UNIVERSITAT POLITÈCNICA DE CATALUNYA
BARCELONATECH
Escola d'Enginyeria de Barcelona Est

FINAL DEGREE THESIS

Bachelor's Degree in energy engineering

GLOBAL CARBON FOOTPRINT ASSESSMENT OF FLOATING WIND ENERGY

Report and Annex

Author: Sergi Vilajuana Llorente
Company tutor: José Ignacio Rapha
Supervisor: Josep Segarra Mullerat

Call: 2024, January

Abstract

Although there are no floating wind energy commercial projects in operation, the floating offshore wind (FOW) sector is now growing significantly. The current situation about the necessity to reduce the carbon emissions, the high potential of the wind resource in offshore deep waters, and the fewer restrictions regarding land use, visual impact and noise, make floating wind a very attractive technology. However, there is still much that is unknown about the effects on the environment. In this work, the global warming potential (GWP) of FOW is presented following the life cycle assessment (LCA) methodology, furthermore, different environmental impacts described in the literature are commented.

The main aim of this work is to analyse the specific emissions of CO_2 for all suitable areas worldwide depending on site conditions; distance to shore, distance to port, water depth, significant wave height and wind potential. Its results show a lot of zones with values below 15 $kgCO_2eq/MWh$, located mainly in countries of north Europe, South America, Egypt, Vietnam, New Zealand, etc. and show a low carbon intensity compared with other technologies that are highly implemented in the actuality.

Resum

Tot i que no hi ha cap projecte comercial d'energia eòlica flotant en funcionament, actualment el sector eòlic flotant està creixent significativament. La situació actual pel que fa la necessitat de reduir les emissions de carboni, l'alt potencial del recurs eòlic en aigües profundes, i les menors restriccions d'ús del sòl, impacte visual i soroll, fan de l'eòlica flotant una tecnologia molt atractiva. No obstant, encara es desconeix molt sobre els efectes sobre el medi ambient. En aquest treball es presenta el potencial d'escalfament global de l'eòlica marina flotant seguint la metodologia d'avaluació del cicle de vida, a més, es comenten diferents impactes ambientals descrits a la literatura.

L'objectiu principal d'aquest treball és analitzar les emissions específiques de CO_2 per a totes les zones viables a tot el món en funció de les condicions del lloc; distància a la costa, distància al port, profunditat de l'aigua, alçada significativa de les onades i potencial eòlic. Els resultats mostren moltes zones amb valors inferiors a 15 $kgCO_2eq/MWh$, localitzades principalment a països del nord d'Europa, Amèrica del Sud, Egipte, Vietnam, Nova Zelanda, etc. i mostra una baixa intensitat de carboni en comparació amb altres tecnologies que són altament implementades en l'actualitat.

Resumen

Aunque no existe ningún proyecto comercial de energía eólica flotante en funcionamiento, actualmente el sector eólico flotante está creciendo significativamente. La situación actual en cuanto a la necesidad de reducir las emisiones de carbono, el alto potencial del recurso eólico en aguas profundas, y las menores restricciones de uso del suelo, impacto visual y ruido, hacen de la eólica flotante una tecnología muy atractiva. Sin embargo, aún se desconocen mucho sobre los efectos sobre el medio ambiente. En este trabajo se presenta el potencial de calentamiento global de la eólica marina flotante siguiendo la metodología de evaluación del ciclo de vida; además, se comentan diferentes impactos ambientales descritos en la literatura.

El objetivo principal de este trabajo es analizar las emisiones específicas de CO_2 para todas las zonas viables en todo el mundo en función de las condiciones del sitio; distancia a la costa, distancia al puerto, profundidad del agua, altura significativa de las olas y potencial eólico. Los resultados muestran muchas zonas con valores inferiores a 15 $kgCO_2eq/MWh$, localizadas principalmente en países del norte de Europa, Sudamérica, Egipto, Vietnam, Nueva Zelanda, etc. y muestra una baja intensidad de carbono en comparación con otras tecnologías que son altamente implementadas en la actualidad.

Appreciations

I would like to express my appreciation to José Ignacio Rapha for his dedication during the supervision of this work. His guidance and expertise, mainly in the field of floating offshore wind, has enabled me to overcome many of the difficulties encountered during this journey.

In addition, I would also like to express my sincere gratitude to the Catalonia Institute for Energy Research (IREC) for the opportunity to carry out the degree thesis with their collaboration. I would like to mention that my internship with them, motivated this study.

I would also like to thank Josep Segarra Mullerat, teacher from UPC, for the tutoring of my work.

And finally, I would be remiss in not mentioning my family and friends for their love and support.

Index

List of figures

List of tables

Acronyms

AC	Alternative current
AEP	Annual energy production
CI	Confidence interval
DC	Direct current
EEZ	Exclusive economic zone
EMF	Electromagnetic field
FOW	Floating offshore wind
FOWF	Floating offshore wind farm
GHG	Greenhouse gas
GIS	Geographic information system
GMF	Geomagnetic field
GWP	Global warming potential
LCA	Life cycle assessment
MRE	Marine renewable energy
O&M	Operation and maintenance
OFAT	One-factor-at-time
OWF	Offshore wind farm
TLP	Tension leg platform

1. Introduction

Globally, 77.6 GW of new wind power capacity was connected to power grids in 2022, bringing total installed wind capacity to 906 GW, a year-on-year growth of 9%. The onshore wind market added 68.8 GW worldwide last year, with China contributing 52%, while offshore wind added 8.8 GW to reach total global offshore wind capacity of 64.3 GW by the end of 2022, 58% lower than the bumper year of 2021 but still made 2022 the second highest year in history for offshore wind installations [1]. This means that the wind power market has been booming for a few years now and focusing more and more on offshore wind. Figure 1.1 shows the historic development of total worldwide installations.

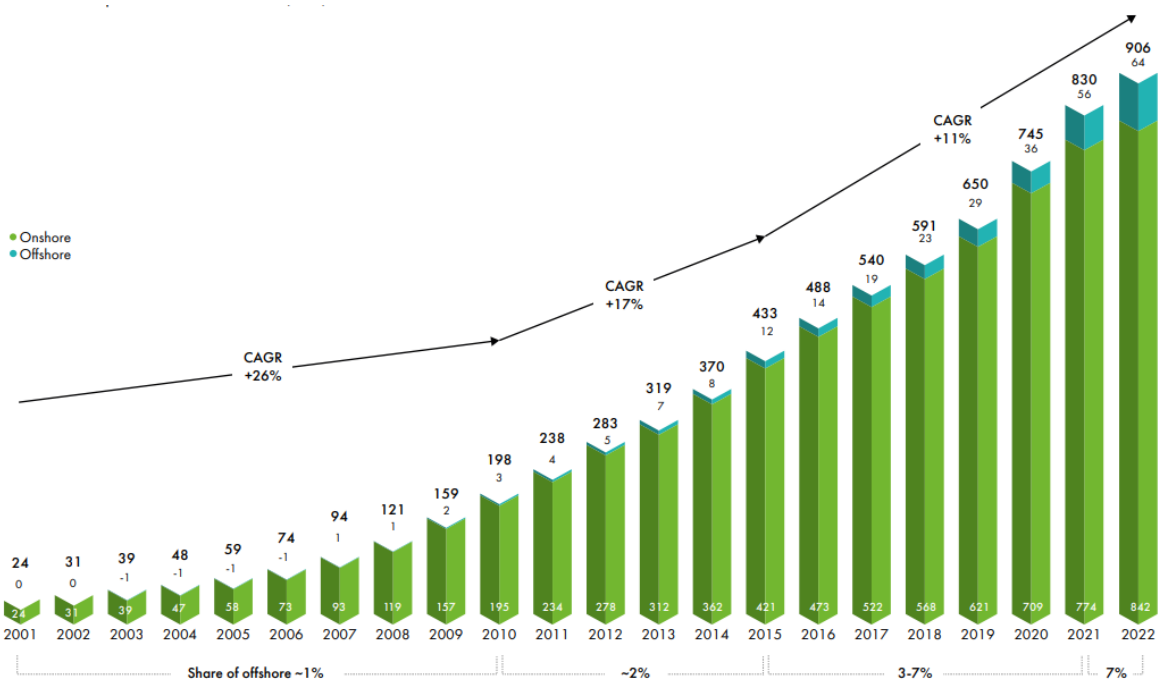

Figure 1.1. Historic development of total installations (GW). (Source: GWEC Global Wind Report 2023 [1])

After 30 years of growth, offshore wind is a mature technology. It is deployment across the globe is now accelerating. However, all these markets have until recently been focused on fixed offshore wind [2]. If offshore wind is to support global action to decarbonise our power system, then we need to seize the opportunity to deploy offshore wind in deeper waters. For most countries around the world, the technical potential of fixed offshore wind is dwarfed by that of floating offshore wind (FOW). Moreover, there are territories as Mediterranean's coasts with high wind potential, but bottom-fixed technology is not an option due to its deep waters.

The huge increase in offshore wind installations has been driven by several factors. On the one hand, the offshore wind speeds tend to be faster and steadier, allowing a steadier supply of energy compared to other renewable energies sources. Furthermore, less restrictions exist regarding land use, visual impact, and noise [3]. Figure 1.2 presents the predicted future worldwide growing of the power capacity of floating wind.

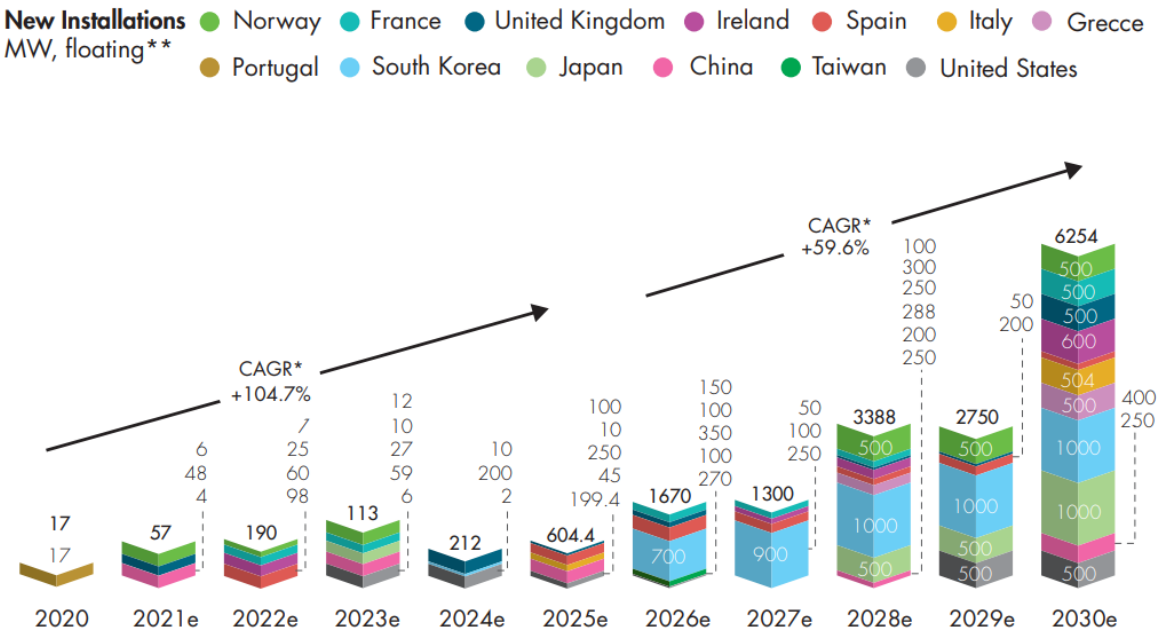

Figure 1.2. New floating wind installations (MW). (Source: GWEC Market Intelligence [2])

80% of the world's offshore wind resource potential lies in waters deeper than 60 m [2], meaning that we must look for opportunities in these deeper waters with floating wind projects if we want to continue efforts to decarbonise the electricity production.

Studies have compared wind power to other generating technologies from a life cycle perspective. The burden of emissions from construction and decommissioning for wind power generation technology, as with other renewable generation technologies, comprises between 97% and 99% of total life cycle greenhouse gas (GHG) emissions [4]. However, there are few studies which evaluate the environmental impacts of floating offshore wind farms (FOWF) as a function of site location, i.e., considering variables as distance to port, distance to shore or water depth, which affects directly on the GHG emissions of the manufacture, installation, operation and maintenance (O&M) and decommissioning.

1.1. Objective

Due to the future growth of the FOW market, and at the same time still unknowing aspects of the technology, the objective of this final degree project is investigate about the different effects that this source of energy has into the environment focusing on the GHG emissions. The main goals of the thesis are summarized below.

- To explain all the aspects on a life cycle of a FOWF which emit GHG emissions.
- To review all the harmful or modifying factors to the ecosystem of the place or the environment.
- To develop a comprehensive model for the LCA of FOWF that allows calculating the GHG emissions for all suitable areas worldwide depending on the main variables.
- To evaluate all the variables involved in the GHG emissions.
- To analyse the carbon intensity results.
- To attribute results to each country and mention the optimal countries regarding the GHG emissions.

1.2. Scope

Firstly, the phases of the life cycle of a floating wind farm that have some type of associated carbon emission and other environmental impacts found in the literature are explained. Then the state-of-art of this topic is collected and analysed to implement many of the found values to achieve the main objective of this study, which is the development of a geospatial model that helps to calculate the carbon intensity worldwide depending on the site conditions with GWP functions and electricity production functions. Also, the validation of the GWP functions is presented. And finally, the analysis of the resultant values with different methods is presented in chapter 6.

2. Environmental impacts of floating wind energy

The aim of this chapter is doing a review of all the impacts that a FOWF has on the environment in which it is installed, in addition to all the activities during its lifetime that involve any alteration or emission.

2.1. LCA of floating wind energy

The LCA is defined as the compilation and evaluation of the inputs, outputs and potential environmental impacts of a product system throughout its life cycle. LCA analyses the environmental burden of products at all stages in their life cycle, from the extraction of resources, through the production of materials, product parts and the product itself, and the use of the product to the management after it is discarded, either by reuse, by recycling or by final disposal [5].

In this technology these stages are, manufacturing, installation, O&M, dismantling and end-of-life, which are described in detail below.

2.1.1. Manufacturing

This stage comprises the raw materials extraction, the transportation of raw materials to the manufacturing facilities and the necessary energy of the heavy equipment used during the production of each part of the wind turbine (tower, nacelle, hub, blades…), substructure, mooring system, and electrical transmission system.

2.1.1.1. Turbine

For wind turbines the main materials used are steel, iron, aluminium, copper, glass, electronics, lubricants and fluids. For example, the V236-15MW model, a Vestas' turbine design for offshore facilities with 143m hub height and total mass of 1530 tons [6], has the typical material breakdown shown in Figure 2.1. The impact of this component will depend mainly on the amount of each material used and the energy consumption for the processing.

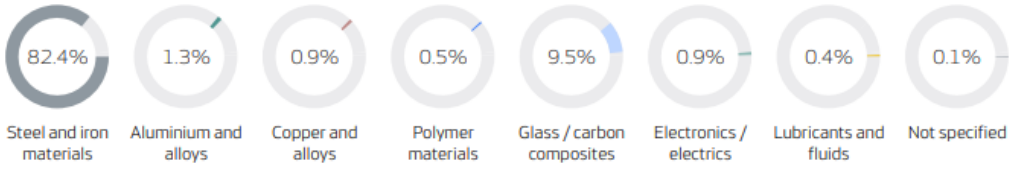

Figure 2.1. Material breakdown for V236-15MW. (Source: Vestas [6])

2.1.1.2. Substructure

Substructure is the component responsible for keeping the turbine afloat, its design will depend on the requirements commented below [7]:

- Ensure design stability in intact conditions.
- Maximum offsets or displacements and limits on dynamic motions.
- Ensure safe operation of wind turbine during the design life of the turbine.
- Maintain acceptable safety for personnel and environment.
- Ensure adequate fatigue strength for 20-30 years operation of the system.

The amount of the materials and the materials itself, are dependent on the design and type of the substructure implemented in each case. These days already exist many options which can be implemented and studies for optimal options are still under development. Its choice depends mainly on the site conditions of the FOWF location. The most recognized types are barge, semisubmersible, spar and tension leg platform (TLP).

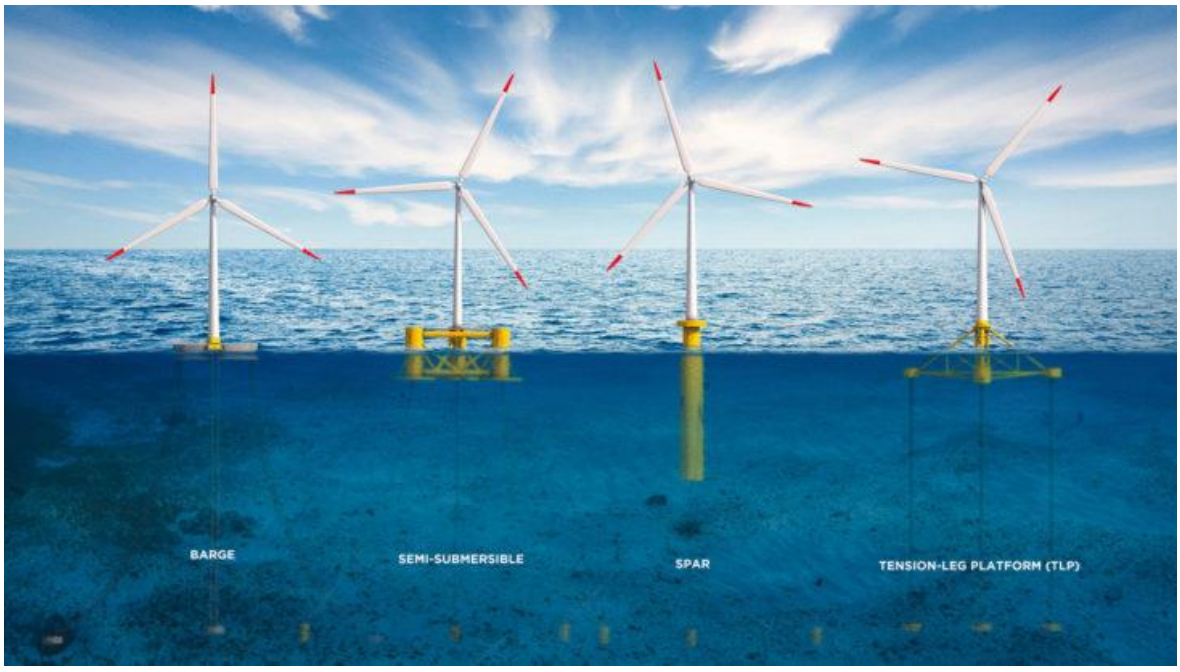

Figure 2.2. Substructure types. (Source: [8])

The substructures are commonly the heaviest component of a FOWF, composite of only steel, steel and concrete, and sometimes if it is necessary a specific ballast material. Its portions will depend on the type and design commented above.

Corewind [9] has two developed Floater designs; WindCrete a spar type with a total mass of 36,840 tons, distributed in 10,230 tons of concrete, 25,860 tons of liquid ballast and 750 tons of steel for the rebar. And Activefloat a semi-submersible concrete floater with a total mass of 21,250 tons, distributed in 19,590 tons of concrete and 1,660 tons of steel for the rebar. Figure 2.3 shows the dimensions of the two substructure designs adding the tower of the wind turbine.

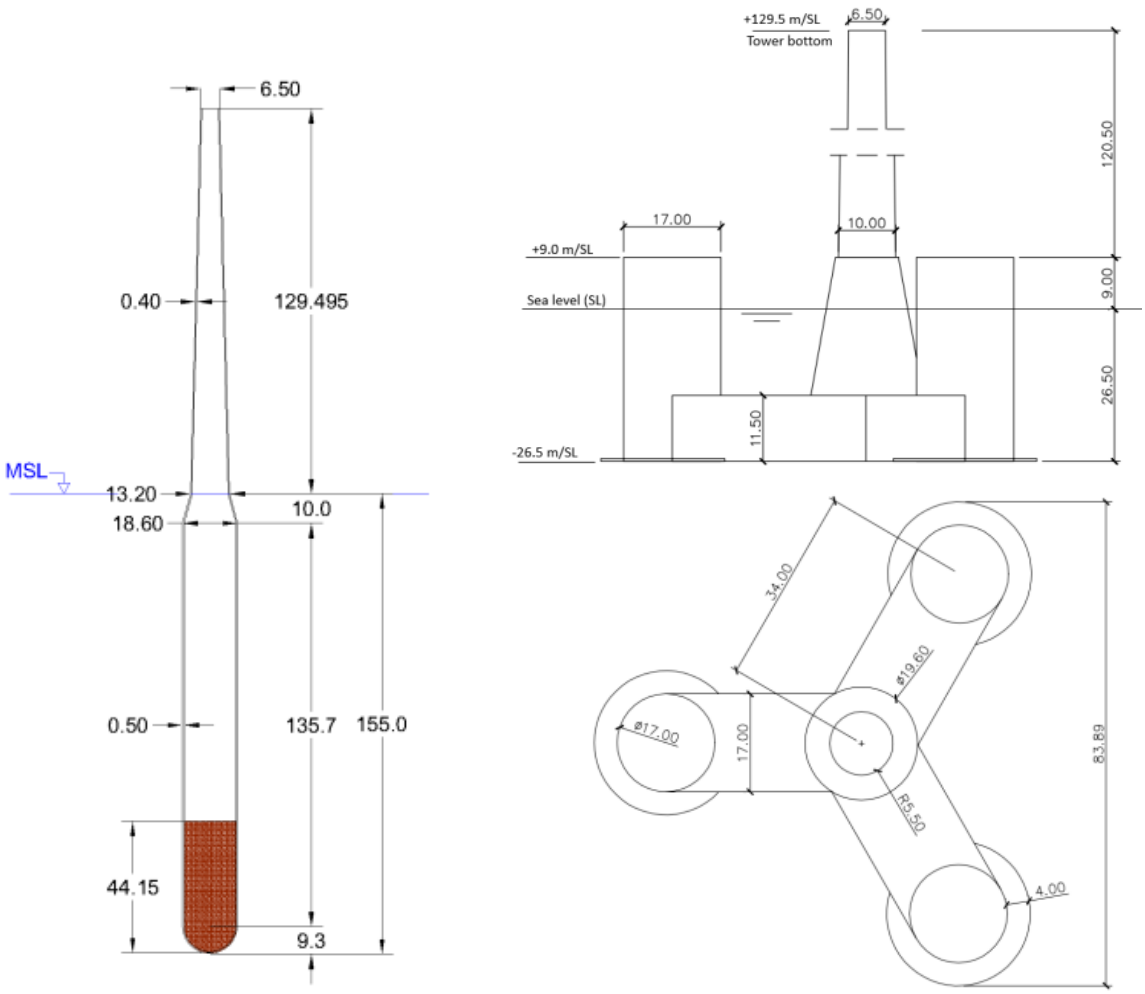

Figure 2.3. a) WindCrete sketch in meters b) Activefloat sketch in meters. (Source: Corewind [9])

These two platforms are designed to support the IEA Wind 15 MW reference wind turbine for a Canary Islands site with conditions, water depth of 200 m, most probable significant wave height of 1.5 m and wind speed at 135 m (hub height of the wind turbine) of 12.26 m/s.

2.1.1.3. Mooring system

Mooring lines connect the anchor with the substructure and are responsible for keeping the wind turbine on site. Different mooring systems configuration exist and each of them can be used for different cases, the three common configurations are illustrated in Figure 2.4.

Tension-leg mooring is the shortest of all three concepts, hence it possesses the smallest carbon emissions. This system provides high vertical loads but is weak for large horizontal forces. Is used for the TLP substructure [3].

Catenary system is the most used system. This system is commonly used for semi-submersible and spar substructures. The curved shape keeps the floating platform in place by laying the lower section of the mooring lines on the seabed with their weight and this supporting the anchor. In case of stormy conditions, the catenary mooring lines act as counterweight to displacements of the platform. The larger material needed for this system transforms a larger carbon footprint than tension-leg mooring system, but at the same time, it helps to be more robust against horizontal loads [3].

The third system, taut-leg mooring system has characteristics of both concepts. The position of the floater is being held by the elasticity of the mooring lines. This one has a bigger carbon footprint than first case, but less than catenary. And it is capable of withstanding considerable vertical and horizontal forces [3].

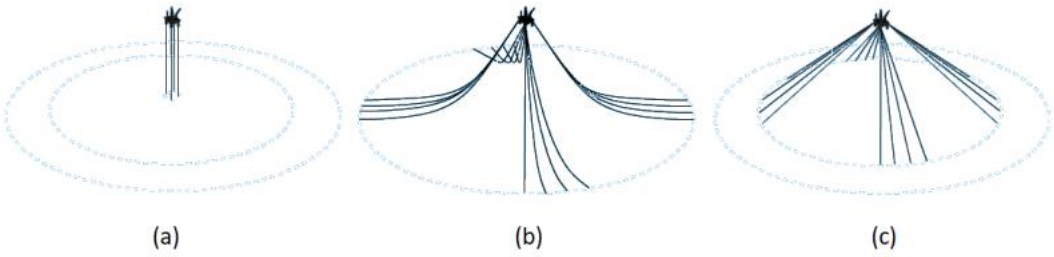

Figure 2.4. a) Tension-leg mooring b) Catenary mooring, and c) taut-leg mooring. (Source: Lerch et al. [3])

Although the most commonly material used for these mooring lines are steel, which is usually the cheapest option, lines made of steel fibres are an alternative solution and have the potential of cost saving due to a lower weight and higher elasticity. Hence, in many cases such as very deep water steel fibres become a better option, which also means a less carbon emissions than steel lines. Synthetic fibre rope is a relatively new material for mooring lines and due its light weight and elasticity are an alternative for taut- and tension-leg mooring systems.

Regarding the anchoring system, its design depends mainly on the aspects commented below [10]:

- Maximum loads supported per line.
- Maximum loads during the transportation and installation.
- Fatigue damage during the lifetime.
- The soil conditions of the site.
- The analysis of the holding capacity to determine the required size and embedment depth of the anchor to achieve the desired capacity.
- Check the ability of the anchor to achieve the required fit and ease of extraction.
- The mooring system selected.

The soil type is classified mainly depending on the grain size distribution. Most commonly soil types found are sand and clay soils. However, other types of soil with higher grain sizes such as rocks or gravel also can be found.

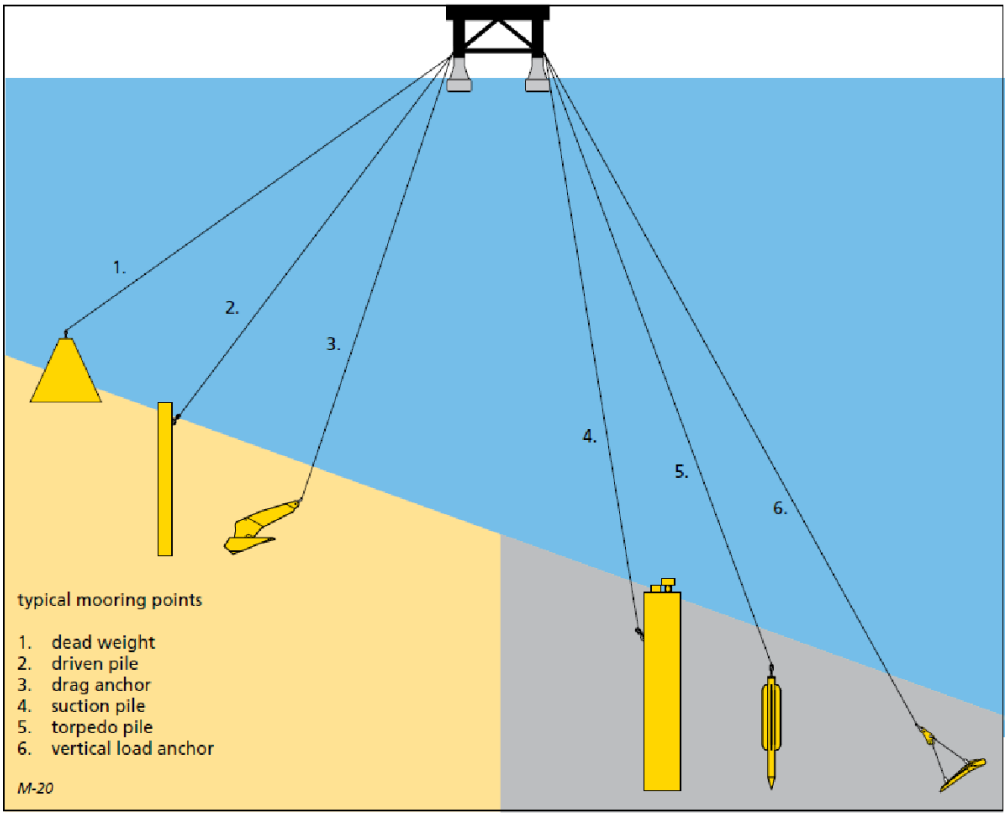

Figure 2.5. Anchor types for floating wind. (Source: Fontana et al. [11])

Gravity anchors are one of the oldest that exist. The holding capacity is based on the weight and material used. Common materials that are used for this type are steel and concrete. However, the portly size and weight can increase the installations costs and the carbon footprint. They are suitable for soft and hard soils and are mostly employed with tension-leg systems due to the high holding capacity [3].

Driven pile is an exceptionally reliable anchor which can achieve a remarkably high load capacities. This anchor has been developed over years with experience in the oil and gas industry. Due to the high reliability, these anchors are the most used for offshore oil production. The main advantages are that stay completely permanent, can be located precisely and are very suitable for supporting vertical loads. The main disadvantage is that this type of anchoring is very expensive, a vibrating or impact hammer is needed. It can be installed in a wide range of soil conditions and are typical for TLP supports as they are also able to withstand large horizontal forces. They are also a viable choice for tensioned and catenary mooring systems [12], [13].

The most commonly used type is drag-embedded anchor, this is dropped on the seabed and dragged to achieve a deeper embedment. Movement over time may not be high risk or critical. The weight of the mooring lines will cause tension in the line which will cause anchor to sink deeper. It has a low cost, are suitable for catenary mooring systems because precise placement is not needed and there are horizontal mooring forces. It is a much cheaper option compared to suction or driven pile, and have a greater load capacity to weight ratio of the anchor. The disadvantages, however, are mainly the lack of precision in the installation and the uncertainty of the load capacity since it mainly depends on the depth of penetration of the anchor and the type of soil. Although uncertainty can be mitigated with tests prior to final installation [12].

Suction piles have a physical appearance of a long tube, which is open at the bottom end and closed at the top. To evacuate the water or suck the pipe on the bottom floor, the closed end is equipped with pump fittings. A transverse stress direction is achieved in the pipe by connecting an anchor line to a bearing eye near the midpoint of the pipe. In this way, the tension line is placed far down in the deepest ground, which allows a large amount of soil to bear the load of the line. A suction anchor is most effective for vertical loading compared to other anchor types [12].

Finally, there is another type of anchor very similar to drag-embedded anchor commented above, vertical load anchor, an adaptation that optimizes resistance to vertical loads. This type is ideal for soft clays [12].

The carbon footprint of these components will depend mainly on the type and amount of raw materials needed, typically steel, steel fibre and/or synthetic fibre and the energy consumption to manufacture them. The specifications of the site as water depth, soil conditions and weather conditions will determine the necessary capabilities of the mooring system and in turn its carbon footprint.

2.1.1.4. Electrical transmission system

The power generated by individual wind turbines is collected through an inter-array connection, and sometimes is transported directly to an onshore substation, to an offshore substation, or to more than

one. The electricity generated is transmitted to shore in either alternative current (AC) or direct current (DC) form through a subsea transmission scheme, which sometimes consists of multiple links to increase the availability and security. Hence, there are three key aspects to complete an electrical transmission system, inter-array cable, substations and export cable [14].

Inter-array cable operates at a voltage of 33 kV or 20 kV although already exists studies to increase this voltage to 66 kV to minimize the power losses. Due to the large distances between wind turbines to minimize the wake effects, this often leads to large sites spanning tens of kilometres in size; such large sites will require substantial cabling distances to connect all turbines to the farm substation [15]. This technology needs dynamic power cable configurations which will depend on how the site conditions affect to the facility, e.g., water depth, large floater lateral motions, floater dynamic rotations, high wave heights, high currents or variations in marine growth over the life of the system. Two common examples are the free/hanging catenary and the lazy wave configuration, as shown in Figure 2.6 a) and Figure 2.6 (b) or the novel design of the fully suspended inter-array power cable configuration shown in Figure 2.6 (c), which is expected to have less dependency on water depth and shorter transmission distance [16].

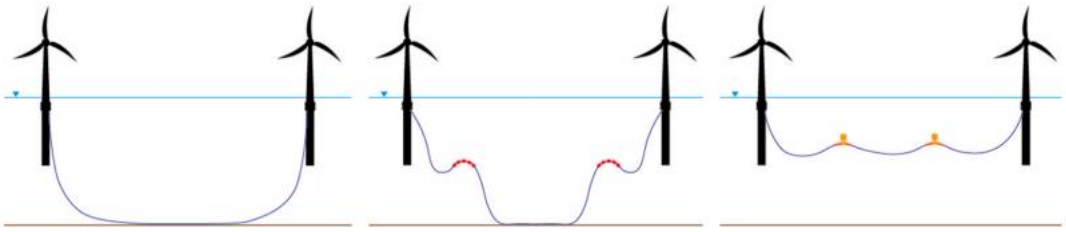

Figure 2.6. Cable configurations. From left, a) Free hanging catenary, b) Lazy wave, c) Fully suspended. (Source: Ahmad et al. [16])

Substations are required for projects larger than 100 MW or when farms are situated at distances greater than 15 km from shore [15]. The main purpose of a substation is to set up the voltage from the collector level, commonly 33 kV, to a higher level suitable to export the electricity produced offshore to the grid, normally 132 kV. The voltage is required to be stepped up to reduced losses that occur with large transmission distances as offshore farms are often located great distances from shore. The large weights of the substations transform into a large carbon footprint mainly due to the great amount of raw material needed.

The final part is the export cables to efficiently transmit the electrical power with minimal loss from the FOWF to the cable connection facility at the landfall point. Export cables may operate with HVDC (High voltage direct current) or HVAC (High voltage altern current) technology, depending on several balancing factors, particularly the offshore distance to shore, the total generated power of the FOWF, material and operational costs [17].

Typical materials needed for this section are copper, electrical steel, steel, lead, etc. which has the largest burden to this section carbon footprint, followed by the energy consumption for the manufacturing. Variables as distance to onshore substation, distance between turbines, substations needed, etc. have effects in the resulting GHG emissions.

2.1.2. Installation

Installation is the last step before commissioning of an FOWF. First step of the installation is delivering components as substructure, tower sections, nacelle, rotor, anchors, etc. to the onshore assembly site, which means fuel consumption due to the necessary trucks or vessels for the transportation of each component that will increase or decrease according to the distance between the manufacturing sites and the harbor site.

Second step is the onshore assembly site at harbor, based on the installation strategy, all component assemblies are completed and, then, components are loaded onto the installation vessel to be transported to the location of the offshore wind farm (OWF). Different strategies exist and its choice depends on minimize the costs and whether the shipyard allows enough area for storage, and has enough draft for the floater. For FOWFs the best strategy is a total turbine assembly onshore so only one lift is necessary [18]. Regarding the floater, the installation will depend on the type of substructure, in the case of the semisubmersible and barge type, due to the good floating performance without moorings and capability to be transported afloat, the floating substructure and turbine are completely assembled and joined together onshore in the harbor and then is towed out to sea by a tugboat as shown in Figure 2.7 and taken to the offshore site where the installation takes place. Since the FOWT is already assembled, only an anchor handling tug vessel is required to perform the final installation, which includes mooring lying and anchor setting [3]. For the spar case, which is not as inherently stable as the types commented above, the turbine and the substructure are transported separately and assembled offshore. The turbine may be transported on a jack-up vessel and the floating substructure is towed by a tugboat [3].

Figure 2.7. Floating turbine being towed for the WindFloat Atlantic project. (Source: WindFloat [19])

The mooring and anchor installation will depend mainly in the type of system chosen, in the case of drag-embedment anchors, an anchor handling vessel is used to lower the anchor to the seabed by using the mooring line. When the anchor reaches the ground, the vessel should move slowly forward to ensure a correct immersion of the anchor into the seabed. Furthermore, a chaser is used to handling the anchor and place it as precisely as possible. For this process exists two options, a pre-installation of the mooring system and later assembly to the floating substructure or an installation of the mooring system simultaneous with the towing of the substructure with the same vessel to minimize the number of vessels needed [20].

For the suction pile, the anchor penetrates up to 60% of its length under its own weight, depending on soil conditions and the pile properties. Then a remote-operated vehicle (ROV) is needed to bury the rest that remained above the sea floor, it pumps water out of the top suction port after sealing pile top valves. Pile top and ROV instrumentation contribute to a precise installation [21].

Prior to the installation of an offshore substation, its foundation should be installed. Typical choices for the foundation are jackets, gravity-based foundations or floating substructure depending on the application. When the foundation is installed, the complete substation should be lifted from the installation vessel and be placed on top of the foundation [22].

Finally, the cable installation is conducted. On the one hand, all wind turbines need to be connected with the offshore substation with the inter-array cables, this process is developed by cable lying vessels with dynamic positioning devices to keep steady position under harsh weather conditions. On the other hand, the installation of export high-voltage cables is carried out by larger cable laying vessels

and ROVs. After export cable installation, precommissioning tests can be developed and the FOWF can be commissioned [22].

With all commented above, installation carbon emissions will depend on the fuel consumption of the crane harbor and vessels, which will be related with the time of installation. This time of installation depends on sites conditions as the distances that will be necessary to travel, the weather conditions and water depth of the site of installation.

2.1.3. Operation and Maintenance

O&M activities consist of scheduled and unscheduled maintenance. As in installation, the main contributor of GHG emissions is the fuel consumption and the fleet required for all the activities. The other contributor is the manufacturing of the replaced components during the entire life of the FOWF.

This section contemplates activities for which vehicles such small boats, helicopters, ROVs or specialized vessels are needed [23].

2.1.4. Decommissioning

Decommissioning can be considered as a reversed installation process and includes the site preparation, the disassembly of the FOWF and the transportation back to port. Hence, the main factors that will affect the emissions of this section will be the same as the commented in the installation section.

2.1.5. End-of-life

This section includes the transportation of the components from the harbor to its management sites and the final treatment which can be recycling, deposition to landfill or incineration with energy recovery in some cases. The final treatment of the wind farm components is usually expressed per material.

This section will depend on the distances between the harbour and final treatment sites and the type and amount of materials used for each component. For example, the greater the amount of steel the greater the bonus will be associated to the part lifespan consumed in the next process. Hence, this section could present negative values of emissions.

2.1.6. Impact categories

There are other impact categories assessed in the literature apart from the GWP, for example Brussa et al. [24] analyse eight impact categories according to International EDP System [25]: global warming

(CO_2/MWh), acidification (kg SO_{2eq}), eutrophication (kg PO), photochemical oxidant formation (kg NMVOC), abiotic depletion of elements (g SB_{eq}), abiotic depletion of fossil fuels (GJ), water scarcity (m^3_{eq}) and ozone layer depletion (g CFC-11_{eq}). However, this study is focused only on the global warming category.

2.2. Environmental effects

Due to the infancy of the floating wind energy, its potential effects on the marine environment during its entire lifetime are speculative. Although a robust empirical study and test of such effects is still not possible, the effects can be estimated with the current literature about other marine industries such as fixed-bottom OWFs, land-based wind energy facilities, marine renewable energy (MRE) devices, oil and gas platforms or some installed prototypes of FOW [5]. In this chapter the different knowledge about the possible potential environmental effects related to FOW will be discussed.

2.2.1. Changes to atmospherics and oceanic dynamics

Studies have evaluated several potential consequences of wind energy extraction on local and regional climate. The most widely documented consequence is the wake effect, or reduction in wind speed and kinetic energy downstream of a wind energy facility [26].

Christiansen et al. [27] produces a simulation to see the cross-scale wake effects near OWF in North Sea. The simulation shows a large-scale reduction in dynamics and the effects to the lateral and vertical transport of heat and salt even far beyond the associated wind farms.

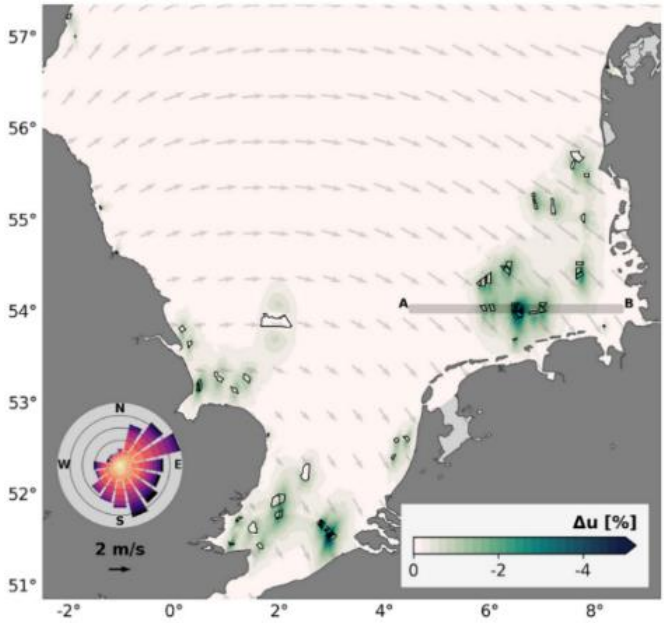

Figure 2.8. Mean wind speed changes for the period of May-September 2013. (Source: Christiansen et al. [27])

Nagel et al. [28] makes an evaluation of the ocean-sediment dynamics in waters depths of 20 m and 50 m. Although these boundaries are for bottom-fixed turbines, it can give an idea about the effects of this aspect. The study shows that turbine wake has impact on both the ocean and the sediment bed layers, but its role is negligible in the air-sea energetic balance. The effects on the ocean surface can generate instabilities and vortex streets. The non-uniformity of the oceanic velocity field induced by wake presence is observed in the local bottom shear stress, responsible for sand erosion and deposition. The wake imprint on the seabed tends to be reduced by largescale vortices and oscillating local velocity which transports sediment back and forth and may increase the turbidity.

Related to the FOWFs, are expected to be less disruptive to ocean currents, waves and sediment dynamics than those with fixed foundations in shallow waters [26]. However, will be needed more studies to see the behaviour of the environment near to these facilities.

2.2.2. Electromagnetic field (EMF) effects

FOWFs increase the distance from shore, so additional, longer and higher capacity subsea cables will be needed to interconnect the FOWFs components to each other, to the seafloor and to shore. The cables emit EMFs along their entire lengths, whether transmitting high-voltage DC or AC. Some prototypes use suspended inter-array cables within the water, rather than solely along the seafloor as is often the case with fixed-bottom OWFs, that may increase the scope of anthropogenic EMFs in the water column and potentially interact with a great diversity of marine organisms [26].

Figure 2.9. Diagrams summarizing the natural and anthropogenic electric fields, induced electric fields and magnetic fields encountered by an electromagnetic-sensitive fish moving across the seabed. (Source: Newton et al.[29])

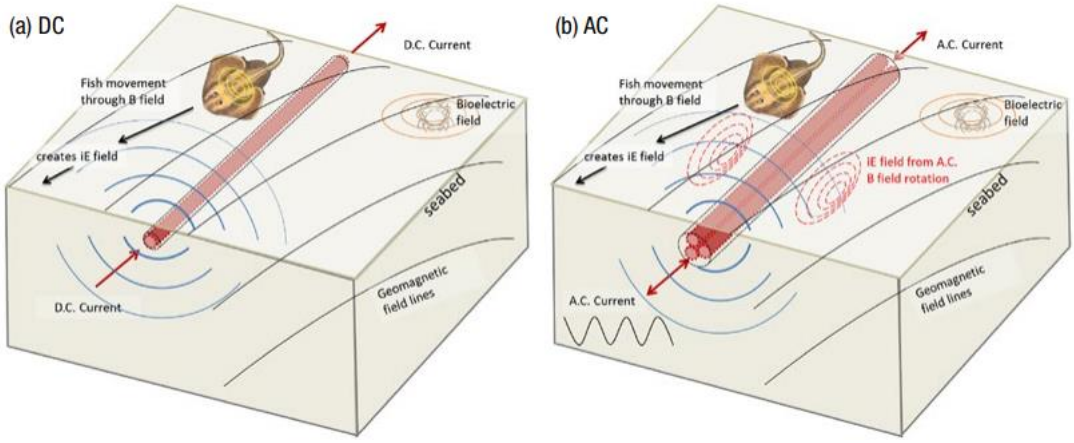

The interactions between EMFs emitted by MRE power generation with the naturally occurring geomagnetic field (GMF) can potentially alter the behaviour of marine animals that are receptive to these fields including potentially altering avoidance or attraction behaviours. The movement and

distribution of the animals also plays a role in the probability of an encounter with an EMF and may depend on the species life stage, as well as the spatial and temporal use of the environment where the EMF occurs.

Although is necessary to continue the exploration on EMFs effects, practically all the studies carried out do not find considerable changes either in invertebrates, in fish (adult, larval or embryonic), or in community species. Whereas based on the current knowledge, biological or ecological impacts associated with MRE subsea power cables may be weak or moderate at the scale is currently being considered or planned [30].

2.2.3. Habitat alterations

The deployment of any novel, offshore structure may induce physical changes in habitats that have the potential to alter species composition and abundance at localized scales or provide opportunities for colonization by new species [26].

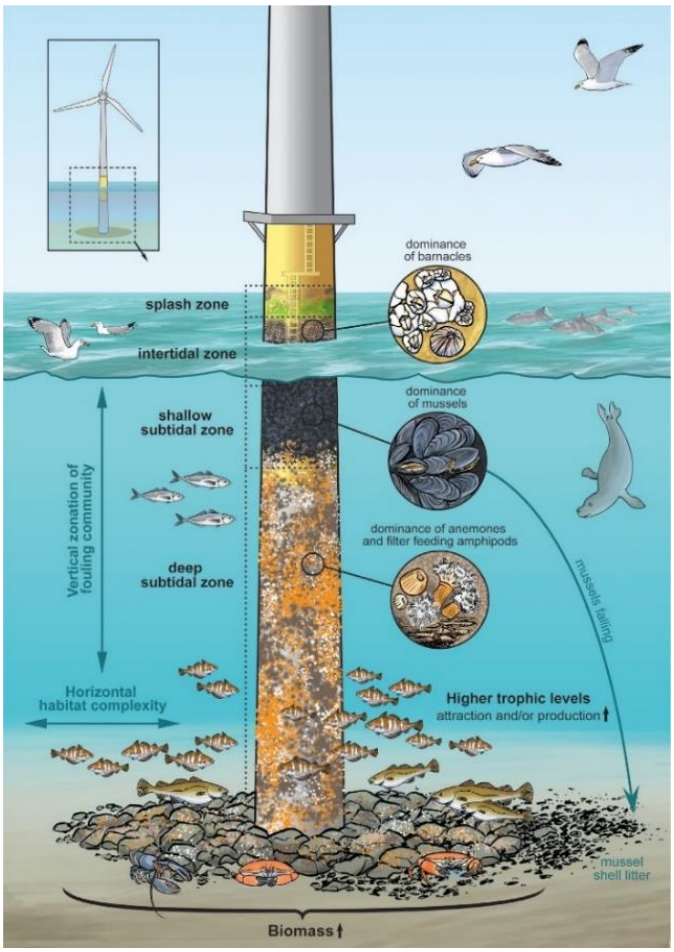

Figure 2.10. Habitat provided by a bottom-fixed offshore wind turbine structure. (source: Degraer et al. [31])

Hammar et al. [32] concludes that OWFs can be at least as effective as existing marine protected areas in terms of creating refuges for benthic habitats, benthos fish and marine mammals. It shows that operational OWFs generate increased biodiversity and abundance for many species. Furthermore, the imposed fishing restrictions can be highly valuable from a conservation point of view. Hence, with regards to marine invertebrates, fish and mammals, the many monitoring programs at existing wind farms support that wind farms and marine conservation interests are compatible, or even synergistic, depending on location. However, several species of seabirds, are negatively affected as they tend to avoid the area and therefore suffer a loss of habitat. Nevertheless, due to the increase of the wind turbines' size, which already reach more than 115 meters in case of the radius rotor or 25 meters between the sea level and the blade, there is enough space for the flight of most birds.

2.2.4. Noise effects

Many marine animals rely on sound for biological functions e.g., communication, social interaction, orientation, foraging, and evasion [30]. Hence, anthropogenic noise sources from turbine or mooring system may have potential interferes with the ability of a fish to detect and respond to biologically relevant sounds, thus can decrease survival and fitness of individuals and populations [33]. However, the worst part comes from the noise during the installation.

Installation of a FOWF may involve a variety of activities that generate sound into marine environment such as: pile driving, drilling, dredging or increased shipping. With respect to these activities there is increasing evidence that for marine mammals and fish there is a risk of phycological response closer to the sound and/or relatively high acoustic doses [34].

During the operation are assumed less noise than during construction, and although this noise still being audible for several species, no study has shown any behavioural impact of sound during the operational phase of wind farms [34].

2.2.5. Structural impediments

The physical presence of offshore structures, whether dynamic or static, may present both novel obstacles and benefits to marine organisms [26]. The deployment of such facilities, for example, may result in displacement of individuals from key habitats such as foraging and breeding grounds. However, there are studies such Russel et al. [35] and Scheidat et al. [36] that shows evidence of an increase in acoustic activity of marine mammals near to OWF facilities. Which can be explained due to an increase in food availability and/or absence of vessels.

As to seabirds, avoidance of OWFs may cause migrating bird species to use more circuitous routes and expend more energy, but studies such as Masden et al. [37] reveals that the additional energy to avoid

in that case the Nysted OWF in the North Sea is insignificant. Skov et al. [38], besides shows the effects of the Thanet OWF in Kent, United Kingdom, where 96.8% of the recorded seabirds fly between the turbine rows while the 3.2% adjusted their flight height to fly below the rotor-swept zone as commented in section 1.3. Which suggest that the responses to that OFW facilities may not require a considerable increased energy expenditure for these seabirds. Although avian collision risk is one of the most popular concerns related to wind facilities, buildings, powerlines, and cats comprise approximately 82% of avian mortality from anthropogenic sources, while land-based wind facilities comprise 0.003% [39]. Furthermore, more distance to shore means less avian collision risks, which also depends considerably on siting carefully the OWF to ensure minimal overlap with the habitat of different species [40].

Additional concerns regarding FOWF are the potential risk of collision and entanglement to marine megafauna, mainly with the mooring lines. Benjamin et al. [41], evaluates the relative degrees of risk posed by different mooring configurations to different megafauna groups. Baleen whales incur the greatest risk of entanglement mainly due to its large size and the greatest risks are generated by catenary moorings. It concludes that although there are no records of marine megafauna entanglement in any mooring system, it is an aspect to take into account in the development of MRE facilities. Furthermore, as in other aspects commented in that sections, the principal factor to consider avoiding this problematic is the site selection.

2.2.6. Changes to water quality

In OWFs are included preemptive measures to prevent corrosion and biofouling, because of the highly corrosive, difficult and expensive maintenance of offshore structures, especially those far from shore [26]. Corrosion protection include numerous epoxy-based coatings, a polyurethane topcoat and cathodic protection [19]. These protections are a direct source of chemical emissions. For example, Vermeirssen et al. [42] demonstrated the release of large amounts of bisphenol A from epoxy resin-based anti-corrosion coatings on onshore infrastructure. However, there is currently no clear evidence of a negative impact on the marine environment from these sources [31]. Furthermore, stricter regulations have initiated the research and development of alternative approaches, and more commonly, the use of various non-toxic, non-biocide-release antifouling coatings [26].

3. State of the art of LCAs of wind energy

Wind energy is one of the cleanest energy resources, it is almost burden-free during its operational phase. The problem comes with the consumption of resources, materials and energy. Hence, LCA methodology is used to evaluate the potential environmental impacts associated with all the activities during the entire life cycle of the wind farm; the supply chain of the components, the impacts of the installation, the maintenance, the dismantling and the end-of-life of all components.

The LCA literature related to onshore wind is extensive, e.g., the reviews Arvesen et al. 2012 [43] and Nugent et al. 2014 [44], find a range of potential global warming of 6-34 gCO_2eq/kWh and 0.4-364.8 gCO_2eq/kWh, respectively. But if we are focusing on OWFs, although is still reaching a lot of studies, we begin to have less information, e.g., Bonou et al. 2016 [45] , estimated the onshore and offshore wind GHG emissions in less than 7 gCO_2eq/kWh and 11 gCO_2eq/kWh, respectively.

But LCA studies of floating wind cases are even less, and all of them are hypothetical cases which provides a speculative results, mainly about the GHG emissions. Specifically, there are 13 studies found which will be commented below.

The first study of the LCA of a FOW turbine is Weinzettel et al. 2009 [46], which present a process based LCA of an offshore floating wind power plant according to the concept developed by Sway Company, designed to be installed at a depth of 100-300 m and up to 50 km from the coast. It concludes that the environmental impact of electricity production from a floating wind power plant does not significantly differ from electricity production in a conventional offshore wind power plant if we assume a better capacity factor. The GHG emissions reach 0.0003 $kgCO_2eq/MJ$, equivalent to 11.52 $kgCO_2eq/MWh$. Elginoz et al. 2017 [47], evaluated the LCA of a multi-use platform, combining 385 MW of wind energy and 265.5 MW of wave energy in the Cantabrian coast (3-13 km from coast) and reach 18.1 $kgCO_2eq/MWh$.

A comparison of the life cycle GHG emissions and energy performance (Energy Payback Ratio and Energy Payback Time) from wind power generation from six different 5 MW offshore wind turbine conceptual designs is presented in Raadal et al. 2014 [48]. Its results give a wide range of carbon intensity from the concept with lower emissions (MIT Tension-Leg-Buoy) with 18 $kgCO_2eq/MWh$ and concept with most emissions (UMaine Semi-Submergible) with 31.4 $kgCO_2eq/MWh$, which change is mainly due to the difference of steel masses required for each platform. Therefore, it transforms to a wide difference between the energy performance results too.

Tsai et al. 2016 [4], aims to enhance the decision of making OWF siting by evaluating the environmental and energy performance of the OWF life cycle and compare the marginal change of environmental burdens in response to the variability of the distance to shore. It compares the GHG emissions for 20

scenarios at 4 different sites and 5 different distances to shore (5, 10, 15, 20 and 30 km), using the most economical foundation according to the water depth between gravity-based, monopile, tripod and floating foundations for 3 MW turbines. It reaches values from 25.56 $kgCO_2eq/MWh$ the case of Oceana at 5 km from shore to 47.32 $kgCO_2eq/MWh$, the case of Huron at 30 km from coast using tripod foundation. The results of floating substructures reach values in the range of 32.88 and 38.1 $kgCO_2eq/MWh$.

In Bang et al. 2019 [23] it is performed the LCA of a FOWF in California, its results show that the emissions are around 15 $kgCO_2eq/MWh$, and compares this with the emissions from hydro and nuclear. Furthermore, it indicates that the turbine manufacturing stage is responsible for the majority of the life cycle GHG emissions, recycling rates for materials have strong implications for reducing life cycle GHG emissions and that the life cycle GHG emissions are most heavily influenced by capacity factor of the turbines and the operational lifetime of the windfarm.

Poujol et al. 2020 [49], presents the LCA of a pilot project in the Mediterranean Sea, specifically on Perpignan coast, of four 6 MW turbines composing a 24 MW FOWF. Its results show an emission of 22.3 $kgCO_2eq/MWh$ and again, the main contributor to environmental impacts is the extraction and transformation of the materials. Furthermore, the study analyses the variability on the environmental impact per kWh produced depending on geographical location and wind data source which transforms in these cases to a significant impact reductions.

Other study focuses on specific type of substructure and compare the environmental effects to other types, Yildiz et al. 2021 [50], analyses the LCA of a 2 MW floating wind turbine on a barge-type platform. Again, the greatest environmental impact corresponds to the manufacturing stage. It concludes that this case has a higher impact with 18.6 $kgCO_2eq/MWh$ than onshore, jacket offshore and floating wind turbines on sway floating platform with 7.09, 9.49 and 11.52 $kgCO_2eq/MWh$, respectively.

Garcia-Teruel et al. 2022 [51], is focused on using an advanced O&M model to quantify the environmental impact of two FOW pilot parks located off the east coast of Scotland, a Spar case inspired by the Hywind deployment and semi-sub case by the Kincardine deployment. The results show GWP values between 27.7 and 45.2 $kgCO_2eq/MWh$ depending on the assumed O&M strategy and vessels, with contribution of the O&M phase to GWP ranging from 21 to 49 %.

Pulselli et al. 2022 [52], concerns a LCA of the environmental performance of two types of FOWT, raft-buoy and spar-buoy, with 6 MW. The study assumes a reference energy production in three areas of the Mediterranean Sea of a 300 MW wind farm installed in Crete (Greece), Split (Croatia) and Larnaca (Cyprus) and considered 22 km from shore for all 3 areas. The results of carbon intensity of electricity fall in range 26.1-78.7 $kgCO_2eq/MWh$, and suppose a mean values of 44 $kgCO_2eq/MWh$ for raft-buoy

and 54.3 $kgCO_2eq/MWh$ for spar-buoy. It concludes that the results variations depend largely on mass balance and the selection of marine areas with different wind energy potentials.

The environmental impacts of a FOWF with 100 wind turbines of 6.7 MW using LCA method are evaluated by Yuan et al. 2023 [53]. The results show a carbon footprint of 25.76 $kgCO_2eq/MWh$. It also affirms that if the average GHG emissions intensity of steel production can be lowered considerably, it will reduce the carbon footprint of the FOW energy.

In Chipindula et al. 2018 [54] the results of the LCA are compared with SimaPro and the Impact 2002+ of individual stages at three locations, onshore, shallow-water and deep-water, in Texas. The results are between 5 and 7 $kgCO_2eq/MWh$ for onshore location, 6 and 9 $kgCO_2eq/MWh$ for shallow-water and 6 and 8 $kgCO_2eq/MWh$ for deep-water. It also reports the payback times for CO_2 and energy consumption which range from 6 to 17 months, with onshore farms having shorter payback times. As in other studies it indicates that material extraction / processing is the dominant stage with an average impact contribution of 72% for onshore, 58% for shallow-water, and 82% for deep-water.

Brussa et al. 2023 [24], reports the LCA of a FOWF of 190 wind turbines with 14.7 MW rated power on a semi-submersible platform in Mediterranean Sea, specifically 60 km from the west coast of Sicily. The estimated carbon intensity is 31.3 $kgCO_2eq/MWh$ with a lifetime of 30 years.

Ferreira et al. 2023 [55] which is the most recent published study, provides an integrated and novel holistic tool to assess the economic aspects and environmental impacts of the life cycle of FOWFs. It allows for identifying the environmental and economic hotspots along the FOW life cycle, driving decision-makers and engineers towards a sustainable floating wind technology and enhancing cost reduction strategies. This study includes the analysis for two sites, 10 km off the coast of Gran Canarias and 60 km off the coast of Morro Bay with spar platform technology and 15 MW turbines for a FOWF of 60, 300 and 1200 MW. The results are between 6.56 and 10.40 $kgCO_2eq/MWh$.

These studies are the key to develop the aim of this thesis, and these values will be used to define the methodology to calculate the carbon intensity for all areas worldwide where is possible to install a FOWF depending on water depth, distance to shore, distance to port, significant wave height and wind potential of each cell evaluated. The results of the carbon intensity are analysed in Table 3.1.

	Carbon intensity ($kgCO_2eq/MWh$)
Minimum	6.56
Maximum	78.70
Average	26.39

Table 3.1. Results assessment of the literature review.

All the studies highlight the importance of the manufacturing stage mainly of the wind turbine, substructure and mooring system on the carbon footprint results, in almost all studies this phase have a burden of more than 50% of the total GHG emissions. Furthermore, the variability due to the capacity factor depending on the site selection is also commented in many of the commented studies, there is a considerably reduction of carbon intensity in sites with high wind potential.

Study	**Power (MW)**	**Water depth (m)**	**Distance from shore (km)**	**Distance from port (km)**	**Carbon intensity ($kgCO_2eq/MWh$)**
Winzettel et al.	200	100-300	50	100	11.52
Elginoz et al. [47]	385	-	3-13	-	18.10
Raadal et al. [48]	500	200	200	-	18.00-31.40
Tsai et al. [4]	300	40-70	10-30	40-70	32.88-38.10
Chipindula et al. [54]	2.3 and 5	140	70	-	7.58 and 6.98
Bang et al. [23]	600	450	35	-	15.35
Poujol et al. [49]	24	-	16	-	22.30
Yildiz et al. [50]	2 and 5	-	-	-	18.60 and 11.52
Garcia-Teruel et al. [51]	30 and 47.5	95-129 and 60-80	25 and 15	25 and 32	36-44 and 31.10-37.40
Pulselli et al. [52]	300	-	22	22	26.10-78.70
Yuan et al. [53]	670	60-80	12-20	-	25.76
Brussa et al. [24]	2793	100-900	60	-	31.30
Ferreira et al. [55]	60, 300 and 1300	200 and 870	10 and 60	-	6.56-6.91 and 9.96-10.40

Table 3.2. Values of interest of the literature review.

4. Methodology for the LCA model

The aim of this chapter is to explain the process during the model development. In section 4.1, the assumptions of the FOWF of the study are described. In section 4.2 the data recollected is commented. Section 4.3 describes the restrictions taken into account. Section 4.4 discusses the variables considered in the model and section 4.5 exposes methodology of the model to compute all necessary functions for the carbon intensity (annual energy production (AEP) and GWP).

4.1. Case of study

This thesis is a case of study of carbon intensity for a FOWF with 20 IEA 15 MW reference wind turbines [56] (total power capacity of 300 MW), with a hub height of 135 m and lifetime of 25 years. Furthermore, separation between turbines of 7Dx7D (where D is the rotor diameter) is considered. Hence, the aim is to find the intensity carbon of this FOWF in all theoretical suitable points over the world.

For the development of the results various data and constraints have to be considered as is explained in the following sections.

4.2. Data processing and collection

In first place, is necessary to consider all the site conditions to determine the suitable areas where is feasible to install a FOWF such as the bathymetry and significant wave height. Also, it is necessary to search the wind speeds to compute the AEP. For this data, is required to use a geographic information system (GIS), which connects data to a map, integrating location data with all types of descriptive information. This provides a foundation for mapping and analysis that is used in science and almost every industry [57]. Hence, the data used for the model, are layers of series of cells which each of them represents information from a specific area in the world map.

For the AEP, apart from wind speed data also capacity factor layers are considered. Specifically, the model work with three turbine classes related to the design requirements to ensure that turbines are appropriately engineered against damage from hazards within the planned lifetime set by the International Electrotechnical Commission [58] (IEC). These turbine classes, depend on the average wind speed, extreme 50-year gust and turbulence, but in this case only average wind speed in the hub height of the wind turbine of the study is taken into account. Turbine classes determines the capacity factor class.

Other data that has to be contemplated is the distance of feasible locations to port, for installation, O&M and dismantling. Therefore, the location of ports is also necessary for the model.

Finally, the exclusive economic zone (EEZ) is implemented as maximum distance to shore. Thus, the final data layer needed is related to EEZ.

All the data layers used for the model and its respective sources are commented below.

Data	**Source**
Bathymetry	GEBCO [59]
Significant wave height	Copernicus [60]
Wind speed	Global Wind Atlas [61]
Capacity Factor 1	Global Wind Atlas [61]
Capacity Factor 2	Global Wind Atlas [61]
Capacity Factor 2	Global Wind Atlas [61]
Ports	AmeriGEO [62]
Exclusive Economic Zones	Marineregions [63]

Table 4.1. Source of the data layers.

The significant wave height layer has to be processed to be useful for the model, there are values from 2011 to 2020 and a mean has to be conducted. Regarding wind speed, the data collection is in heights of 100 m and 150 m.

4.3. Restrictions

The restrictions are carried out to provide the feasible and unfeasible areas to apply this technology. Water depth is the first contemplated constraint, it is considered that this technology is feasible in the

range of 60 to 1000 m, in the lower range the bottom-fixed is a better option and in the upper range the technology is considered economically and technologically unfeasible. Hence, shallow and very deep waters are excluded of the study.

Another restriction is a maximum of average significant wave height, which is settled in 3 m to ensure suitable weather windows for installation, O&M and decommissioning.

Finally, due to the aim to analyse the values for each country, only the cells inside the EEZs are considered. These are the zones of the ocean extending up to 200 nautical miles (370 km) immediately offshore from a country's coastline [64], where an exclusive sovereign state has rights regarding the exploration and use of marine resources, including energy production from water and wind [65].

4.4. Variables

The functions commented below to calculate the carbon emissions of each phase of the life cycle of the FOWF will be implemented for the feasible locations worldwide, therefore, many conditions of the feasible cells will be taken into account. The independent variables for the CO_2 emissions per megawatt calculations are water depth, average significant wave height, distance to shore and distance to port. While the energy delivered to the onshore substation have into account the distance to shore, average wind speed, capacity factor and average significant wave height.

For the distance to shore, a function based on Haversine formula [66] is used with help of MATLAB, to compute the distances between each feasible cell and the coast, which corresponds to the nearest 0 m of bathymetry cell. The process applied for the distance to port is the same as in the distance to shore case, but for the nearest port.

4.5. Functions

The methodology carried out to find the functions for the GHG emissions is a regression of the values obtained from current projects and studies commented in chapter 3. Hence, the first step was recollecting the useful information from as many studies and projects as possible.

At the beginning, because of the simplicity and larger number of values than for the final method, which will be commented later, the idea was to use the total CO_2 emissions per MW as dependent variables, and water depth, distances and significant wave height of each study as independent variables. But the results although statistically were not unfavourable, the result of the regression presents a lot of negative coefficients for the variables, which transforms in the final results to some negative CO_2 emissions cases, which is impossible.

On the second try, the idea was to directly consider the carbon intensity as a dependent variable and add the capacity factor as independent variable. In this case, the calculation of energy is not necessary because the results already take into account the energy production. As the case commented above some of the coefficients of the regression result negative and transforms again to some cases which the carbon intensity is negative.

In the two previous cases mentioned, two statistic tools, explained below, were applied to see if there is a possibility to achieve better results.

- COX-BOX: is a model used when there is no lineal relationship between the dependent and independent variables. This uses a transformation of variables to achieve linearization, specifically a group of new variables that depend on λ. These variables are denoted as Z(λ) and its value is [67]:

$$Z(\lambda) = \frac{y^{\lambda} - 1}{\lambda} \qquad \textbf{(Eq. 4.1)}$$

  With help of RStudio the first step was find the value of λ that achieve the greatest normalization of the regression model. Then, the transformation was applied to all the variables, and assumptions could be made with the values resulting from this new regression, e.g., what variables has to be included or excluded of the model, depending on its significances.
- Stepwise: this is a variable selection system which make the necessary iterations to select the variables that meet conditions related to a required p-value [67]. This system was applied with RStudio, as the model commented above, but the results were not good enough and the function to apply in the model was not feasible.

After proving that these cases do not work, the third try was the one used in the model. This one works with the results in tCO_2eq/MW as in the first attempt, but in this case the calculations are separated in different stages, substructure manufacturing, mooring system manufacturing, wind turbine manufacturing, installation, O&M, dismantling and end-of-life. The useful values for the calculations are mentioned in Table 4.2, Table 4.3 and Table 4.4. The 6 first cases, which are not mentioned in chapter 3 are provided by IREC.

Case	Capacity Power (MW)	Energy production (GWh)	Carbon intensity ($kgCO_2eq/MWh$)	Total CO_2eq emissions (tCO_2eq)	tCO_2eq/MW
West of Barra Activefloat	300	54,700	11.110	607,717	2026
Gran Canaria Activefloat	300	56,100	10.09	565,993	1887
Gran Canaria WindCrete	300	56,500	7.38	417,140	1390
Morro Bay Activefloat	300	40,200	11.23	451,446	1505
Morro Bay Windcrete	300	40,000	11.12	444,840	1483
"Undisclosed for privacy"	180	17,500	15.42	269,903	1499
Brussa et al. [24]	2793	264,129	31.40	8,293,651	2969
Poujol et al. [49]	24	1,447	22.28	32,239	1343
Barbara et al. [23]	600	65,700	15.35	1,008,495	1681
Raadal et al. [48]	500	40,296	31.40	1,265,294	2531
Garcia-Teruel et al. [51] Semi-sub case	47.5	4,161	33.89	141,016	2969
Garcia-Teruel et al. [51] Spar case	30	3,285	39.25	128,936	4298
Yildiz et al. [50]	2	120	18.60	2,232	1,116
Pulselli et al. [52] Raft-buoy case	300	23,400	26.1	610,740	2036
Pulselli et al. [52] Spar-Buoy case	300	23,400	32.20	753,480	2,512

Table 4.2. Values of interest of the cases used in the model.

Many of the values that appear in the table above are commented directly in the corresponding studies, while others as total emissions or emissions per MW was necessary to calculate them with the information provided.

Case	Water depth (m)	Distance to shore (km)	Distance to installation port (km)	Distance to maintenance port (km)	Distance to dismantling port (km)	Average Significant wave height (m)
West of Barra Activefloat	104	19	320	205	240	3
Gran Canaria Activefloat	426	11	1300	50	2100	1.3
Gran Canaria WindCrete	426	11	1300	50	2100	1.3
Morro Bay Activefloat	500	58	350	240	370	2.2
Morro Bay Windcrete	500	58	350	240	370	2.2
"Undisclosed for privacy"	101	95	95	95	95	1.8
Brussa et al. [24]	200	60	60	0	60	1.1
Poujol et al. [49]	80	16	16	16	16	0.73
Barbara et al. [23]	450	35	35	35	35	2.5
Raadal et al. [48]	200	200	200	200	200	1.65
Garcia-Teruel et al. [51] Semi-sub case	70	15	32	32	32	1.5
Garcia-Teruel et al. [51] Spar case	112	25	25	25	25	1.8
Yildiz et al. [50]	50	22	54	54	54	1.5
Pulselli et al.[52] Raft-buoy case	110	22	22	22	22	1.8
Pulselli et al. [52] Spar-Buoy case	110	22	22	22	22	1.8

Table 4.3. Independent variables of the cases used in the model.

For the variables, many of them are directly commented on the studies and others is necessary to make assumptions or investigate other studies e.g., take the distance to shore as distance to port, investigate what subsequent studies or projects the calculations are based on or analyse the supplementary data available.

Case	Substructure	Turbine	Electric system	Mooring system	Installation	O&M	Decommissioning	End-of-Life
West of Barra Activefloat	465.68	614.28	28.63	655.85	390.13	280.26	128.19	-537.53
Gran Canaria Activefloat	304.25	613.92	27.68	367.62	280.13	274.14	387.81	-368.21
Gran Canaria WindCrete	269.51	588.35	30.13	92.10	203.40	274.21	179.56	-227.40
Morro Bay Activefloat	377.21	614.26	46.36	89.11	190.00	299.88	156.53	-268.00
Morro Bay Windcrete	292.80	587.60	45.60	72.40	237.89	299.13	271.16	-323.74
“Undisclosed for privacy”	358.85	588.10	85.17	50.07	377.65	152.45	153.59	-266.50
Brussa et al. [24]	725.81	650.16	205.69	271.88	340.45	293.16	312.08	75.65
Poujol et al. [49]	510.69	445.16	155.38	84.27	32.54	72.64	14.27	6.22
Barbara et al. [23]	948.49	755.55	44.35	397.81	120.45	295.65	120.45	-1007.40
Raadal et al. [48]	1265.29	378.78	145.07	177.30	249.84	96.7	217.60	-537.53
Garcia-Teruel et al. [51] Semi-sub case	581.38	457.68	141.02	198.02	235.13	1208.29	148.44	-368.21
Garcia-Teruel et al. [51] Spar case	770.18	770.18	107.45	322.34	322.34	1762.13	214.89	-
Yildiz et al. [50]	-	-	-	-	33.48	11.16	-	-
Pulselli et al. [52] Raft-buoy case		1467.67	23	59.33	152.67	197.33		123.67
Pulselli et al. [52] Spar-Buoy case		1566.33	23	134.67	446.67	197.33		135.00

Table 4.4. tCO_2eq/MW emissions per stage.

These are all cases and values used for the categorized model regression. For the two first methodologies proposed, there are more values than used in this case, all of them mentioned in chapter 3. There have been requests to the authors of some of the studies that appear in the state-of-art because the emissions' breakdowns are not shown to provide extra data. However, it was not possible.

In order to select the best functions to suit all the stages, a selection criterion is followed for each function. The first step is to select the variables that should have significance on the results, e.g., for the mooring system the distance to shore will not have a repercussion. Hence, to avoid false relationship between independent and dependent variables as a result of chance, this variable is removed from the mooring system regression. The second step is to apply the stepwise regression commented above in this section, developed with RStudio. This regression removes in this case, coefficients with p-values above 0.2 (this value is an assumption of the study). Although is considered that this value has to be 0.05 or less to be significant, many of the values worked with do not present this good relationship. The resulting functions are further explained in the following subsections.

4.5.1. Substructure

Due to the several types of existing substructures and the non-relationship found with any of the independent variables, an average of all cases is used for the substructure emissions. Its result is 572.512 tCO_2eq/MW.

4.5.2. Wind turbine

This stage covers all wind turbine components and the tower. As in the substructure case, for wind turbine emissions an average of the values found is used. The result is 588.669 tCO_2eq/MW.

4.5.3. Electrical system

The electrical system covers the inter-array, the export cable and the offshore substation. For the inter-array cable, the variables involved are the horizontal movement of wind turbines, water depth and distance between turbines [68], while for the export cable the main variable is the distance to shore that determines the length of the cable. Hence, in this case the site conditions could be water depth and distance to shore as mentioned above and significant wave height related to the horizontal movement of the turbine. However, because this is a variable rarely mentioned in the studies except in the case of the mooring system, significant wave height will not be included in the regression. The resultant function of the stepwise regression is (in $kgCO_2eq/MW$):

$$\boldsymbol{Electrical}(\boldsymbol{x},\boldsymbol{y}) = \mathbf{58975} + \mathbf{437} \cdot \boldsymbol{DistONS}(\boldsymbol{x},\boldsymbol{y}) \quad \textbf{(Eq. 4.2)}$$

Where "*DistONS*" is the distance to the onshore substation in the coordinates x and y related to the distance from shore.

4.5.4. Mooring system

The length and the type selected for this system, will depend mainly on the water depth, and the loads capacity which is related to the significant wave height, which affect the type and the number of mooring lines to keep the wind turbine afloat reliably [69]. In this case, many of the mooring systems of the studies are based on existing projects, therefore, the average significant wave height of this projects is taken into account. Hence, the variables used for the stepwise regression in this case are average significant wave height and water depth. The resultant equation is showed below.

$$\boldsymbol{Mooring\ system}(\boldsymbol{x},\boldsymbol{y}) = -\mathbf{25432} + \mathbf{135704} \cdot \boldsymbol{SWH}(\boldsymbol{x},\boldsymbol{y}) \quad \textbf{(Eq. 4.3)}$$

Where "*SWH*" is the average significant wave height of the site.

4.5.5. Installation

The main variables involved in the installation process are the farm size, the distance to port, water depth and climate conditions [22]. Again, climate conditions can be related to the significant wave height but as mentioned above it is not considered in the regression due to how little it is mentioned in the studies. The resultant function is:

$$\boldsymbol{Installation}(\boldsymbol{x},\boldsymbol{y}) = \mathbf{240850} \quad \textbf{(Eq. 4.4)}$$

Although, the variables taking into account affect the emissions of this stage, the p-values of the coefficients are bigger than the expected 0.2. Hence, the variables are removed from this function, and its result is an independent value from the site conditions.

4.5.6. Operation and maintenance

Different maintenance strategies exist, but all depends mainly on the failure rates of each component, vessel and equipment requirements, distances to port, farm size, water depths and weather conditions [70]. Hence, the variables considered are water depth and distance to port. For this regression the resultant function is:

$$\boldsymbol{O\&M}(\boldsymbol{x},\boldsymbol{y}) = \mathbf{112481} + \mathbf{394} \cdot \boldsymbol{Depth}(\boldsymbol{x},\boldsymbol{y}) \quad \textbf{(Eq. 4.5)}$$

The O&M emissions will depend only on the water depth of the site.

4.5.7. Decommissioning

Decommissioning can be considered as the reversed installation process, therefore, the variables taking into account are the same as in the installation stage. The resultant function is:

$$\boldsymbol{Decommissioning}(x, y) = \mathbf{164194} + \mathbf{59} \cdot \boldsymbol{DistPort}(x, y) \quad \textbf{(Eq. 4.6)}$$

Where "*DistPort*" is the distance from the site to the nearest port.

4.5.8. End of life

The last function required regarding life cycle GHG emissions is related to the end-of-life, this function involve the transportation of the components from harbour to the treatment site and the treatment itself. Therefore, it will depend on the distance between harbour and treatment sites, and the mass of the components, so it will be directly related to the water depth and distance to shore. This stage has less values to work with due to the lack of values provided in the literature. The resultant function is:

$$\boldsymbol{End\ of\ Life}(x, y) = -\mathbf{238690} \quad \textbf{(Eq. 4.7)}$$

As in installation none of the variables have enough significance to be considered in the model. Therefore, this stage is a fix value and does not depend on site-conditions.

4.5.9. Annual energy production

The AEP or rather the annual energy supplied to the onshore substation by each cell is calculated with four steps:

1. Computing the average wind speed at 135 m (the hub height of the wind turbine being evaluated) with the interpolation of average wind speed data at an elevation of 100 m and 150 m.

2. Finding the capacity factor for each cell of the worldwide map, with the interpolation of three capacity factor layers depending on the average wind speed results of point 1. Cells with wind speed below 7.5 m/s are equivalent to capacity factor class 3, between 7.5 and 8.75 m/s are equivalent to the interpolation between class 2 and 3, between 8.75 and 10 m/s are equivalent to the interpolation between class 1 and 2, and above 10 m/s are equivalent to capacity factor class 1. This process is more understandable with the following diagram:

$$\boldsymbol{WS < 7.5\frac{m}{s}} \quad \rightarrow \quad \boldsymbol{Class\ III}$$

$$\boldsymbol{7.5\frac{m}{s} < WS < 8.75\frac{m}{s}} \quad \rightarrow \quad \boldsymbol{Interpolation\ Class\ II\ and\ III}$$

$$\boldsymbol{8.75\frac{m}{s} < WS < 10\frac{m}{s}} \quad \rightarrow \quad \boldsymbol{Interpolation\ Class\ I\ and\ II}$$

$$\boldsymbol{WS > 10\frac{m}{s}} \quad \rightarrow \quad \boldsymbol{Class\ I}$$

Hence the greatest capacity factors are in capacity factor class 1 layer.

3. Calculating the ideal AEP per MW with equation 4.8.

$$\boldsymbol{AEP(x,y) = CF(x,y) \cdot 1\ MW \cdot\ 365.25\ days \cdot 24h} \qquad \textbf{(Eq. 4.8)}$$

Where *"CF"* is the capacity factor in coordinates x and y selected in the previous point.

4. Applying different factors that affect the efficiency of generation and distribution; wake efficiency (93%), array efficiency (99%), export efficiency depending on the distance from shore as shown in equation 4.9, substation efficiency (98%) [71] and availability depending on average significant wave height as shown in equation 4.10.

$$\boldsymbol{ExportEff(x,y) = \frac{99 - DistONS(x,y) \cdot 0.02}{100}} \qquad \textbf{(Eq. 4.9)}$$

$$\boldsymbol{Availability(x,y) = \frac{98 - SWH(x,y)^3}{100}} \qquad \textbf{(Eq. 4.10)}$$

The result of this subsection is multiplied by the years of the FOWF lifetime (25 years) to compute the total energy supplied to the onshore substation.

4.5.10. Carbon intensity function

Once the total CO_2 emissions and energy supplied is calculated, the division provides the final result required in $kgCO_2eq/MWh$. The layers and functions are connected with a MATLAB code and the carbon intensity layer is obtained.

5. Model Validation

In this section, the basic diagnostic plots and interesting values are presented as coefficient of determination R^2 or p-values of the coefficients of each regression, to assess the appropriateness of the model, appreciate the strength of the conclusions being drawn from this model, and to check that the model is appropriate fit for the data and is likely to perform similarly in the case that new values are involved [72].

5.1. Mooring system

```
> summary(RLM.Stepwise)

Call:
lm(formula = MandA ~ SWH, data = Book1)

Residuals:
    Min      1Q  Median      3Q     Max
-200.72 -140.67  -10.82  129.16  274.17

Coefficients:
            Estimate Std. Error t value Pr(>|t|)
(Intercept)   -25.43     139.94  -0.182   0.8588
SWH           135.70      76.00   1.786   0.0994 .
---
Signif. codes:  0 '***' 0.001 '**' 0.01 '*' 0.05 '.' 0.1 ' ' 1

Residual standard error: 161 on 12 degrees of freedom
Multiple R-squared:  0.2099,    Adjusted R-squared:  0.1441
F-statistic: 3.188 on 1 and 12 DF,  p-value: 0.09944
```

Figure 5.1. Summary of mooring system regression.

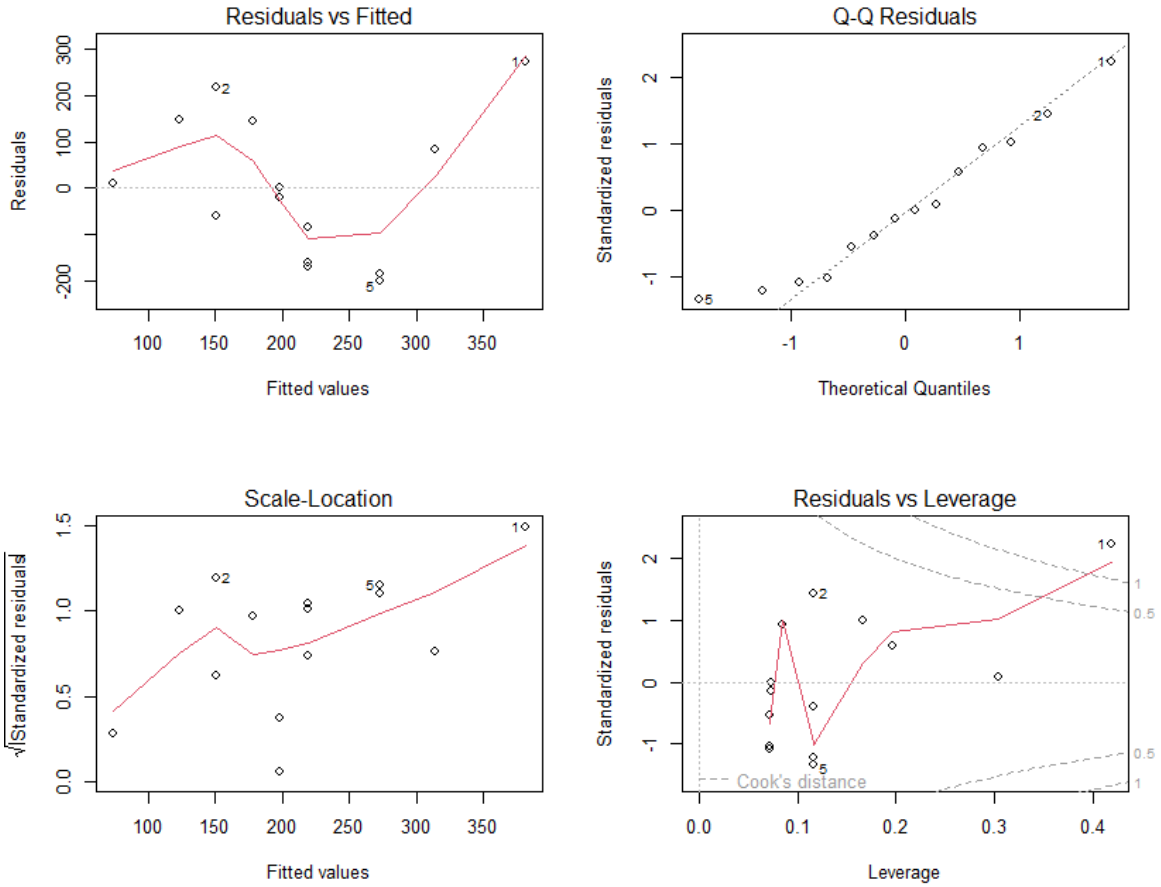

Figure 5.2. Diagnostic plots mooring system regression.

5.2. Electrical System

First electrical system regression presents a negative coefficient as shown Figure 5.3.

```
> summary(RLM.Stepwise)

Call:
lm(formula = ElectricalSystem ~ Depth + Distshore, data = Book1)

Residuals:
    Min      1Q  Median      3Q     Max
-64.577 -29.138  -4.425  14.126 114.429

Coefficients:
            Estimate Std. Error t value Pr(>|t|)
(Intercept) 93.77040   29.47029   3.182  0.00873 **
Depth       -0.14377    0.08808  -1.632  0.13086
Distshore    0.43736    0.30276   1.445  0.17645
---
Signif. codes:  0 '***' 0.001 '**' 0.01 '*' 0.05 '.' 0.1 ' ' 1

Residual standard error: 55.29 on 11 degrees of freedom
Multiple R-squared:  0.3016,    Adjusted R-squared:  0.1746
F-statistic: 2.375 on 2 and 11 DF,  p-value: 0.1389
```

Figure 5.3. Summary first electrical system regression.

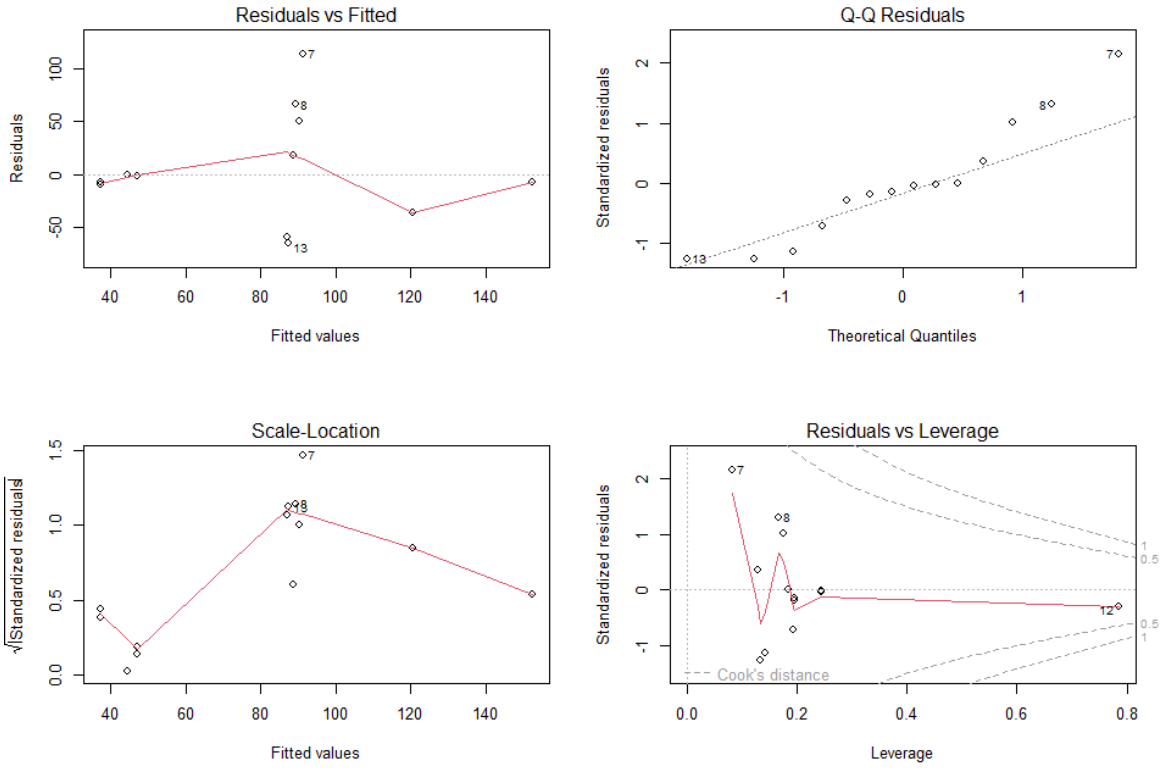

Figure 5.4. Diagnostic plots first electric system regression.

Although the validation is statistically good, a negative coefficient related to depth is not possible in a real case. Hence, in this case this variable is excluded from the regression. The resultant regression is showed below.

```
> summary(RLM.Stepwise)

Call:
lm(formula = Electrical ~ DistShore, data = Book1)

Residuals:
   Min     1Q Median     3Q    Max
-45.59 -38.48 -31.79  27.82 120.48

Coefficients:
            Estimate Std. Error t value Pr(>|t|)
(Intercept)  58.9752    21.7166   2.716   0.0188 *
DistShore     0.4372     0.3231   1.353   0.2010
---
Signif. codes:  0 '***' 0.001 '**' 0.01 '*' 0.05 '.' 0.1 ' ' 1

Residual standard error: 59 on 12 degrees of freedom
Multiple R-squared:  0.1324,    Adjusted R-squared:  0.06008
F-statistic: 1.831 on 1 and 12 DF,  p-value: 0.201
```

Figure 5.5. Summary second electrical system regression.

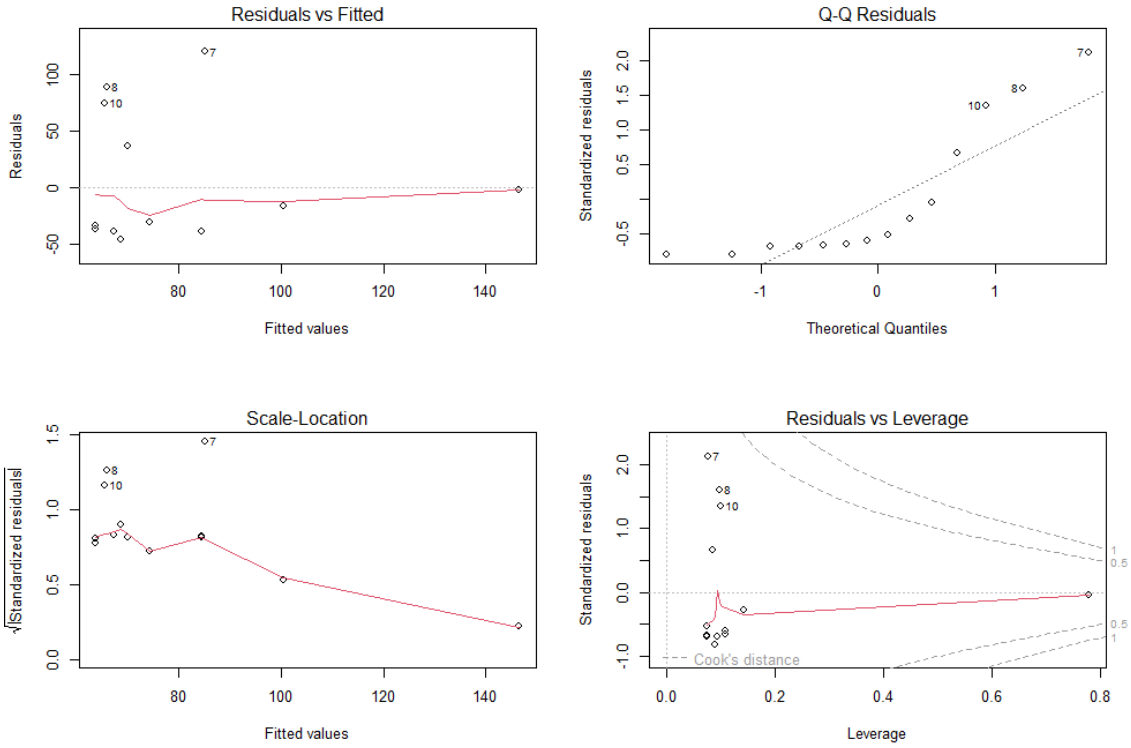

Figure 5.6. Diagnostic plots second electric system regression.

The resultant coefficient related to the distance to onshore substation has a p-value slightly above the assumed 0.2. Due to the small difference and the importance considered of this variable to this function, the coefficient it is included.

5.3. Installation

```
> summary(RLM.Stepwise)

Call:
lm(formula = Installation ~ 1, data = Book1)

Residuals:
     Min       1Q   Median       3Q      Max
-208.311  -69.515   -2.963   90.543  205.817

Coefficients:
            Estimate Std. Error t value Pr(>|t|)
(Intercept)   240.85      31.94   7.541 2.71e-06 ***
---
Signif. codes:  0 '***' 0.001 '**' 0.01 '*' 0.05 '.' 0.1 ' ' 1

Residual standard error: 123.7 on 14 degrees of freedom
```

Figure 5.7. Summary installation regression.

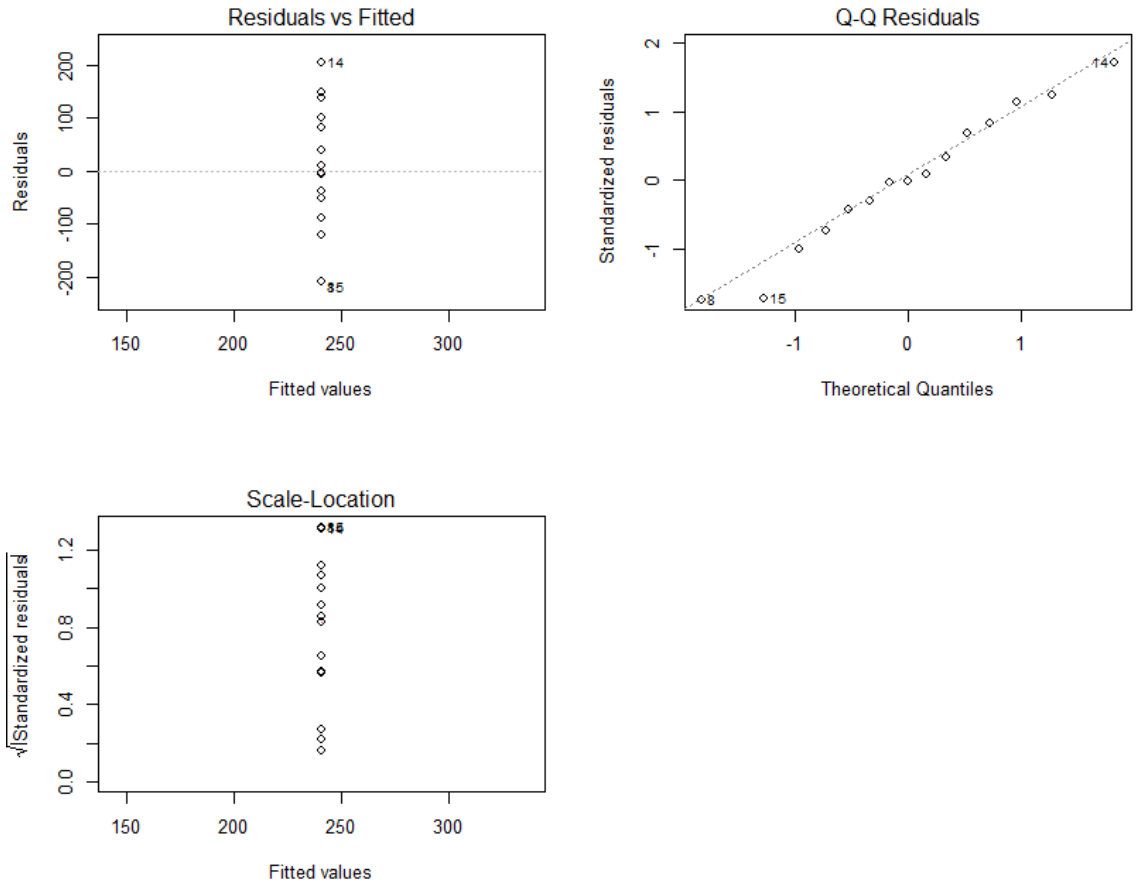

Figure 5.8. Diagnostic plots installation regression.

5.4. Operation and maintenance

The initial idea, as in all cases, is to consider the 15 values available, but in this case the procedure has a little change. The first regression shown in Figure 5.9 proved as in other cases, that the result is an independent value. However, analyzing the behavior of the regression is easy to see extreme points. In all plots, these outliers points (14 and 15) are located too far away from the rest, e.g., in quantile-quantile plot, these residuals are clearly not following the normal distribution marked by the straight line. Furthermore, the standard error is even greater than the intercept itself. Hence, although taken into account that the small size of the sample can cause these events, these values are considered outliers and removed from the regression to achieve better linearization.

```
> summary(RLM.Stepwise)

Call:
lm(formula = Maintenance ~ 1, data = Book1)

Residuals:
    Min      1Q  Median      3Q     Max
-369.80 -206.07 -106.75  -83.58 1381.16

Coefficients:
            Estimate Std. Error t value Pr(>|t|)
(Intercept)    381.0      121.2   3.143  0.00719 **
---
Signif. codes:  0 ‘***’ 0.001 ‘**’ 0.01 ‘*’ 0.05 ‘.’ 0.1 ‘ ’ 1

Residual standard error: 469.5 on 14 degrees of freedom
```

Figure 5.9. Summary first O&M regression.

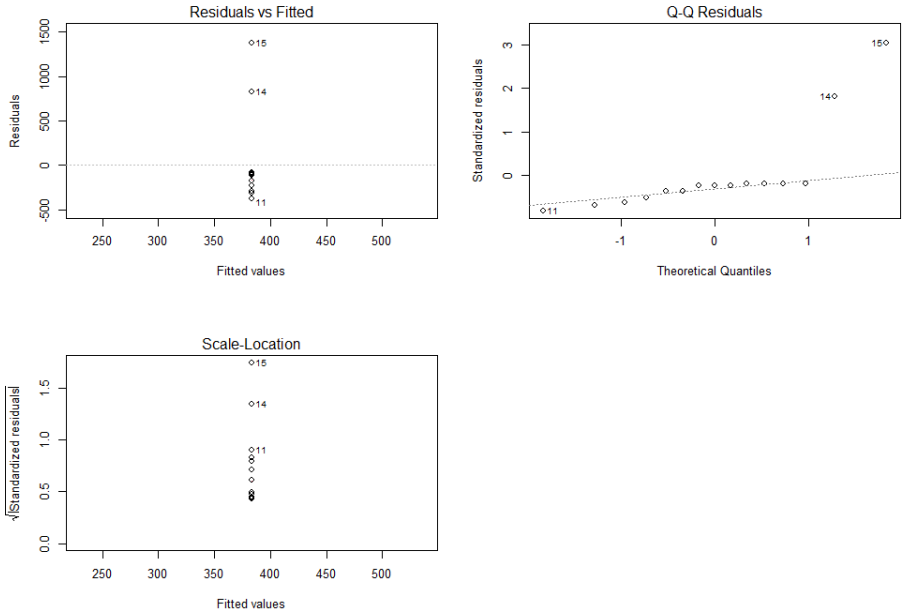

Figure 5.10. Diagnostic plots first O&M regression.

In the following case, without Garcia-Teruel et al. [51] cases, which are the outliers, the regression achieves a significant coefficient related to water depth and the plots have a better behaviour.

```
> summary(RLM.Stepwise)

Call:
lm(formula = Maintenance ~ Depth, data = Book1)

Residuals:
     Min       1Q   Median       3Q      Max
-125.912   -9.657   -6.334   53.700  122.584

Coefficients:
            Estimate Std. Error t value Pr(>|t|)
(Intercept) 117.9926    36.8257   3.204  0.00839 **
Depth         0.3816     0.1212   3.148  0.00928 **
---
Signif. codes:  0 '***' 0.001 '**' 0.01 '*' 0.05 '.' 0.1 ' ' 1

Residual standard error: 75.08 on 11 degrees of freedom
Multiple R-squared:  0.4739,    Adjusted R-squared:  0.426
F-statistic: 9.907 on 1 and 11 DF,  p-value: 0.009282
```

Figure 5.11. Summary second O&M regression.

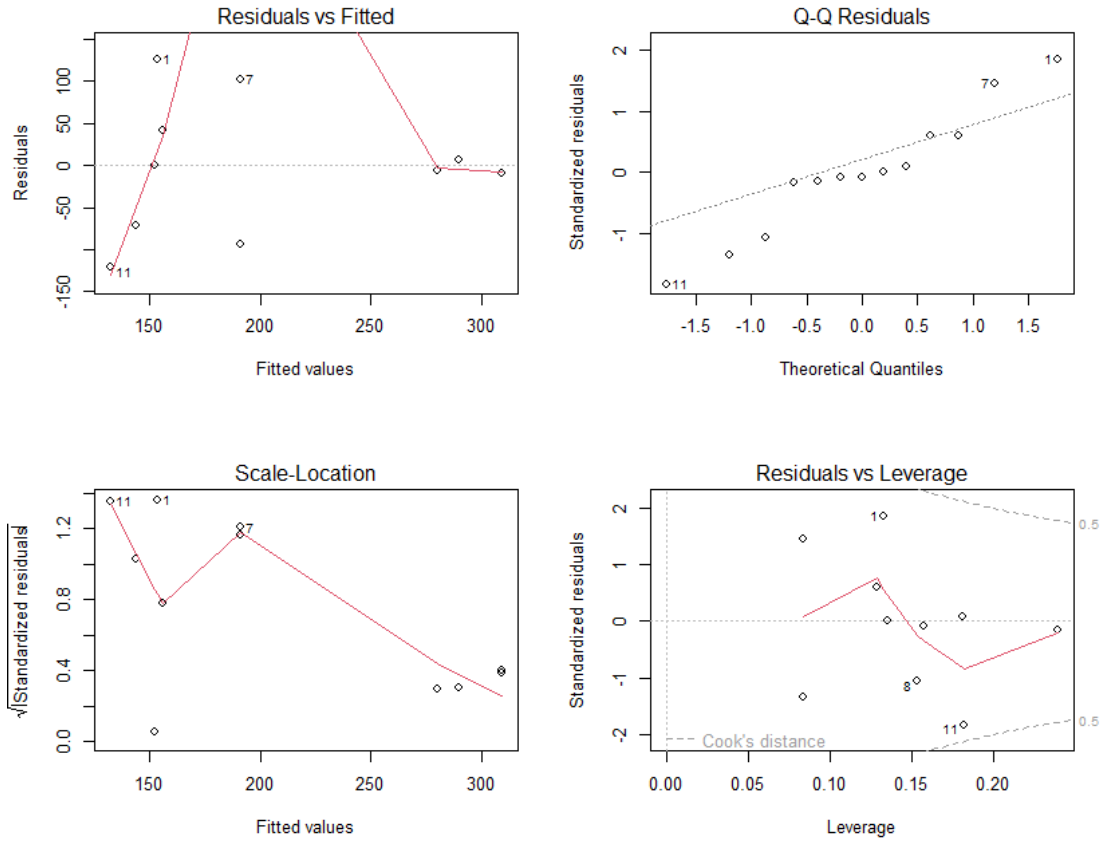

Figure 5.12. Diagnostic plots second O&M regression.

5.5. Decommissioning

```
> summary(RLM.Stepwise)

Call:
lm(formula = Decommissioning ~ DistPort, data = Book1)

Residuals:
    Min      1Q  Median      3Q     Max
-150.87  -46.92  -16.94   58.18  144.33

Coefficients:
             Estimate Std. Error t value Pr(>|t|)
(Intercept) 164.19394   31.13125   5.274 0.000361 ***
DistPort      0.05923    0.03554   1.667 0.126567
---
Signif. codes:  0 '***' 0.001 '**' 0.01 '*' 0.05 '.' 0.1 ' ' 1

Residual standard error: 90.98 on 10 degrees of freedom
Multiple R-squared:  0.2174,    Adjusted R-squared:  0.1391
F-statistic: 2.777 on 1 and 10 DF,  p-value: 0.1266
```

Figure 5.13. Summary decommissioning regression.

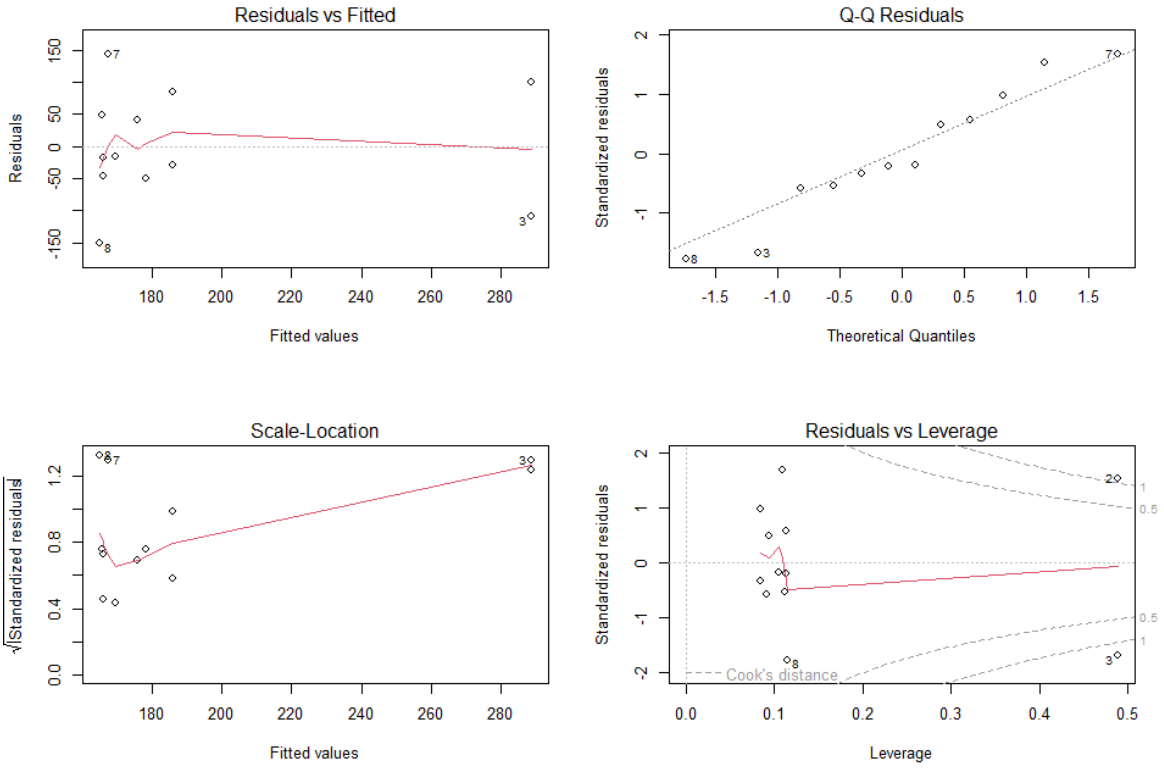

Figure 5.14. Diagnostic plots decommissioning regression.

5.6. End of Life

In this case something like in O&M occurs. If all values available of end of life are used in the regression, it produces the results shown in Figure 5.15 and Figure 5.16.

```
> summary(RLM.Stepwise)

Call:
lm(formula = EoL ~ 1, data = Book1)

Residuals:
    Min      1Q  Median      3Q     Max
-683.30  -44.11   56.10   96.70  399.76

Coefficients:
            Estimate Std. Error t value Pr(>|t|)
(Intercept)   -324.1      105.4  -3.076   0.0152 *
---
Signif. codes:  0 '***' 0.001 '**' 0.01 '*' 0.05 '.' 0.1 ' ' 1

Residual standard error: 316.1 on 8 degrees of freedom
```

Figure 5.15. Summary first end of life regression.

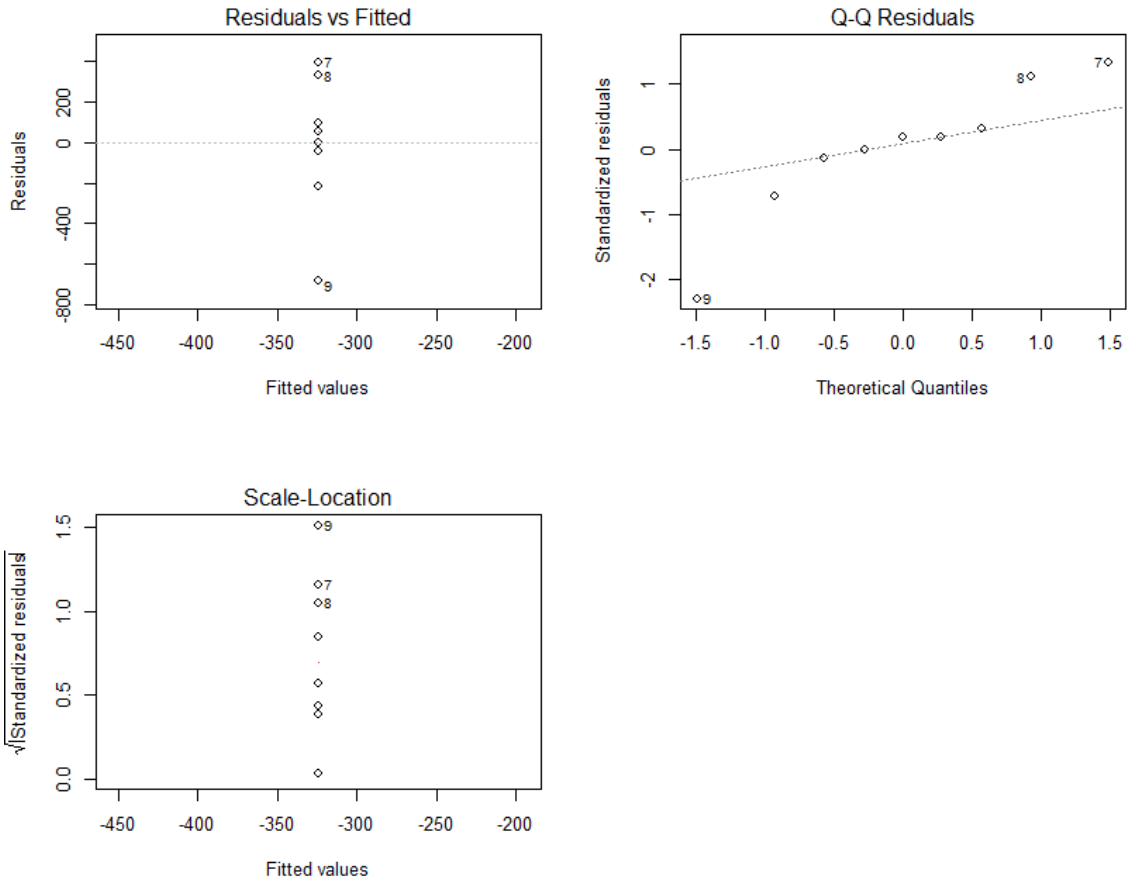

Figure 5.16. Diagnostic plots first end of life regression.

On the three plots shown above, the point number 9 stands out for its difference between the trend of the other points. Besides, the standard error is almost the same magnitude of the intercept itself. Hence, this point is removed from the regression. The results of the new regression are shown in Figure 5.17 and Figure 5.18.

```
> summary(RLM.Stepwise)

Call:
lm(formula = EoL ~ 1, data = Book1)

Residuals:
    Min      1Q  Median      3Q     Max
-298.84  -96.17  -28.56   69.69  314.34

Coefficients:
            Estimate Std. Error t value Pr(>|t|)
(Intercept)  -238.69      69.93  -3.413   0.0112 *
---
Signif. codes:  0 ‘***’ 0.001 ‘**’ 0.01 ‘*’ 0.05 ‘.’ 0.1 ‘ ’ 1

Residual standard error: 197.8 on 7 degrees of freedom
```

Figure 5.17. Summary second end of life regression.

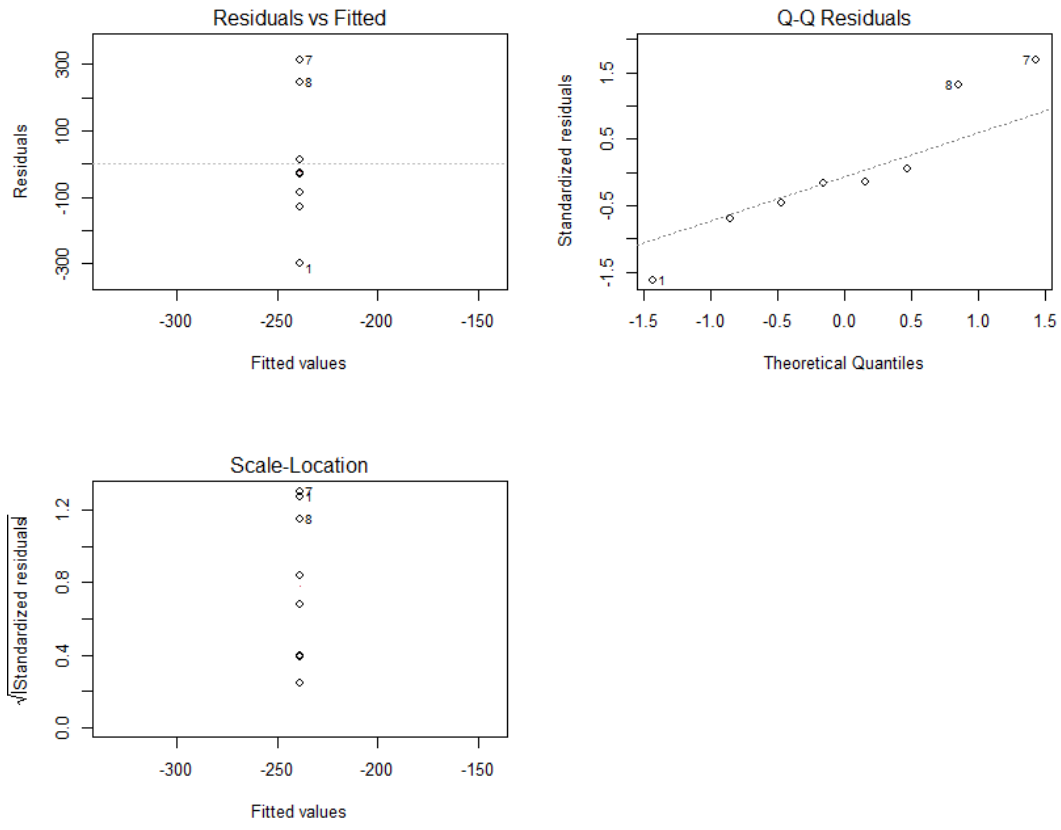

Figure 5.18. Diagnostic plots second end of life regression.

5.7. Conclusions of the chapter

In this chapter valuable informations related to the regressions carried out for the FOW LCA model to determine its consistency are presented.

Regarding the coefficients and intercepts p-values, as commented in section 4.5, all of them larger than 0.2 are removed from the regressions. Hence, although a variable is considered significant when this value is lower than 0.05, and in an ideal case the functions would consider all site conditions that should have an effect on the result, the coefficients obtained in this study are considerably good.

The coefficients of determination R^2, 0.4739 for O&M function, can be interpreted as large effect size, which means this function have practical significance [73]. While mooring system, decommissioning and electrical system, with 0.2099, 0.2174 and 0.1324 respectively, are considered medium effect size.

The diagnostic graphics determines the linearity, homoscedasticity, normality and independence of the regressions and analyse if the models are appropriate to use for the particular data worked with [74]. Is considered that none of the resultant plots violate none of the 4 assumptions, except in two cases. Point 1 on the residuals vs leverage plot of mooring system shown in Figure 5.2 is outside the cook's distance (marked by the dashed line), thus, this point is overly influential. However, due to the other resultant plots and the considered realistic influence of this point, this case is not removed from the regression. In the same plot type in Figure 5.14, related to decommissioning regression, something similar occurs with point 2 and 3. However, this happens due to the large magnitude of the value of the variable distance to port related to this two points (as seen in Table 4.3 the distance to dismantling port of cases 2 and 3 is 2100 km, much greater than the other cases), hence, it is not excluded from the regression.

Standard errors are significant, therefore, they will be taken into account when analysing the results computing the confidence intervals (CIs).

The evaluation of the regressions is not bad, but the premature situation of the technology makes difficult to find useful values to integrate in this model. Therefore, the main weaknesses of the model are the few values that it is working with and the uncertainty of the adjustment to reality that these values have. This transforms to a low consistency of the model, and the great dependency on the quality of the data recollected, i.e., if the values were better, the results obtained would also be better. Furthermore, the entry of new cases could significantly modify the regressions or at least the coefficients of each stage, therefore, also the final results.

6. Results

The results of the model are presented, analysed and compared to the existing literature in this chapter. First sections present the results and provide a first analysis without getting into detail. As the sections appear, the level of detail becomes deeper.

6.1. Map

The layer of the results of the model are plotted on a world map to have a first impression about the locations with the lower values of FOW carbon intensity which, as seen in Figure 6.1, correspond to the blue areas. These areas are cells with the higher wind potential and closest to the shore and do not exceed the 15 $kgCO_2eq/MWh$, located mainly in Peru, Argentina, Egypt, Vietnam, Taiwan, New Zealand, Mauritania and some parts of the north Europe and north South America. These results are also plotted in a web map shown in Annex A .

The graphic results showed in this map only allows a superficial analysis of the results, hence, in the subsequent sections it is deepened.

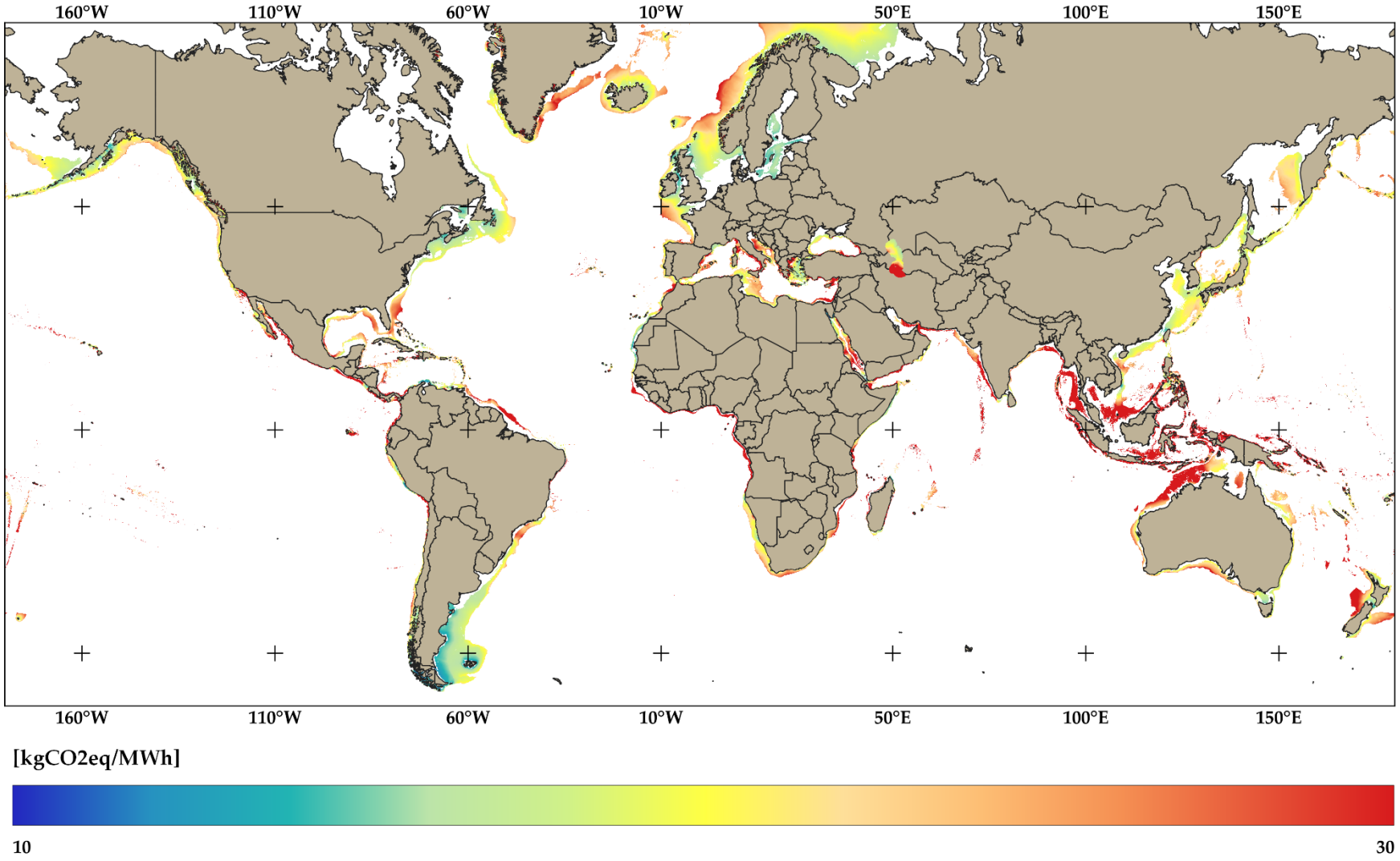

Figure 6.1. Carbon intensity map.

6.2. First analysis of the results

The results present a minimum registered of 10.35 $kgCO_2eq/MWh$, an average of 30.80 $kgCO_2eq/MWh$ and a maximum value of 2,730.80 $kgCO_2eq/MWh$. Hence, the study found a large number of results that can be interesting for the analysis, however, others that can be discarded. The histogram helps to see the general behaviour of the obtained results. In Figure 6.2 the amount of area with results between 10 and 50 $kgCO_2eq/MWh$ is presented in intervals of 2 $kgCO_2eq/MWh$. Although it cannot be appreciated, the lower values are between 10 and 12 $kgCO_2eq/MWh$ and add up an area of 3,499 km^2. The area quantity does not stop increasing until the interval from 18 to 20 $kgCO_2eq/MWh$, which is the greatest amount of area registered with 2,519,050 km^2. Since 20 $kgCO_2eq/MWh$, the tendency of the area amount per interval is to decrease. Therefore, the maximum value of the study and even values above the limit of the histogram can be considered as extreme values.

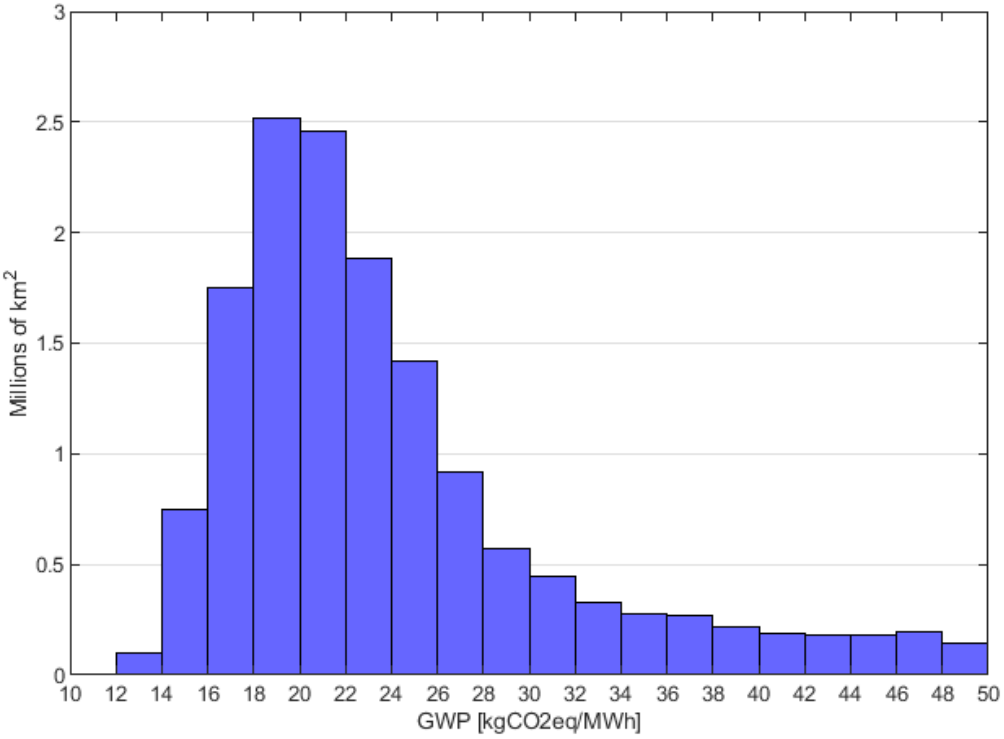

Figure 6.2. Carbon Intensity histogram.

The results obtained are similar to the observed in the literature. Although the minimums, 10.35 $kgCO_2eq/MWh$ for this study and 6.56 $kgCO_2eq/MWh$ for the literature, are considerably different, the average is similar. Furthermore, the maximum of 78.70 $kgCO_2eq/MWh$ registered in the state-of-art is by far, greater than average of the study.

6.3. Sensitivity analysis

Sensitivity analysis determines how different values of an independent variable (input) affect a particular dependent variable (output) under a given set of assumptions [75].

6.3.1. Variables

In this case, the dependent variable is the carbon intensity in $kgCO_2eq/MWh$. The independent values are all needed for the calculations related to the GHG emissions and energy production. The quantification of uncertainty in the input is given by a specific range of variation, in this case 25 % above and below. Although many sensitivity analysis exist, the one-factor-at-a-time (OFAT) is selected for the analysis. The OFAT technique consists of changing one input while keeping everything else constant to see the effect on the final results and repeat the process to all input parameters [76]. In Figure 6.3, the influence of the site conditions are showed.

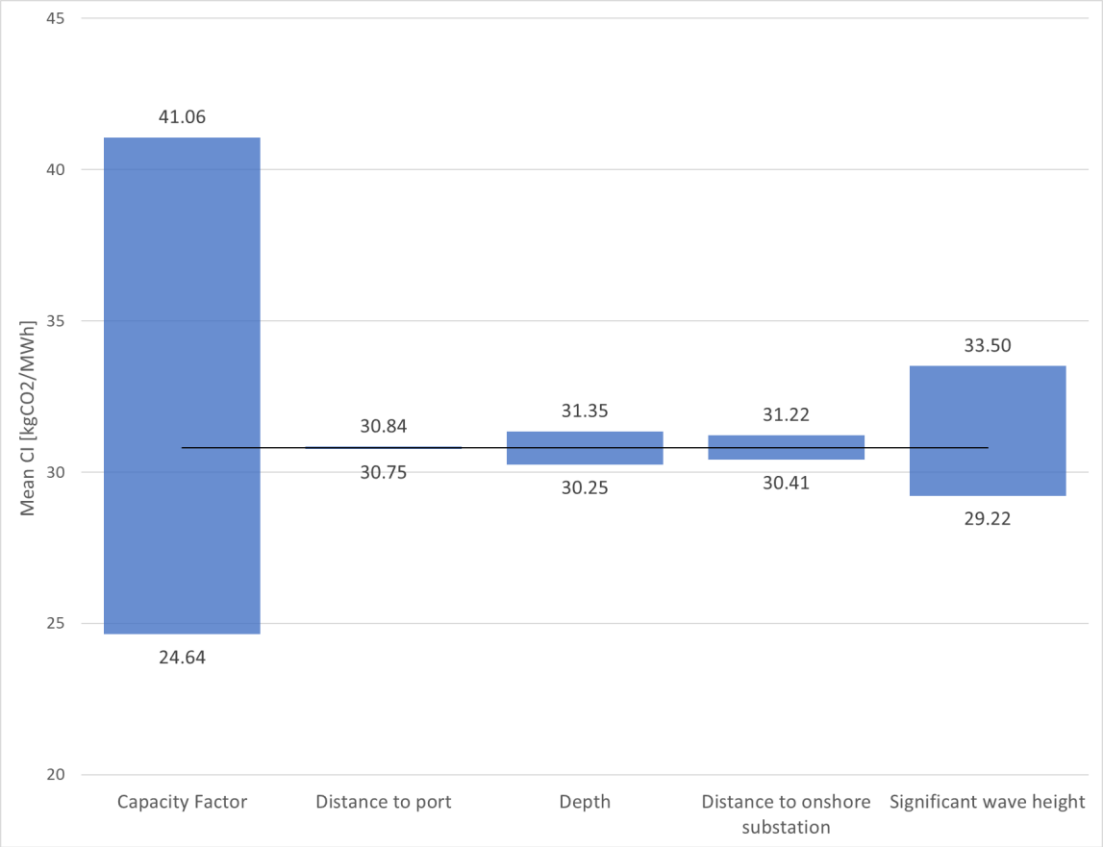

Figure 6.3. Carbon intensity variation by change of independent variables.

An increase or decrease of the variable that has a direct impact on the energy production has by far the biggest effect on the results, this is the case of capacity factor. If capacity factor increase by 25 %, the carbon intensity decreases -20.00%, meanwhile decreasing 25 % affects +33.33 %. The second

variable with most importance is average significant wave height, which affects in one of the GWP functions and in the energy production efficiency as showed above in equation 4.10. Increasing and decreasing the average significant wave height have an effect of 8.79 % and - 5.11 % respectively. The higher effect on increasing the variable is due to the cubed relation in equation 4.10. The less significant are the distances and depth, these variables only effect on the GWP functions, while in the case of distance to onshore substation, it also affects distribution efficiency (the larger the export cable distance, the bigger power losses). When increasing these variables by 25 %, the variability in the mean carbon intensity is 0.14 % for distance to port, 1.36 % for distance to onshore substation and 1.78 % for water depth. For decreasing is - 0.14 %, - 1.27 % and - 1.78 % respectively.

Therefore, the results show that the variables with the highest effect on the carbon intensity are the ones directly related to the energy production that appear in equation 4.8 and the results effects of distance to port are almost negligible.

6.3.2. Stages

To identify the highest potential GWP reductions of FOW and analyse the burden of each stage described in section 2.1 and developed in section 4.5, a sensitivity analysis is also applied for these values.

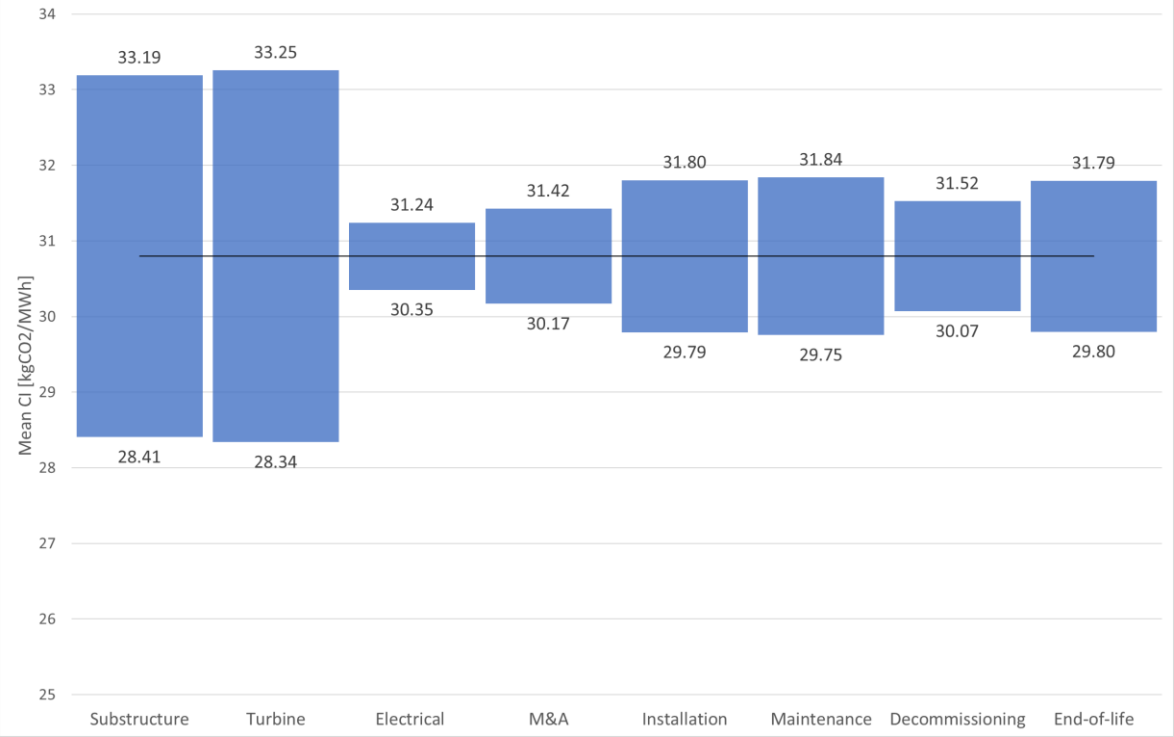

Figure 6.4. Carbon intensity variation by change of stages

The biggest impact comes from the substructure and turbine manufacturing, with ± 7.76 % and ± 7.98 %, followed by installation, maintenance and end-of-life, which have a similar impact when increasing or decreasing of ± 3.25 %, ± 3.38 % and ± 3.25 % respectively. Finally, the stages with less impact are decommissioning, mooring system and electrical system respectively, with variations between ± 1.44 % and ± 2.36 %.

The burden of each stage is similar as the found in literature, the importance of the supply phase of the turbine and substructure are the greatest ones.

6.4. Single cell analysis

The aim of this section is to analyse one cell to describe the procedure to obtain each value and evaluate the quality of the final result mentioning the possible failures during the calculations, the CIs and the relation between the input (depth, distances, etc.) and output (carbon intensity) parameters.

6.4.1. Cell selection

Before the execution of the subsequent analyses, there are other considerations that make impossible the installation of a FOWF apart from the restrictions taken into account in the carbon intensity map, e.g., protected areas, heritage restriction zones, military areas, minimum distance to shore and licensed areas for exploration and exploitation of hydrocarbons [77]. Hence, in order to achieve realest results a few of these restrictions are considered in these sections. Due to the difficulty in finding these restrictions for the entire world map, only protected zones, heritage restriction areas and minimum distance to shore are considered. The layers of protected and heritage restriction areas are provided by Protected Planet [78] and distance constraint, which depends on the country of installation, for this study is selected at 10 km from shore, i.e., all cells inside protected, heritage restriction area or closer than 10 km from shore are removed for the following analyses.

Figure 6.5 shows the results obtained after the applied criteria mentioned above in Spain. The areas with lowest values of FOW carbon intensity, which corresponds to the areas plotted with darkest blue and marked by two rectangles, are located mainly in the south and northwest. In this case, due to the current interest of the FOW sector in the Gulf of Roses, e.g., with “Parc Tramuntana” project [79], this section will analyse the cell with the minimum carbon intensity of this zone.

In Figure 6.6, the map is zoomed to the cell interest zone and the point analysed is marked in red. The resultant carbon intensity in this cell is 16.53 $kgCO_2eq/MWh$. This is located 14.66 km from the nearest point of the coast, which distance is represented with a red line, 23.09 km from the nearest port located on the purple point (Roses’ port), which distance is represented with a black line, has a water depth of 132 m and an average significant wave height of 0.91 m.

Distance to shore is taken into account as the distance to the onshore substation connection, i.e., it has an effect on the electrical system and power losses. Distance to port is considered for decommissioning operations, which is the only function where this independent variable has the necessary significance regarding the procedure commented in section 4.5 to be implemented. Water

depth has an effect on maintenance and significant wave height on the mooring system and availability. Regarding the energy production, the capacity factor obtained in this cell is 0.5294.

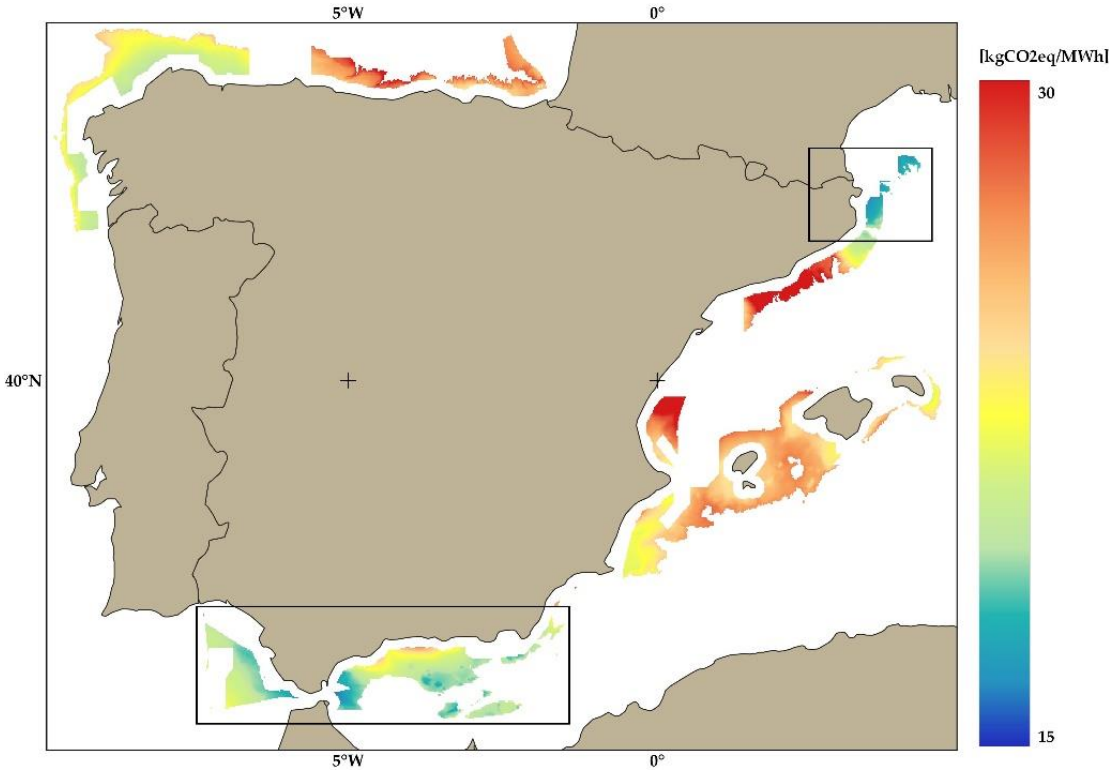

Figure 6.5. Feasible areas in Spain's EEZ with restrictions.

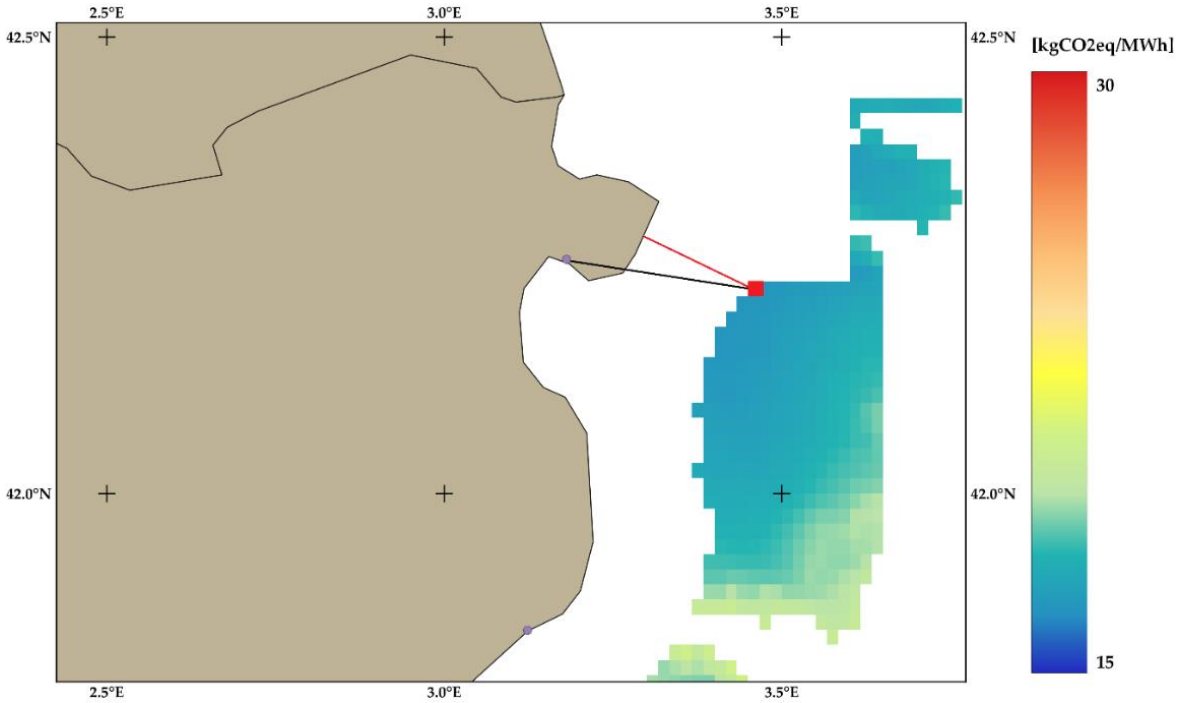

Figure 6.6. Selected cell for the analysis.

6.4.2. Procedure

First step is computing the carbon footprint of each stage with its respective CI, which is selected in 95 %:

$$\boldsymbol{Substructure}(x,y) = \mathbf{572512\ kgCO_2eq/MW} \quad \textbf{(Eq. 6.1)}$$

$$\boldsymbol{Turbine}(x,y) = \mathbf{588669\ kgCO_2eq/MW} \quad \textbf{(Eq. 6.2)}$$

CIs are not considered for substructure and turbine.

$$\boldsymbol{Mooring}(x,y) = -25432 + 135704 \cdot 0.91 = \mathbf{98059\ kgCO_2eq/MW} \quad \textbf{(Eq. 6.3)}$$

Standard errors, which are necessary for the CIs calculations are showed in chapter 5. For mooring system is 161,000. For the CI selected, it will be 1.96 times the standard error [80], hence the calculation applied for all cases is:

$$\boldsymbol{CI_{95\%} = X \pm 1.96\sigma = 98059 \pm 1.96 \cdot 161000 = 98059 \pm 315558} \quad \textbf{(Eq. 6.4)}$$

Where "*X*" in this case is the result of the mooring system in the analysed cell and "*σ*" is the standard error.

$$\boldsymbol{Electrical}(x,y) = 58975 + 437 \cdot 14.66 = \mathbf{65383\ kgCO_2eq/MW} \quad \textbf{(Eq. 6.5)}$$

$$\boldsymbol{CI_{95\%} = 65383 \pm 115640} \quad \textbf{(Eq. 6.6)}$$

$$\boldsymbol{Installation}(x,y) = \mathbf{240850\ kgCO_2eq/MW} \quad \textbf{(Eq. 6.7)}$$

$$\boldsymbol{CI_{95\%} = 240850 \pm 242452} \quad \textbf{(Eq. 6.8)}$$

$$\boldsymbol{O\&M}(x,y) = 112481 + 394 \cdot 132 = \mathbf{168417\ kgCO_2eq/MW} \quad \textbf{(Eq. 6.9)}$$

$$\boldsymbol{CI_{95\%} = 168417 \pm 147157} \quad \textbf{(Eq. 6.10)}$$

$$\boldsymbol{Decommissioning}(x,y) = 164194 + 59 \cdot 23.09 = \mathbf{165557\ kgCO_2eq/MW} \quad \textbf{(Eq. 6.11)}$$

$$\boldsymbol{CI_{95\%} = 165557 \pm 178321} \quad \textbf{(Eq. 6.12)}$$

$$\boldsymbol{End\ of\ Life(x,y) = -238690\ \mathrm{kgCO_2eq/MW}} \quad \textbf{(Eq. 6.13)}$$

$$\boldsymbol{CI_{95\%} = -238690 \pm 387688} \quad \textbf{(Eq. 6.14)}$$

The total carbon footprint per MW is the sum of all the results computed above, therefore, the total CI also will be its sum.

$$\boldsymbol{CF(x,y) = 1660755 \pm 1386816\ \mathrm{kgCO_2eq/MW}} \quad \textbf{(Eq. 6.15)}$$

For AEP, CI is not considered, hence its value is:

$$\boldsymbol{AEP(x,y) = 0.5294 \cdot 1\ \mathrm{MW} \cdot 365.25\ \mathrm{days} \cdot 24\mathrm{h} = 4640.63\ \mathrm{MWh}} \quad \textbf{(Eq. 6.16)}$$

Appling the losses, the annual delivered energy is:

$$\boldsymbol{ADE(x,y) = AEP \cdot WEff \cdot AEff \cdot EEff \cdot SSEff \cdot Av = 4019.22\ \mathrm{MWh}} \quad \textbf{(Eq. 6.17)}$$

Where *"WEff"* is the wake efficiency, *"AEff"* is the array efficiency, *"EEff"* is the export efficiency, *"SSEff"* is the substation efficiency and *"Av"* is the availability. The value of each parameter is explained in subsection 4.5.9.

If the total carbon footprint is divided by the total delivered energy the carbon intensity is obtained:

$$\boldsymbol{CIn(x,y) = \frac{CF}{ADE \cdot lifetime} = \frac{1660755}{4019.22 \cdot 25} = 16.53\ \mathrm{kgCO_2eq/MWh}} \quad \textbf{(Eq. 6.18)}$$

With the values of the CI:

$$\boldsymbol{CIn-(x,y) = \frac{1660755 - 1386816}{4019.22 \cdot 25} = 2.73\ \mathrm{kgCO_2eq/MWh}} \quad \textbf{(Eq. 6.29)}$$

$$\boldsymbol{CIn^{+}(x,y) = \frac{1660755 + 1386816}{4019.22 \cdot 25} = 30.33\ \mathrm{kgCO_2eq/MWh}} \quad \textbf{(Eq. 6.20)}$$

The result is 16.53 ± 13.80 $kgCO_2eq/MWh$, which is a CI considerably big.

6.5. Carbon intensity per country

The aim of this section is to find a value of FOW carbon intensity associated with all countries with feasible cells in their EEZ and identify the countries with the greatest potential regarding this environmental impact.

6.5.1. Criteria

First step is to select the criteria to find a meaningful value for each country to be compared between others. The assumption is to find the average carbon intensity of the necessary cells with the minimum carbon intensity to produce the 20 % of the electricity production of each country in 2022. Hence, it is necessary to find the total 2022 electricity production per country. This data is provided by Our World in Data [81].

Another necessary assumption is to compute the delivered energy from the FOWF to the onshore substation for each cell to be evaluated. Given the difference in area depending on the position of the cell, each of them will have a different power installed depending on the installation space. Hence, the followed methodology is the commented below:

1. Distance between turbines of 7D as commented in section 4.1 and a margin of 3.5D for the space occupied by mooring system are considered. Hence, for a FOWF distribution of 5 x 4 turbines as shown in Figure 6.7, the area of the farm will be:

$$\boldsymbol{FOWFArea} = (\mathbf{7} \cdot \boldsymbol{D} \cdot \mathbf{5}) \cdot (\mathbf{7} \cdot \boldsymbol{D} \cdot \mathbf{4}) \qquad \textbf{(Eq. 6.1)}$$

where "*D*" is the 240 m of the rotor diameter.

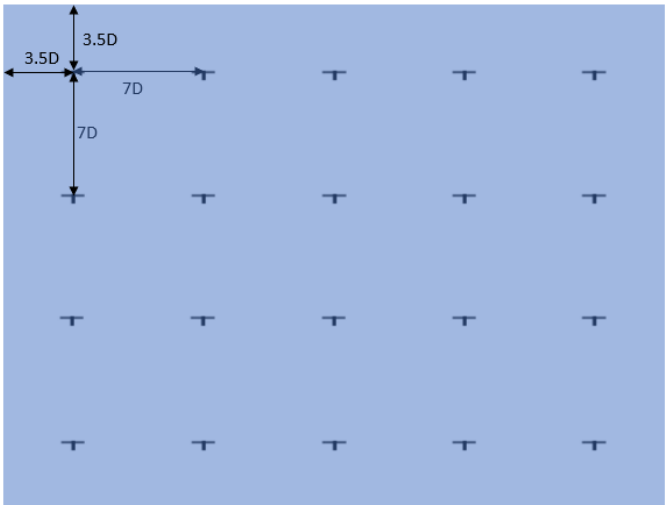

Figure 6.7. Area considered for the floating offshore wind farm**.**

Therefore, the relation will be the 300 MW of the FOWF of the study divided by the resulting area (56.4 km^2), which results in a power density of 5.32 MW/km^2. This FOW power density does not differ much from the offshore wind value obtained by Enevoldsen et al. 2021 [82] of 7.2 MW/km^2.

2. With the relation calculated above, the next step is to compute the area of the cell. One cell in equator has an area of 3.43 km^2, which comes from ~1.852 km squared. The equation used for each cell is:

$$\boldsymbol{CellArea = 3.43 \cdot cos(lat)} \qquad \textbf{(Eq. 6.1)}$$

where "lat" is the latitude of the cell position.
The resultant MWs per cell is computed from multiplying the relation obtained in point 1 by the cell area.

3. Appling the equation described in subsection 4.5.9, for the variables related to the cell and multiplying by the resultant MWs commented in the point 2, the delivered energy is obtained.
4. Finally, using a MATLAB code, with the correct assumptions and conditions the values per country are obtained.

6.5.2. Representation of the carbon intensity per countries

The first analysis of the values obtained in this section can be seen in Figure 6.8, the countries with lowest carbon intensity values are represented in dark green. The lowest value is 12.16 $kgCO_2eq/MWh$ reached in Venezuela, and the maximum value is 101.77 $kgCO_2eq/MWh$, but almost all values are in range of 10 to 50 $kgCO_2eq/MWh$. Hence, the results are plotted in two stages, between 10 to 50 the values are organized in intervals of 5 and all values from 50 to 100 are included on a single interval. Furthermore, the countries or territories without coast, with coast but without cells to work with, or without the electricity production data, appear on the map with black stripes, i.e., Belarus as the first case commented, Netherlands as the second case or Western Sahara as the third case.

As seen in Figure 6.8, the countries with the darkest green, which composes a large group of countries, can be the most relevant information provided by this map. These countries have a resultant associated carbon intensity for FOW between 10 and 15 $kgCO_2eq/MWh$. At first glance, it can be seen that this group is made up of countries in northern Europe, South American countries, Egypt, Mauritania, Madagascar, Canada, Alaska (which is considered an individual territory), Vietnam, Taiwan, New Zealand, etc. These results are also plotted in the web map as shown in Annex A .

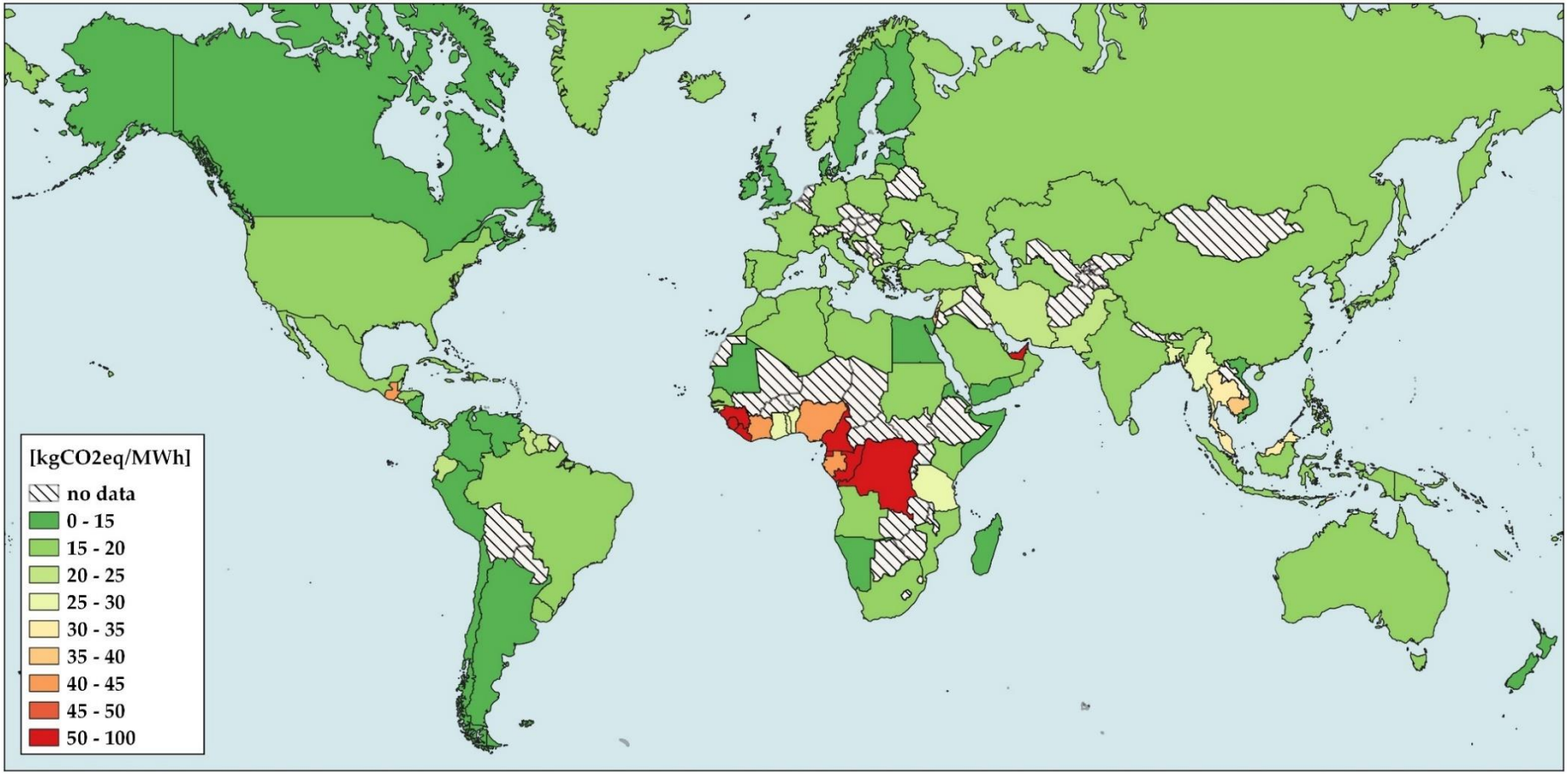

Figure 6.8. Map of results of carbon intensity per country.

6.5.3. Countries ranking

To get more into detail, the aim of this subsection is to provide a ranking of the 20 optimal countries regarding carbon intensity of FOW. The lower the carbon intensity obtained in the previous point the higher will be the position in the ranking. However, there are territories or countries that have been taken into account for the representation of the map that do not have enough cells to provide the 20 % of the electricity generation and others that with a single cell or a little number of cells, already reach more than the 20 % required. This second affirmation imply that these sites have a considerably little electricity consumption and probably a little population. Hence, to exclude territories with small values of electricity productions and add to the ranking others that may be more interesting, the territories with necessary FOW power less than 300 MW, which corresponds to the FOWF power of the study, are not taking into account in the analysis. Therefore, these sites will be removed from the selection ranking procedure. Appling what is commented above and ordering the countries from lowest to highest carbon intensity value the ranking is:

Position	Countries	FOW Carbon Intensity ($kgCO_2eq/MWh$)	Carbon intensity of 2022 electricity production ($kgCO_2eq/MWh$)	FOW Power (MW)
1	Venezuela	12.24	212.48	5472
2	Argentina	12.32	357.79	8540
3	Colombia	12.50	181.07	4638
4	Peru	12.54	230.65	3267
5	Alaska	13.16	591.49	437
6	Vietnam	13.79	448.22	16069
7	New Zealand	14.03	132.43	2809
8	Ireland	14.44	363.61	2382
9	Estonia	14.44	481.22	487
10	United Kingdom	14.48	268.33	20142
11	Sweden	14.48	45.82	11879
12	Finland	14.51	145.54	5084
13	Denmark	14.51	221.42	2336
14	Canada	14.54	128.46	43459
15	Nicaragua	14.54	354.21	345
16	Taiwan	14.60	573.28	19449
17	Egypt	14.80	464.43	13538

18	Costa Rica	14.92	33.04	921
19	Latvia	14.92	223.93	411
20	Chile	14.97	416.88	5793

Table 6.1. Ranking of 20 countries regarding the carbon intensity of FOW.

This table shows the FOW carbon intensity reached, the carbon intensity of the electricity production in 2022 and the necessary FOW power for the production of the 20 % of total electricity produced per country. In all cases, the carbon intensity from the electricity produced in 2022 is higher than the considered for FOW. The largest difference is registered in Alaska, where the carbon intensity for FOW is 45 times lower than the registered in the country, while the lowest differences are registered in Costa Rica and Sweden due to its low carbon electricity mix, where the value for FOW is almost the half of the values of country electricity produced. However, the difference between the FOW carbon intensity reached of the first and last country of the ranking is 2.73 $kgCO_2eq/MWh$. Hence, the values reached for all these countries are similar. These results shows that FOW represents a good option for the reduction of the carbon emissions of many countries. The values of all countries and territories, are provided in Annex A .

6.5.4. Detailed results of Top 10 countries

The aim of this subsection is to analyse each of the 10 countries with lower carbon emissions for FOW reached in the previous subsection, showing all the cells after the constrictions mentioned above are applied and remarking the cells used for the results.

6.5.4.1. Venezuela

Venezuela is the country with the lowest resultant carbon intensity. This result is mainly due to the high wind potential of the west coast of the country, where the used cells for the analysis are located. The carbon intensity reached for FOW is almost 20 times lower than the registered for the electricity production of the country in 2022. Furthermore, the necessary FOW power in this case is about 5,500 MW. The map below shows the feasible cells of the country highlighting the ones used for this analysis, which are plotted in black.

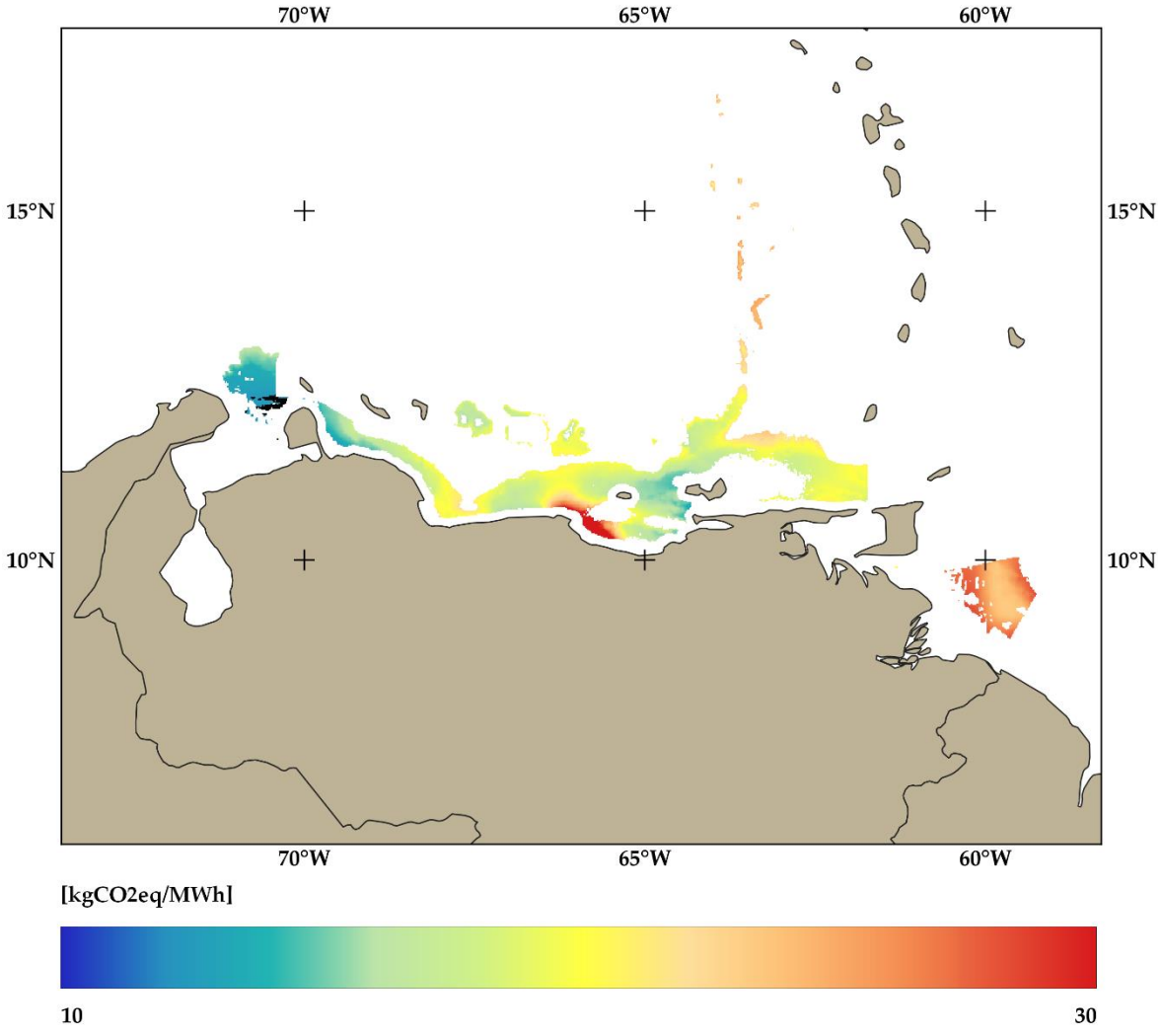

Figure 6.9. Venezuela's results map.

6.5.4.2. Argentina

Argentina reaches the second lowest value of the ranking but its difference with the carbon intensity of the country is larger than in the Venezuela's case. Here the carbon intensity for FOW is about 30 times lower than the registered in 2022. This country has a large area with carbon intensity between 10 to 15 $kgCO_2eq/MWh$, mostly in the northern part of the country, where the cells taking into account for the analysis are located as shown in Figure 6.10.

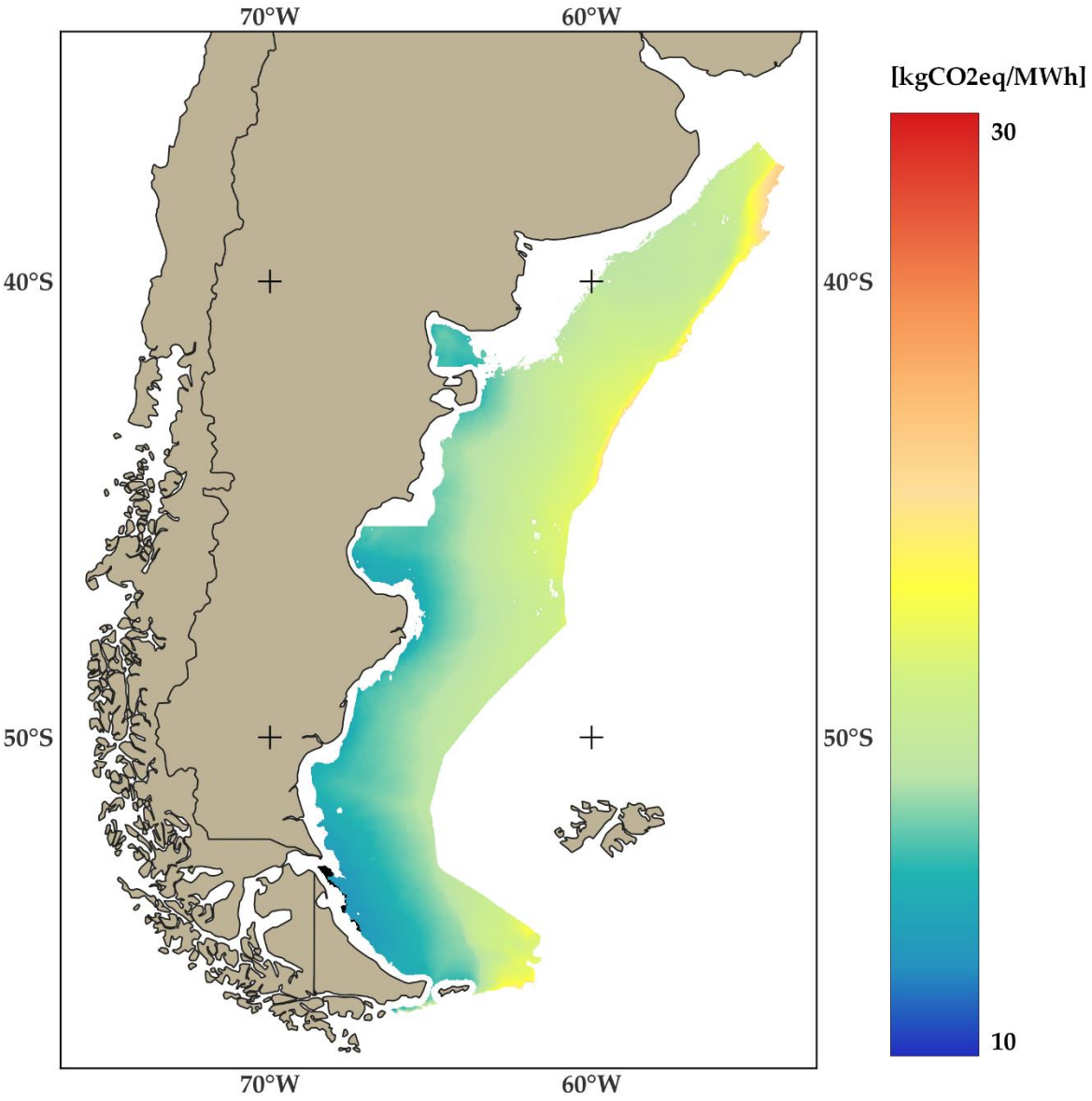

Figure 6.10. Argentina's results map.

6.5.4.3. Colombia

Colombia is a bordering country with Venezuela and has low value cells near the zone with high wind potential mentioned above in Venezuela. In this case located in its northeast coast, where the cells used for the analysis are situated. Figure 6.11 shows that there is only one zone with low values located in the north of the country, while in the rest of the country's coast the values are above 30 $kgCO_2eq/MWh$. It is the country with the lowest carbon intensity of the electricity production of 2022 and the lowest FOW power necessary to satisfy the conditions set of the top 3 with 181.07 $kgCO_2eq/MWh$ and about 4,600 MW.

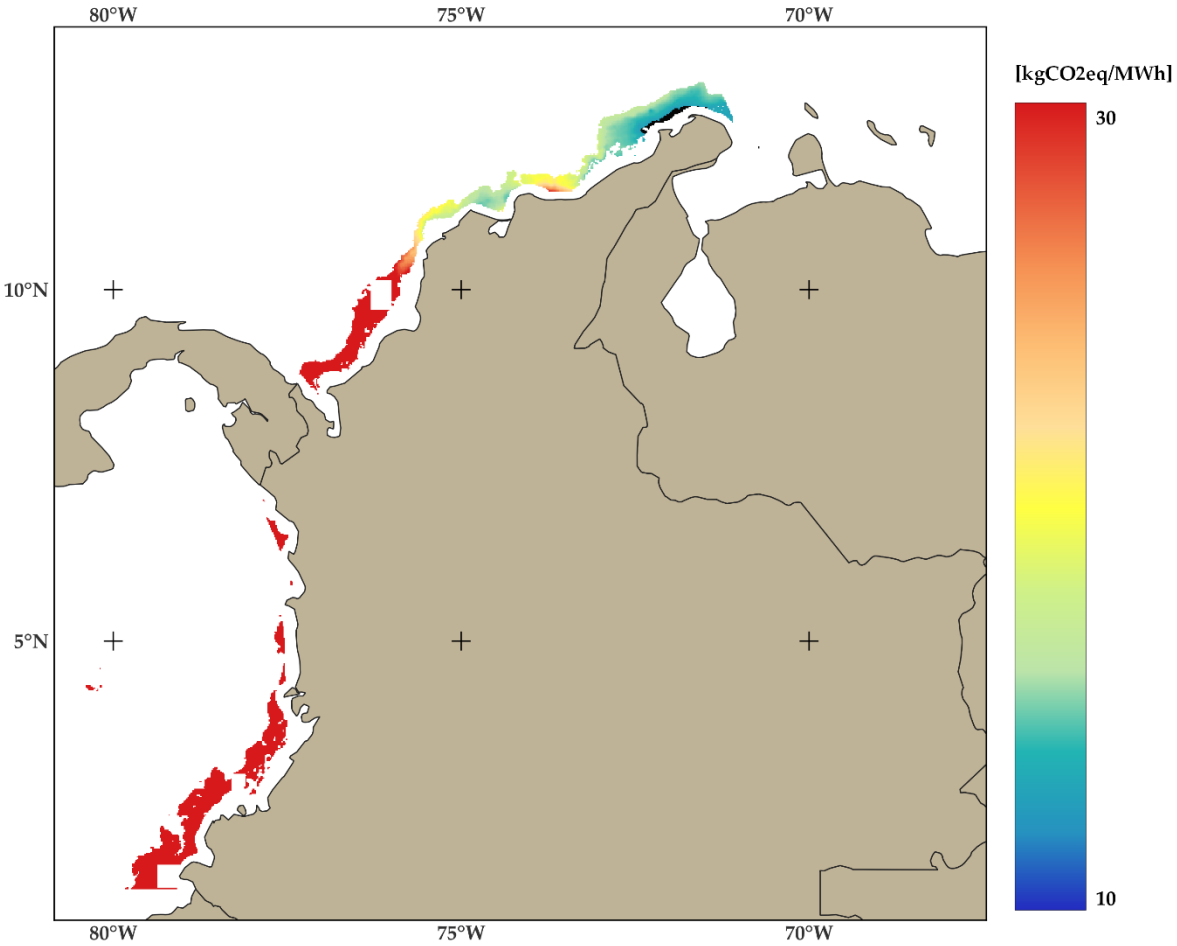

Figure 6.11. Colombia's results map.

6.5.4.4. Peru

Peru has a large coast, and many zones with low values, but the optimal zone considering emission factor, is located near to the *"Bahia de la independencia"* where the cells for the analysis are situated. It had a carbon intensity of 2022 electricity production of 230.65 $kgCO_2eq/MWh$ and FOW power required about 3,300 MW, the lowest so far.

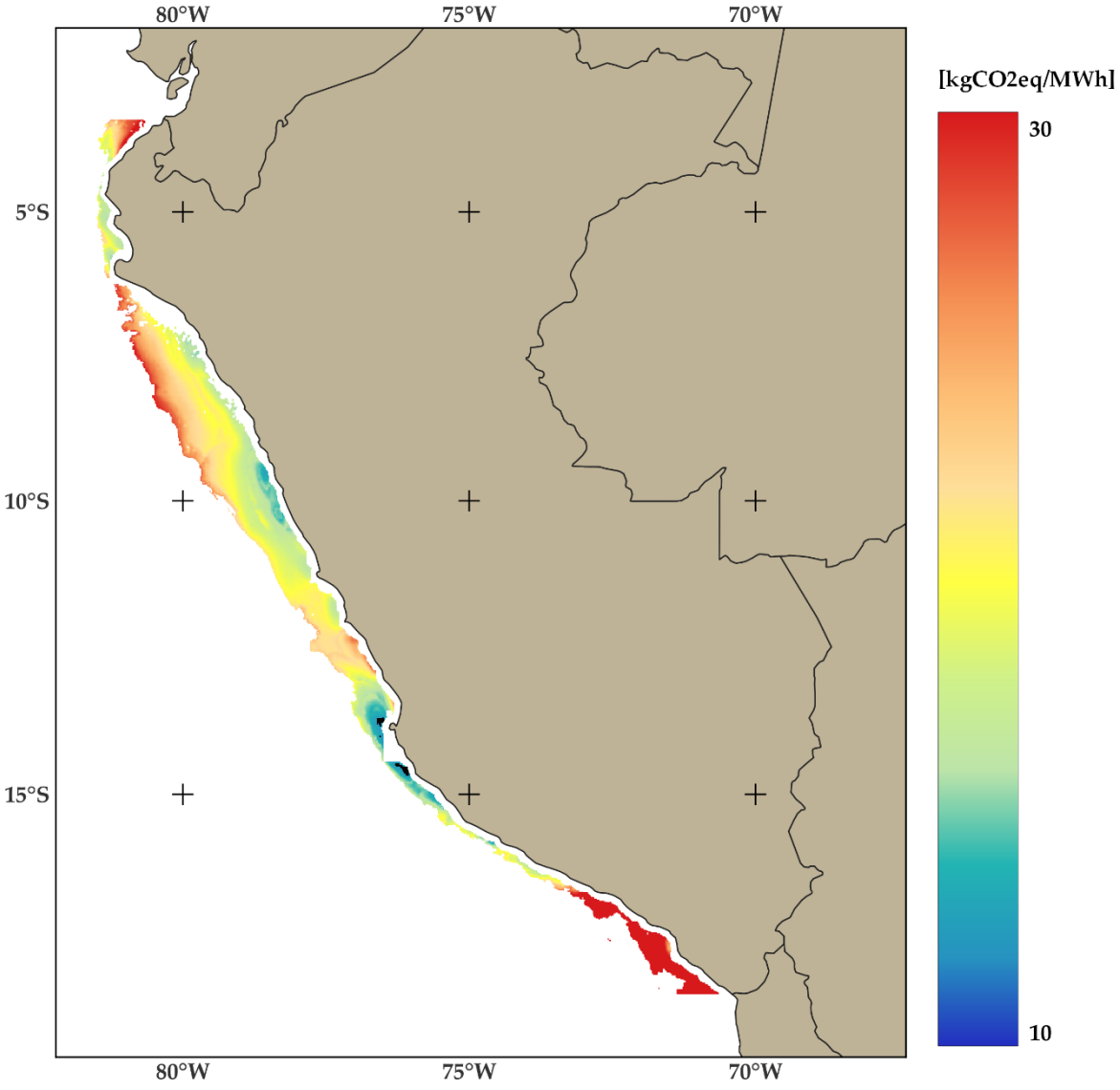

Figure 6.12. Peru's results map.

6.5.4.5. Alaska

Although Alaska is a state of United States is considered as individual territory due to the large distance between its territory and Washington's territory, which corresponds to the closest state to Alaska. It has the lowest FOW power of the top with about 440 MW, hence, is probably the territory with smallest population and minimum energy consumption. The points used for the analysis are all in the zone observed near to 155º W, 60º N point in Figure 6.13, which fortunately also corresponds to one of the most populated areas of Alaska. Furthermore, the carbon intensity of the 2022 electricity production for this country is 591.49 $kgCO_2eq/MWh$ the highest of the top.

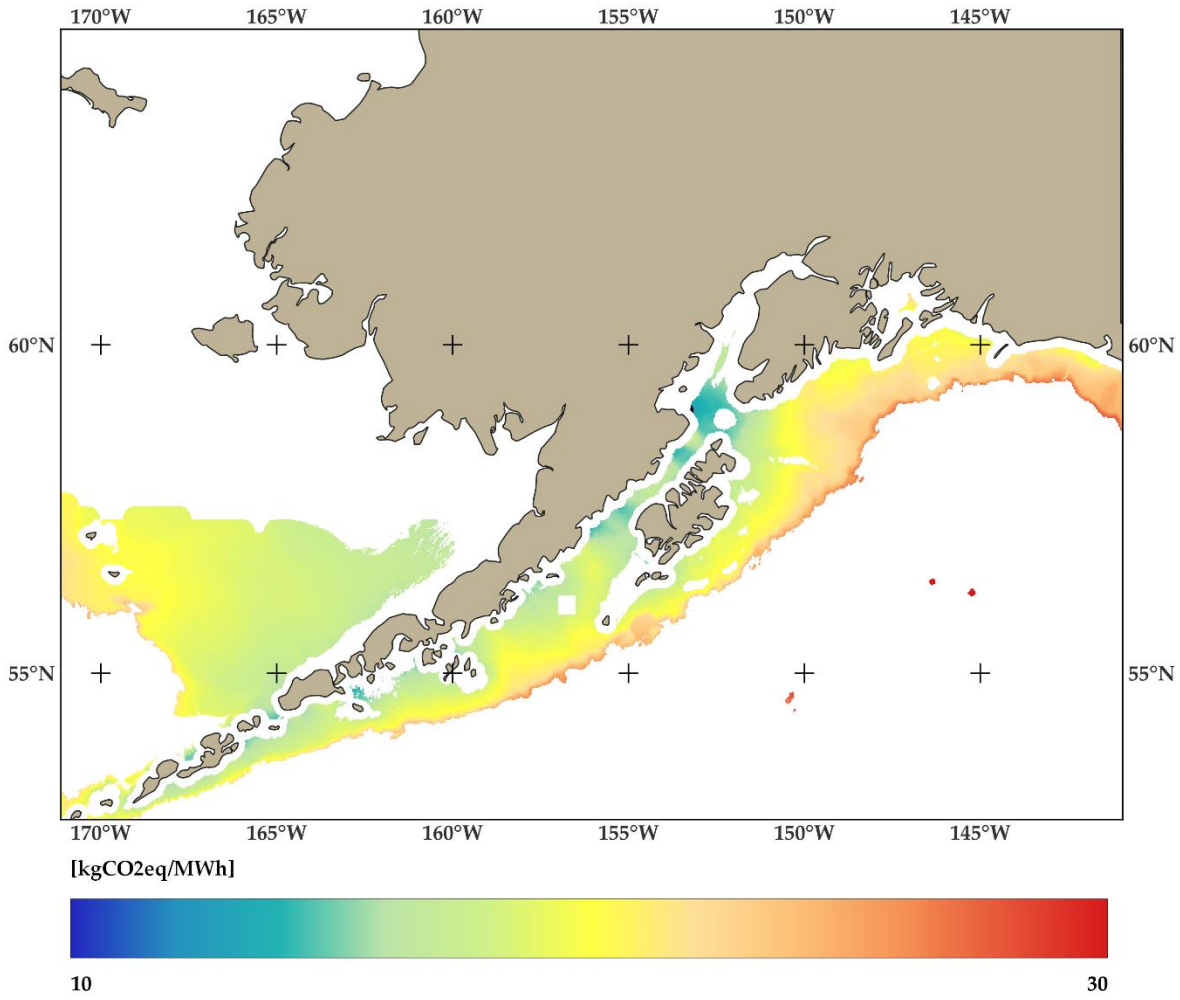

Figure 6.13. Alaska's results map.

6.5.4.6. Vietnam

Vietnam has a FOW carbon intensity of 13.79 $kgCO_2eq/MWh$, while the carbon intensity of electricity production in 2022 for this country is about 33 times higher, and the FOW power required is about 16,000 MW, the greatest so far. The highest potential of the country is mainly located in one zone, where all cells for the analysis are located, shown in Figure 6.14 in black.

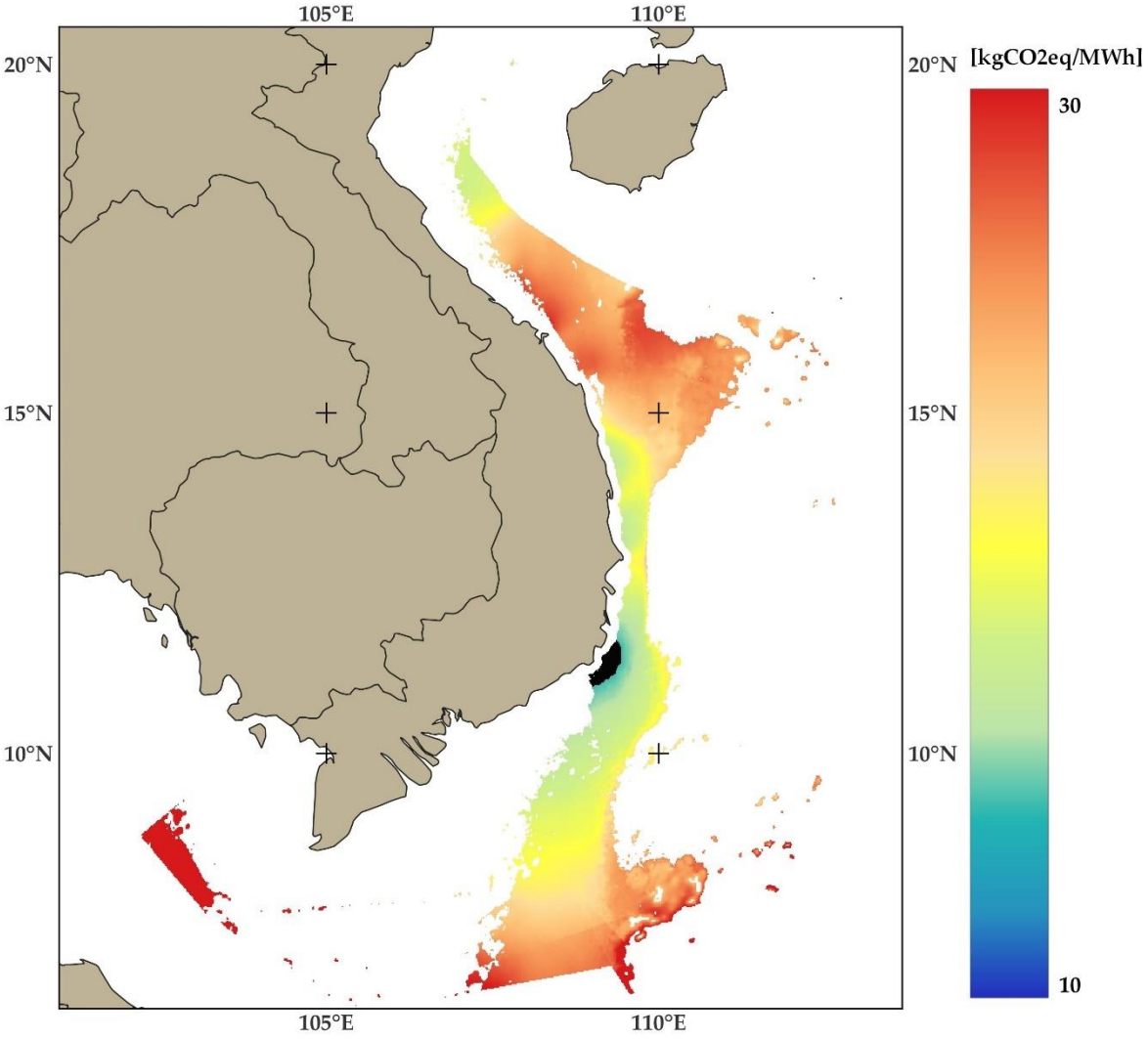

Figure 6.14. Vietnam's results map.

6.5.4.7. New Zealand

New Zealand has the lowest carbon intensity of 2022 electricity production of the top. However, the difference still considerably large, the carbon intensity of the FOW is about 10 times lower with 14.03 $kgCO_2eq/MWh$. Furthermore, it needs about 2,800 MW to satisfy the set condition. As shown in Figure 6.15, the zone with the highest potential is located between the North and South Island where the cells for the analysis are situated (plotted in black). In this case, the position of the cells may have a high maritime density, which can be a restriction for the FOWF installation that is not considered in this study. The rest of the country has values above 15 $kgCO_2eq/MWh$.

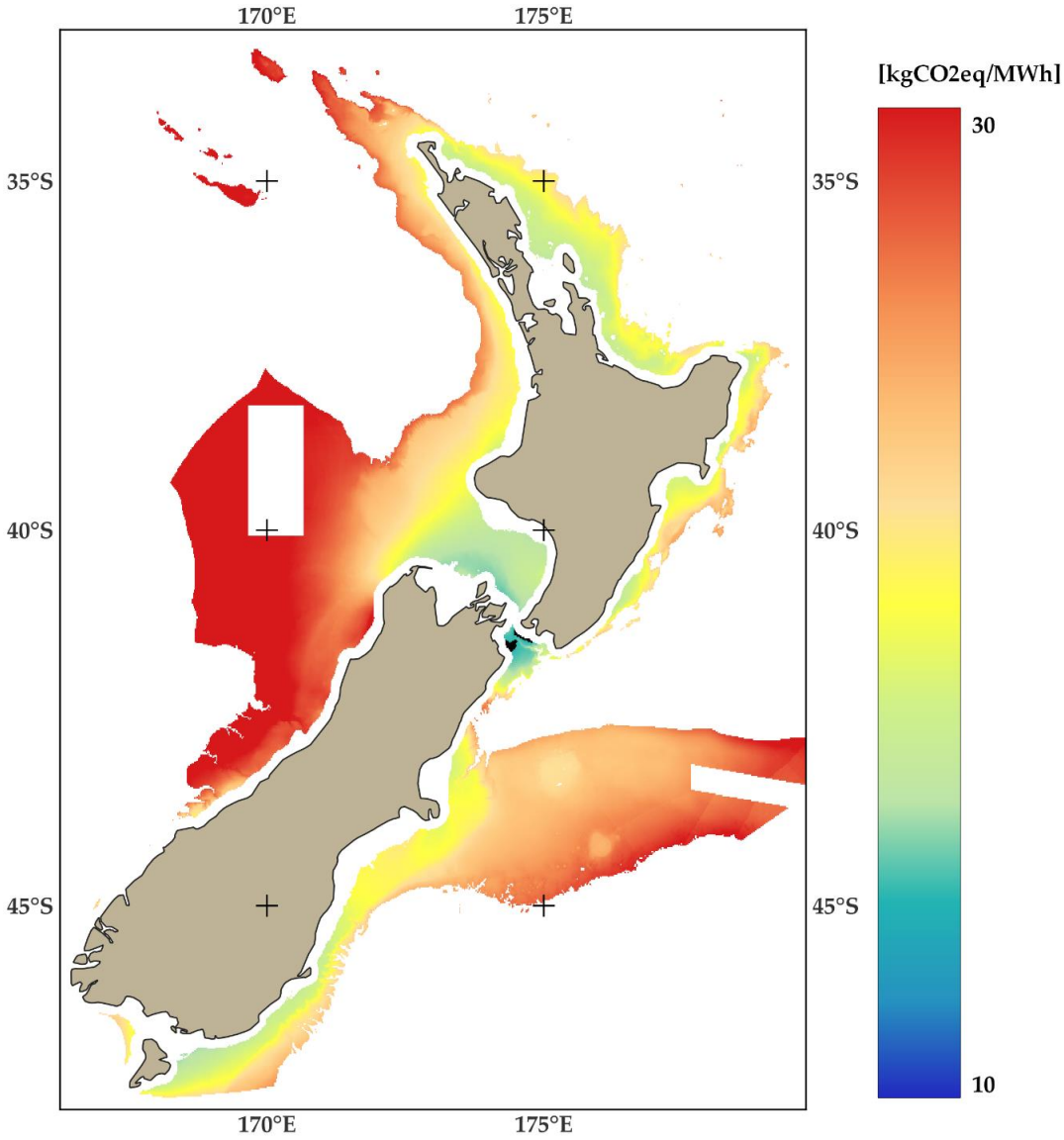

Figure 6.15. New Zealand's results map.

6.5.4.8. Ireland

Ireland is the second smallest country of the top and needs a FOW power about 1,500 MW to set the conditions. However, as shown in the Figure 6.16, it has a lot of potential cells below the 15 $kgCO_2eq/MWh$, mainly in the east coast. The cells taking into account for the analysis are located on the border with United Kingdom, plotted in the map in black.

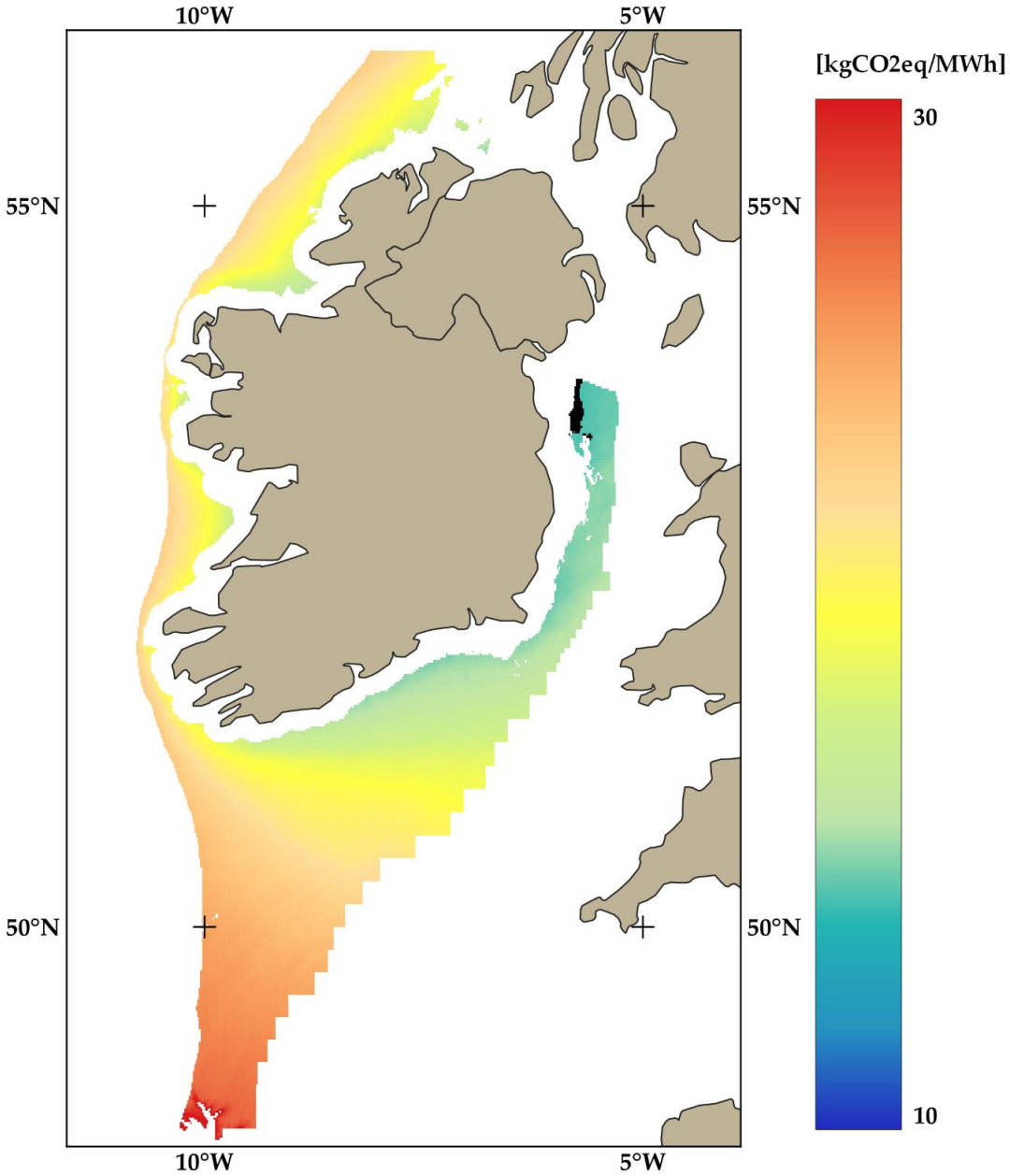

Figure 6.16. Ireland's results map.

6.5.4.9. Estonia

Estonia is the only country with coast in the Baltic Sea, which is one of the zones leading the development of offshore wind sector, that reach a position in the top 10. It is the smallest country in the top and has the second lowest FOW power with 487 MW, little more than Alaska. All its coast reach values below 16.5 $kgCO_2eq/MWh$, however, the lower values are in the east coast, where the values used for the study are located, as seen in Figure 6.17. Estonia has the second highest carbon intensity of the 2022 electricity production of the top.

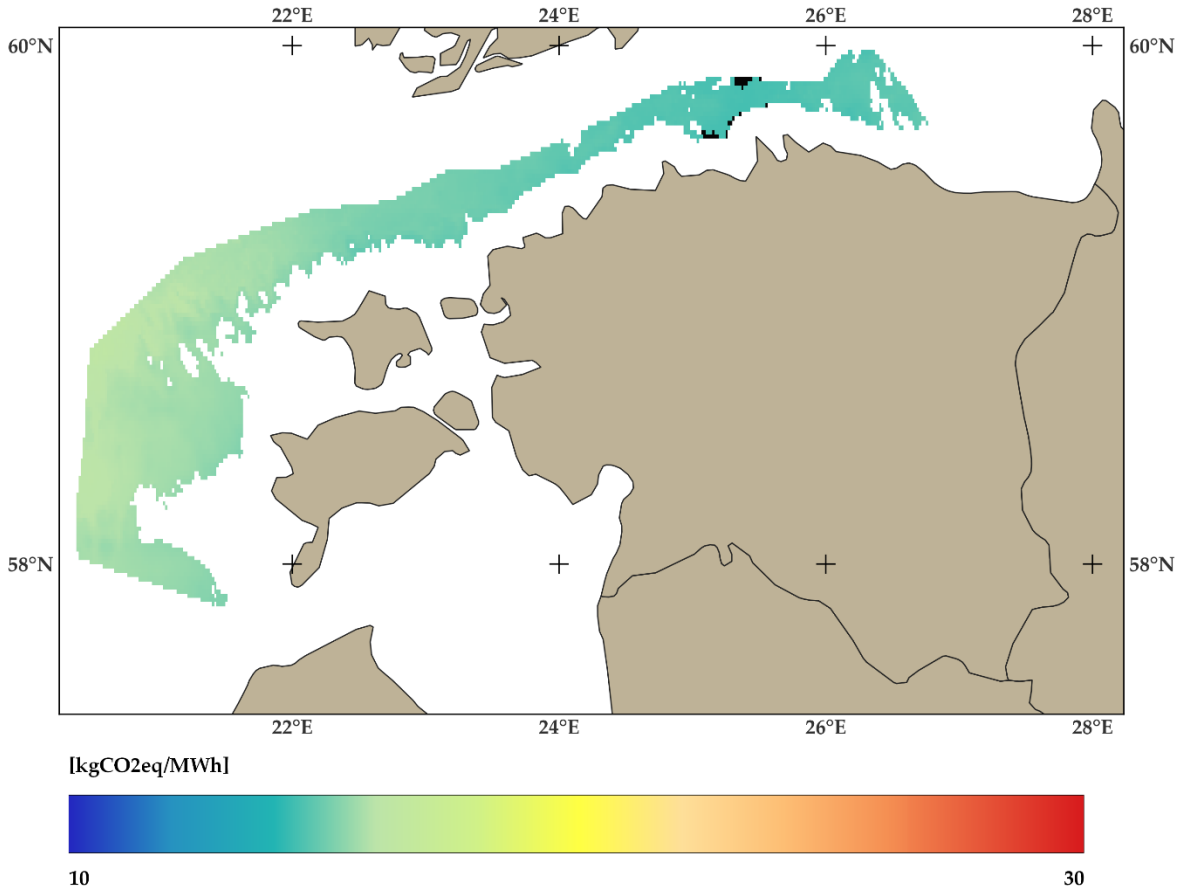

Figure 6.17. Estonia's results map.

6.5.4.10. United Kingdom

United Kingdom is the leading country in offshore wind energy, but almost all their projects are installed with bottom-fixed technology due its large areas with shallow water and its high wind potential. However, it also has a large potential for FOW. It has the greatest FOW power registered in the top 10 with about 20,000 MW. Hence, it is probably the country with most electricity production of the top. Although almost all the coast has values below the 16 $kgCO_2eq/MWh$, the cells used in the analysis are all between the two great British islands, near the cells used in the Ireland case. These cells are plotted in black in the map. In this case, as in New Zealand, this zone is a strait with high maritime density which can be a restriction for the FOWF installation.

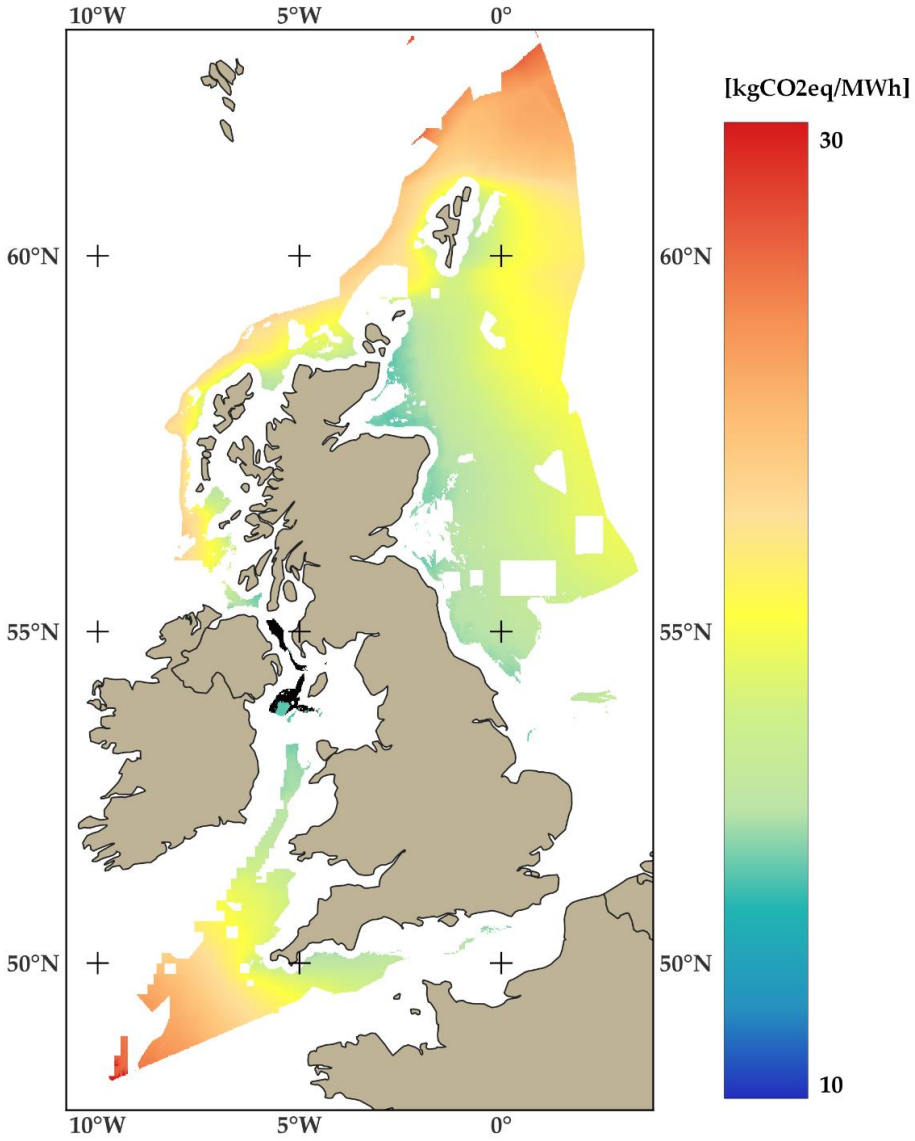

Figure 6.18. United Kingdom's results map.

6.6. FOW carbon intensity

The aim of this chapter is to find an emission factor value associated to FOW regarding the results obtained from the model and compare to other electricity generation technologies, both renewable and non-renewable.

6.6.1. Criteria for the resultant carbon intensity

Due to the number of values reached with the model, the assumption is to select the carbon intensities found per country (values showed in Annex A) as values for the GHG emissions estimations. These values have a minimum, first quarter (Q1), average, third quarter (Q3) and maximum that correspond to 12.15, 15.64, 23.21, 23.49 and 101.77 $kgCO_2eq/MWh$ respectively.

6.6.2. Comparison with literature

Finding the same values commented above for the literature, the results are those shown in Table 6.2.

Generation technology	Emission factor ($kgCO_2eq/MWh$)				
	Min	**1Q**	**Med**	**3Q**	**Max**
FOW (Study)	*12.32*	*15.90*	*23.68*	*23.79*	*101.77*
FOW (Literature)	6.56	18.05	26.39	33.01	78.70

Table 6.2. Comparison with literature values.

As seen in Table 6.2 and Figure 6.19 the results in both cases are similar, the main differences are on one hand the minimums, which the one related to the literature is about the half of the study and on the other hand the maximums, which the one related to the study is greatest due to the consideration of all countries in the analysis.

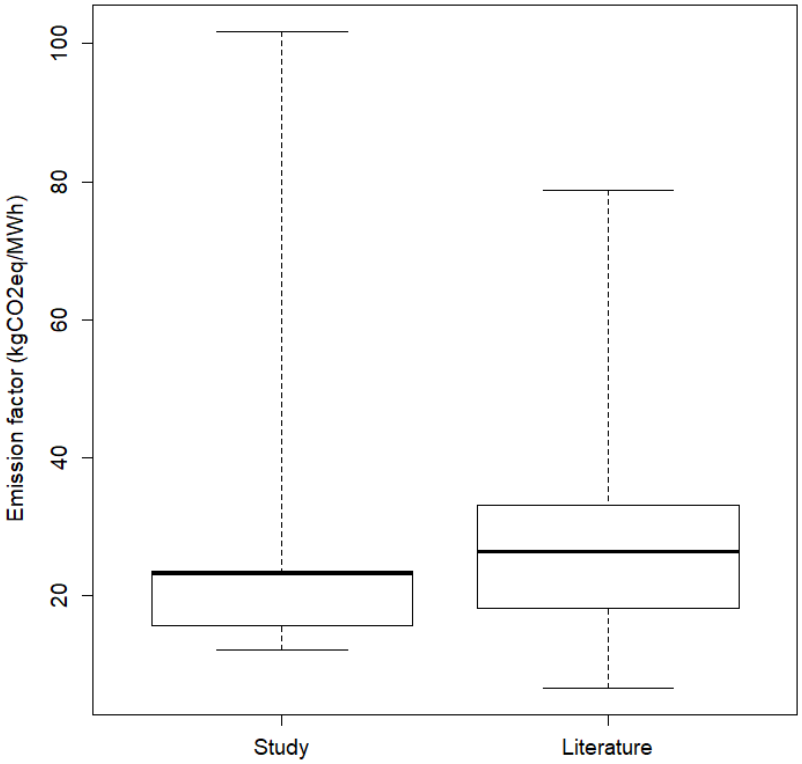

Figure 6.19. Boxplot comparison with literature values.

6.6.3. Comparison with renewable technologies

The technologies with lowest factor emissions are commonly the renewable ones. The values of emission factor from renewable energies according to National Renewable Energy Laboratory (NREL) [83] and the values regarding this study are shown in table below:

Generation technology	Emission factor ($kgCO_2eq/MWh$)				
	Min	**1Q**	**Med**	**3Q**	**Max**
FOW (Study)	*12.32*	*15.90*	*23.68*	*23.79*	*101.77*
Onshore wind	1.30	7.90	12.15	20.85	81.00
Bottom-fixed wind	5.28	12.06	19.33	28.48	43.70
Biopower	-1000.00	28.00	52.00	110.00	1300.00
Photovoltaic	10.90	30.00	43.40	62.00	226.00
Concentrating Solar Power	11.00	20.00	28.00	44.00	241.00
Geothermal	5.60	21.90	36.70	51.50	245.20

Hydropower	0.57	8.37	20.50	27.37	74.88
Ocean	2.00	6.00	8.00	9.00	23.00

Table 6.3. Comparison with renewable energy sources.

Focusing on the mean values, FOW has the fifth lowest factor emission, behind ocean, onshore wind, bottom-fixed wind and hydropower. This means that in terms of wind energy, FOW has by little, larger GHG emissions than the other two options. However, it has lower carbon intensity than biopower, concentrating solar power, geothermal and photovoltaic. These values are represented with a boxplot in Figure 6.20. In conclusion and considering that values from countries that have a low wind potential are also considered in the emission factor result for FOW, the values reached are considerably low compared to other generation technologies.

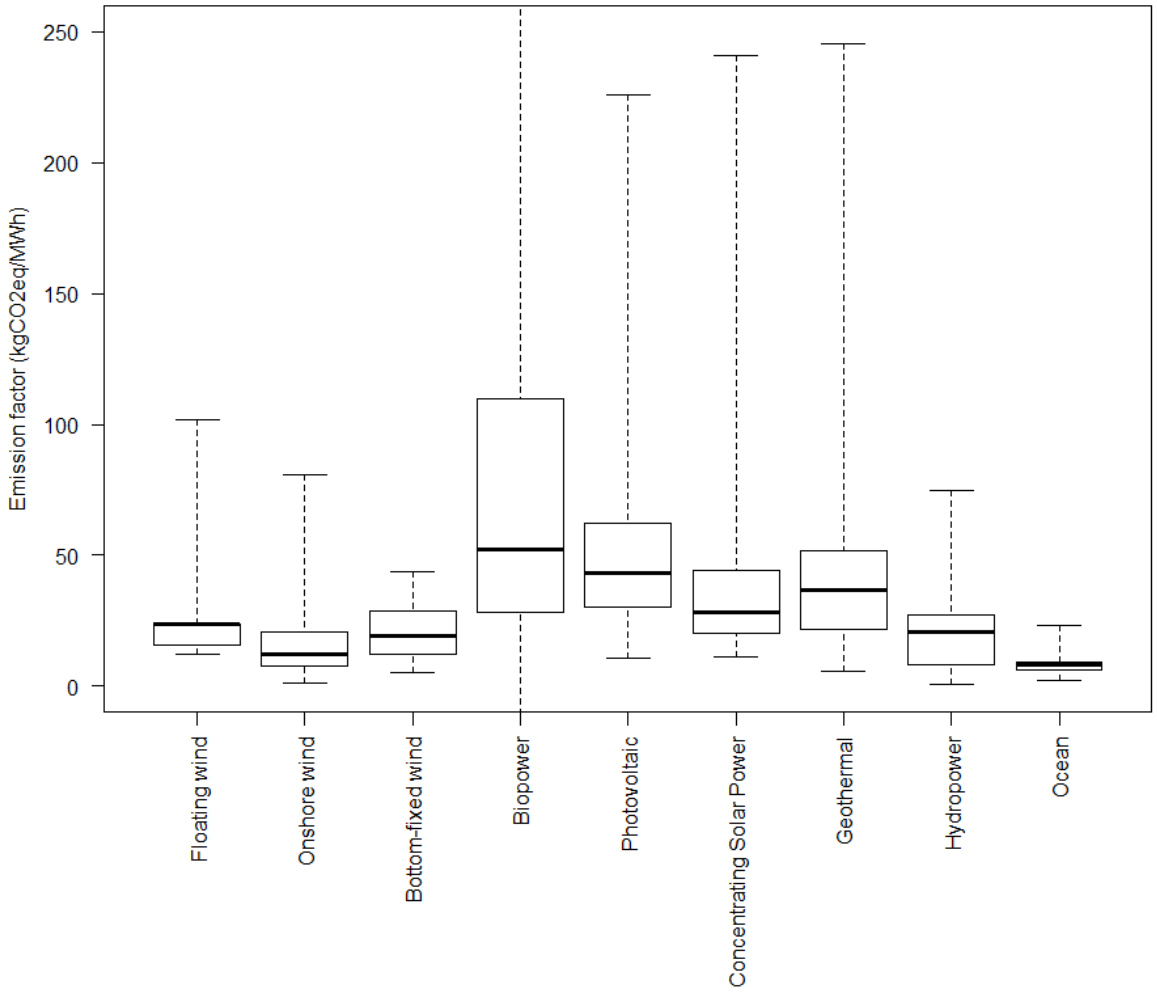

Figure 6.20. Boxplot comparison with renewable energy sources.

6.6.4. Comparison with non-renewable technologies

In Table 6.4 are presented the factor emissions of non-renewable energy according to NREL [83].

Generation technology	Emission factor ($kgCO_2eq/MWh$)				
	Min	**1Q**	**Med**	**3Q**	**Max**
FOW (Study)	*12.32*	*15.90*	*23.68*	*23.79*	*101.77*
Nuclear	3.10	7.70	13.00	31.00	220.00
Natural gas	307.00	427.25	486.00	550.50	988.00
Oil	510.00	722.00	840.00	907.00	1170.00
Coal	675.00	891.00	1001.00	1134.00	1689.00

Table 6.4. Comparison with non-renewable energy sources.

Comparing with the average of emissions factor of non-renewable technologies, FOW has the second lowest value, behind nuclear energy. However, the subsequent technology, natural gas has more than 20 times the emission factor reached for FOW energy. This can be seen in Figure 6.21.

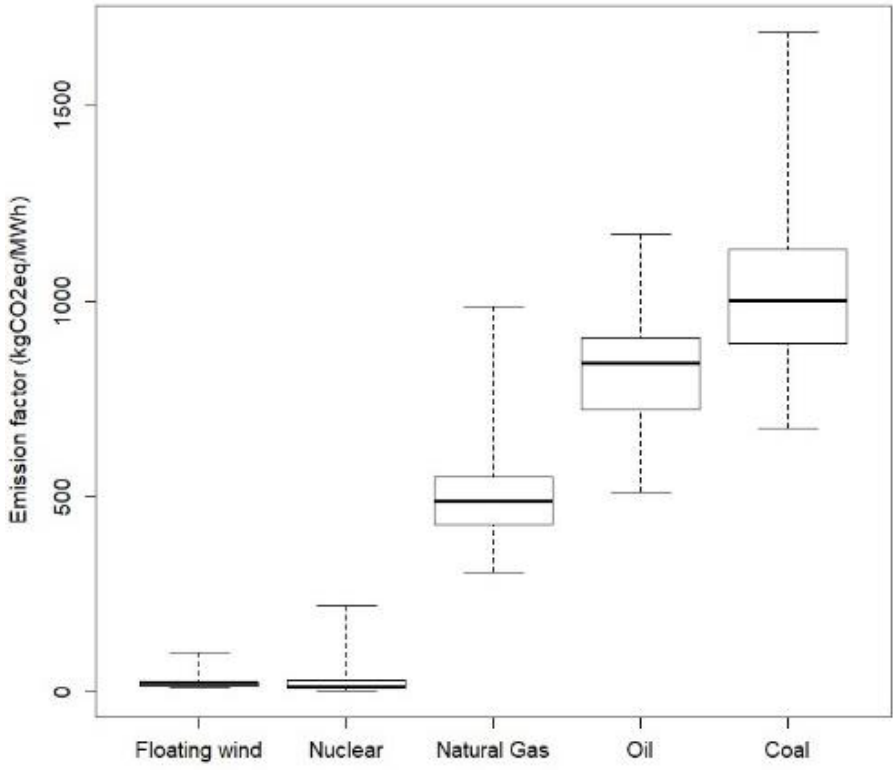

Figure 6.21. Boxplot comparison with non-renewable energy sources**.**

Natural gas, oil and coal has by far the largest GHG emissions of all generation technologies.

Conclusions

This thesis presents a geospatial model that helps calculating the carbon intensity of FOW in every feasible area worldwide, using the values of existing studies and considering site conditions as wind resource, distance to shore, distance to port, water depth and average significant wave height. Furthermore, the results of the model are mapped and analyzed in chapter 6.

Model validation in chapter 5, shows the lack of existing values needed for the model, exposes its vulnerability to the possibility of adding new values and the large dependence on the quality of the data used. However, it also shows the existence of practical significance in the functions.

The results present 850,000 km^2 with low factor emissions, which for the values obtained, can be taking into account below 16 $kgCO_2eq/MWh$. These are zones with high wind potential, considerably small depths and close to the coast.

The variables of the study are compared with the OFAT method. The independent variable related to energy production, capacity factor, has the biggest effect on the carbon intensity results as it is observed in the literature. Regarding the LCA phases, the larger burden comes from the manufacturing stage, mainly related to the turbine and substructure. Hence, according to the results, the FOW carbon intensity reduction potentials are the increment of the energy production or the decrease of the carbon footprint during the substructure or turbine manufacturing process.

In section 6.5 a value of FOW carbon intensity is attributed to every country with feasible cells in its EEZ. These FOW carbon intensity values allow a comparison between countries. Furthermore, for each country, the difference between the carbon footprint of the electricity produced in 2022 and the carbon footprint associated with the production of 20% of that energy in the case that it was produced with FOW on the coasts of that country is shown. Annex A shows the results for 161 countries, which the three with lower carbon intensity are in first place Venezuela with 12.24 $kgCO_2eq/MWh$, in second place Argentina with 12.32 $kgCO_2eq/MWh$ and in third place Colombia with 12.50 $kgCO_2eq/MWh$.

The emission factor attributed to the FOW is the average of values per country, 23.68 $kgCO_2eq/MWh$, which is slightly smaller than the found in the literature. Besides, it is similar to other renewable sources, but considering that it is still a nascent sector and that carbon footprint values regarding its life cycle stages will probably decrease, the resultant emission factor is considerably low.

To sum up, it can be concluded that this research work can be of great interest for people mainly from the wind sector to investigate about the emission factor related to the FOW, to locate the sites of most interest for this technology or analyze the potential reductions of carbon footprint.

Further work

There are several processes that can be implemented to the model of this thesis that could reinforce the forcefulness of the results obtained:

- Add new values from future studies and projects to improve the regressions.
- Consider more variables as the distance between port and manufacturing sites or to the waste treatment site.
- Decipher the ports with capabilities to carry out the installation, maintenance and dismantling activities of a FOWF.
- Locate grid connections to consider distance to grid connection rather than distance to shore.

Regarding the analysis of the results there is additional research work that can be of interest:

- Perform a background analysis of values related to a single country.
- Analyse areas with lower carbon intensity values by adding economic cost analysis (LCOE).

References

[1] GWEC, "Global Wind Report 2022," 2022.

[2] GWEC, "FLOATING OFFSHORE WIND-A GLOBAL OPPORTUNITY," 2022.

[3] M. Lerch, "Technical-economic analysis, modeling and optimization of floating offshore wind farms," 2020. [Online]. Available: http://www.tdx.cat/?locale-

[4] L. Tsai, J. C. Kelly, B. S. Simon, R. M. Chalat, and G. A. Keoleian, "Life Cycle Assessment of Offshore Wind Farm Siting: Effects of Locational Factors, Lake Depth, and Distance from Shore," *J Ind Ecol*, vol. 20, no. 6, 2016, doi: 10.1111/jiec.12400.

[5] E. Masanet, "Life Cycle Assessment of Renewable Energy Sources," *Annu Rev Environ Resour*, vol. 36, no. 1, 2010, doi: 10.1146/annurev-environ-010710-100408.

[6] Vestas, "Material use in Vestas turbines," 2022.

[7] A. Ojo, M. Collu, and A. Coraddu, "Multidisciplinary design analysis and optimization of floating offshore wind turbine substructures: A review," *Ocean Engineering*, vol. 266. 2022. doi: 10.1016/j.oceaneng.2022.112727.

[8] "OffshoreTronic," https://offshoretronic.tech/floating-wind.

[9] CoreWind, "Public design and FAST models of the two 15MW floater-turbine concepts," 2020.

[10] K.-T. Ma, Y. Luo, T. Kwan, and Y. Wu, "Chapter 8 - Anchor selection," in *Mooring System Engineering for Offshore Structures*, 2019.

[11] C. M. Fontana *et al.*, "Multiline anchor force dynamics in floating offshore wind turbines," *Wind Energy*, vol. 21, no. 11, 2018, doi: 10.1002/we.2222.

[12] "Floating wind turbines," http://floatingwindfarm.weebly.com/anchoring-systems.html.

[13] K. T. Ma, Y. Luo, T. Kwan, and Y. Wu, *Mooring system engineering for offshore structures*. 2019. doi: 10.1016/C2018-0-02217-3.

[14] C. Ng and L. Ran, "Introduction to offshore wind energy," in *Offshore Wind Farms: Technologies, Design and Operation*, 2016. doi: 10.1016/B978-0-08-100779-2.00001-5.

[15] O. Anaya-Lara, "Offshore wind farm arrays," in *Offshore Wind Farms: Technologies, Design and Operation*, 2016. doi: 10.1016/B978-0-08-100779-2.00012-X.

[16] I. Bin Ahmad, A. Schnepf, and M. C. Ong, "An optimisation methodology for suspended inter-array power cable configurations between two floating offshore wind turbines," *Ocean Engineering*, vol. 278, 2023, doi: 10.1016/j.oceaneng.2023.114406.

[17] N. Srinil, "Cabling to connect offshore wind turbines to onshore facilities," in *Offshore Wind Farms: Technologies, Design and Operation*, 2016. doi: 10.1016/B978-0-08-100779-2.00013-1.

[18] C. Maienza, A. M. Avossa, F. Ricciardelli, D. Coiro, G. Troise, and C. T. Georgakis, "A life cycle cost model for floating offshore wind farms," *Appl Energy*, vol. 266, 2020, doi: 10.1016/j.apenergy.2020.114716.

[19] T. Duarte, A. Peiffer, and J. M. Pinheiro, "WindFloat Atlantic Project: Technology Development Towards Commercial Wind Farms," in *Proceedings of the Annual Offshore Technology Conference*, 2022. doi: 10.4043/32058-MS.

[20] Vryhof Anchors, *Anchor Manual 2015 – The guide to Anchoring*. 2015.

[21] "ACTEON," https://acteon.com/blog/how-do-suction-piles-work/.

[22] M. Asgarpour, "Assembly, transportation, installation and commissioning of offshore wind farms," in *Offshore Wind Farms: Technologies, Design and Operation*, 2016. doi: 10.1016/B978-0-08-100779-2.00017-9.

[23] S. Barbara *et al.*, "Life Cycle Assessment of Greenhouse Gas Emissions for Floating Offshore Wind Energy in California Committee in charge," 2019.

[24] G. Brussa, M. Grosso, and L. Rigamonti, "Life cycle assessment of a floating offshore wind farm in Italy," *Sustain Prod Consum*, vol. 39, 2023, doi: 10.1016/j.spc.2023.05.006.

[25] "The International EDP System," https://www.environdec.com/home.

[26] H. Farr, B. Ruttenberg, R. K. Walter, Y. H. Wang, and C. White, "Potential environmental effects of deepwater floating offshore wind energy facilities," *Ocean Coast Manag*, vol. 207, 2021, doi: 10.1016/j.ocecoaman.2021.105611.

[27] N. Christiansen, U. Daewel, B. Djath, and C. Schrum, "Emergence of Large-Scale Hydrodynamic Structures Due to Atmospheric Offshore Wind Farm Wakes," *Front Mar Sci*, vol. 9, 2022, doi: 10.3389/fmars.2022.818501.

[28] T. Nagel, J. Chauchat, A. Wirth, and C. Bonamy, "On the multi-scale interactions between an offshore-wind-turbine wake and the ocean-sediment dynamics in an idealized framework – A numerical investigation," *Renew Energy*, vol. 115, 2018, doi: 10.1016/j.renene.2017.08.078.

[29] K. C. Newton, A. B. Gill, and S. M. Kajiura, "Electroreception in marine fishes: chondrichthyans," *Journal of Fish Biology*, vol. 95, no. 1. 2019. doi: 10.1111/jfb.14068.

[30] A. Copping and L. Hemery, "OES-Environmental 2020 State of the Science Report: Environmental Effects of Marine Renewable Energy Development Around the World. Report for Ocean Energy Systems (OES)," 2020.

[31] T. Kirchgeorg, I. Weinberg, M. Hörnig, R. Baier, M. J. Schmid, and B. Brockmeyer, "Emissions from corrosion protection systems of offshore wind farms: Evaluation of the potential impact on the marine environment," *Marine Pollution Bulletin*, vol. 136. 2018. doi: 10.1016/j.marpolbul.2018.08.058.

[32] L. Hammar, D. Perry, and M. Gullström, "Offshore Wind Power for Marine Conservation," *Open Journal of Marine Science*, vol. 06, no. 01, 2016, doi: 10.4236/ojms.2016.61007.

[33] A. N. Popper and A. D. Hawkins, "An overview of fish bioacoustics and the impacts of anthropogenic sounds on fishes," *Journal of Fish Biology*, vol. 94, no. 5. 2019. doi: 10.1111/jfb.13948.

[34] F. Thomsen and M. H. Andersson, "MaRVEN-Environmental Impacts of Noise, Vibrations and Electromagnetic Emissions from Marine Renewable Energy," 2016, doi: 10.2777/272281.

[35] D. J. F. Russell *et al.*, "Marine mammals trace anthropogenic structures at sea," *Current Biology*, vol. 24, no. 14. 2014. doi: 10.1016/j.cub.2014.06.033.

[36] M. Scheidat *et al.*, "Harbour porpoises (Phocoena phocoena) and wind farms: A case study in the Dutch North Sea," *Environmental Research Letters*, vol. 6, no. 2, 2011, doi: 10.1088/1748-9326/6/2/025102.

[37] E. A. Masden, D. T. Haydon, A. D. Fox, R. W. Furness, R. Bullman, and M. Desholm, "Barriers to movement: Impacts of wind farms on migrating birds," *ICES Journal of Marine Science*, vol. 66, no. 4, 2009, doi: 10.1093/icesjms/fsp031.

[38] H. Skov, S. Heinänen, T. Norman, R. Ward, S. Méndez-Roldán, and I. Ellis, *ORJIP bird collision and avoidance study - Final Report*, vol. 66. 2018.

[39] W. P. Erickson, G. D. Johnson, and D. P. Y. Jr, "A Summary and Comparison of Bird Mortality from Anthropogenic Causes with an Emphasis on Collisions 1 Fatality Rates," *Most*, 2005.

[40] C. White, B. S. Halpern, and C. V. Kappel, "Ecosystem service tradeoff analysis reveals the value of marine spatial planning for multiple ocean uses," *Proc Natl Acad Sci U S A*, vol. 109, no. 12, 2012, doi: 10.1073/pnas.1114215109.

[41] S. Benjamin *et al.*, "Understanding the potential for marine megafauna entanglement risk from marine renewable energy developments," *Scottish Natural Heritage Commissioned Report No. 791*, no. 7, 2014.

[42] E. L. M. Vermeirssen, C. Dietschweiler, I. Werner, and M. Burkhardt, "Corrosion protection products as a source of bisphenol A and toxicity to the aquatic environment," *Water Res*, vol. 123, 2017, doi: 10.1016/j.watres.2017.07.006.

[43] A. Arvesen and E. G. Hertwich, "Assessing the life cycle environmental impacts of wind power: A review of present knowledge and research needs," *Renewable and Sustainable Energy Reviews*, vol. 16, no. 8. 2012. doi: 10.1016/j.rser.2012.06.023.

[44] D. Nugent and B. K. Sovacool, "Assessing the lifecycle greenhouse gas emissions from solar PV and wind energy: A critical meta-survey," *Energy Policy*, vol. 65, 2014, doi: 10.1016/j.enpol.2013.10.048.

[45] A. Bonou, A. Laurent, and S. I. Olsen, "Life cycle assessment of onshore and offshore wind energy-from theory to application," *Appl Energy*, vol. 180, 2016, doi: 10.1016/j.apenergy.2016.07.058.

[46] J. Weinzettel, M. Reenaas, C. Solli, and E. G. Hertwich, "Life cycle assessment of a floating offshore wind turbine," *Renew Energy*, vol. 34, no. 3, 2009, doi: 10.1016/j.renene.2008.04.004.

[47] N. Elginoz and B. Bas, "Life Cycle Assessment of a multi-use offshore platform: Combining wind and wave energy production," *Ocean Engineering*, vol. 145, 2017, doi: 10.1016/j.oceaneng.2017.09.005.

[48] H. L. Raadal, B. I. Vold, A. Myhr, and T. A. Nygaard, "GHG emissions and energy performance of offshore wind power," *Renew Energy*, vol. 66, 2014, doi: 10.1016/j.renene.2013.11.075.

[49] B. Poujol, A. Prieur-Vernat, J. Dubranna, R. Besseau, I. Blanc, and P. Pérez-López, "Site-specific life cycle assessment of a pilot floating offshore wind farm based on suppliers' data and geo-located wind data," *J Ind Ecol*, vol. 24, no. 1, 2020, doi: 10.1111/jiec.12989.

[50] N. Yildiz, H. Hemida, and C. Baniotopoulos, "Life cycle assessment of a barge-type floating wind turbine and comparison with other types of wind turbines," *Energies (Basel)*, vol. 14, no. 18, 2021, doi: 10.3390/en14185656.

[51] A. Garcia-Teruel, G. Rinaldi, P. R. Thies, L. Johanning, and H. Jeffrey, "Life cycle assessment of floating offshore wind farms: An evaluation of operation and maintenance," *Appl Energy*, vol. 307, 2022, doi: 10.1016/j.apenergy.2021.118067.

[52] R. M. Pulselli *et al.*, "Benchmarking Marine Energy Technologies Through LCA: Offshore Floating Wind Farms in the Mediterranean," *Front Energy Res*, vol. 10, 2022, doi: 10.3389/fenrg.2022.902021.

[53] W. Yuan *et al.*, "Floating wind power in deep-sea area: Life cycle assessment of environmental impacts," *Advances in Applied Energy*, vol. 9, 2023, doi: 10.1016/j.adapen.2023.100122.

[54] J. Chipindula, V. S. V. Botlaguduru, H. Du, R. R. Kommalapati, and Z. Huque, "Life cycle environmental impact of onshore and offshore wind farms in Texas," *Sustainability (Switzerland)*, vol. 10, no. 6, 2018, doi: 10.3390/su10062022.

[55] V. J. Ferreira, G. Benveniste, J. I. Rapha, C. Corchero, and J. L. Domínguez-García, "A holistic tool to assess the cost and environmental performance of floating offshore wind farms," *Renew Energy*, vol. 216, 2023, doi: 10.1016/j.renene.2023.119079.

[56] E. Gaertner, J. Rinker, L. Sethuraman, B. Anderson, F. Zahle, and G. Barter, "IEA Wind TCP Task 37: Definition of the IEA 15 MW Offshore Reference Wind Turbine," *Technical Report NREL/TP-5000-75698 March 2020*, 2020.

[57] "Esri," https://www.esri.com/en-us/what-is-gis/overview.

[58] "International Electrotechnical Commission ."

[59] "GEBCO," https://www.gebco.net/.

[60] "Copernicus," https://www.copernicus.eu/es.

[61] "Global Wind Atlas," https://globalwindatlas.info/en.

[62] "AmeriGEO," https://data.amerigeoss.org/.

[63] "Marineregions," https://marineregions.org/downloads.php.

[64] M. Metych, "exclusive economic zone," Encyclopedia Britannica.

[65] "PART V - Exclusive Economic Zone (II)," in *United Nations Convention on the Law of the Sea*, 2014. doi: 10.1163/ej.laos_9780792324713_489-510.

[66] "Havesine Formula," https://en.wikipedia.org/wiki/Haversine_formula.

[67] R. Montero, "Modelos de regresión lineal múltiple," *Documentos de Trabajo en Economía Aplicada*, vol. 3, no. 12, 2016.

[68] D. Song *et al.*, "Optimization of floating wind farm power collection system using a novel two-layer hybrid method," *Appl Energy*, vol. 348, 2023, doi: 10.1016/j.apenergy.2023.121546.

[69] A. Campanile, V. Piscopo, and A. Scamardella, "Mooring design and selection for floating offshore wind turbines on intermediate and deep water depths," *Ocean Engineering*, vol. 148, 2018, doi: 10.1016/j.oceaneng.2017.11.043.

[70] A. Myhr, C. Bjerkseter, A. Ågotnes, and T. A. Nygaard, "Levelised cost of energy for offshore floating wind turbines in a lifecycle perspective," *Renew Energy*, vol. 66, 2014, doi: 10.1016/j.renene.2014.01.017.

[71] Shayan Heidari, "Economic modelling of floating offshore wind power," Degree Project in Industrial Engineering and Management with Specialization in Energy Engineering, School of Business, Society and Engineering, 2017.

[72] *Secondary Analysis of Electronic Health Records*. 2016. doi: 10.1007/978-3-319-43742-2.

[73] P. Bhandari, "What is Effect Size and Why Does It Matter? (Examples)," *Scribbr*, 2020.

[74] Zach, "How to Interpret Diagnostic Plots in R."

[75] W. Kenton, D. Kindness, and V. Velásquez, "Sensitivity analysis definition," Investopedia.

[76] "SSDSI."

[77] E. Sourianos, K. Kyriakou, and G. A. Hatiris, "GIS-based spatial decision support system for the optimum siting of offshore windfarms," *European Water*, vol. 58, no. August 2018, 2017.

[78] UNEP-WCMC and IUCN, "Protected planet: The world database on protected areas (WDPA)," *Database*, no. January. 2010.

[79] "Parc Tramuntana," https://parctramuntana.com/es/inicio/.

[80] P. Bhandari, "What Is Standard Error? | How to Calculate (Guide with Examples)," Scribbr.

[81] Ember - with major processing by Our World in Data, "Yearly Electricity Data," https://ourworldindata.org/grapher/electricity-generation.

[82] P. Enevoldsen and M. Z. Jacobson, "Data investigation of installed and output power densities of onshore and offshore wind turbines worldwide," *Energy for Sustainable Development*, vol. 60, 2021, doi: 10.1016/j.esd.2020.11.004.

[83] NREL, "Life Cycle Greenhouse Gas Emissions from Electricity Generation: Update," *NREL*. 2021.

Annex A

A1. Values for all countries

Countries	FOW Carbon intensity ($kgCO_2eq/MWh$)	Carbon intensity of 2022 electricity production ($kgCO_2eq/MWh$)	FOW share of 2022 electricity production (%)	FOW Power (MW)
Alaska	13.16	591.49	20.00	437
Albania	20.67	23.44	20.00	804
Algeria	19.75	498.90	20.00	7088
American Samoa	26.80	687.50	29.17	28
Angola	19.08	195.98	20.00	1232
Antigua and Barbuda	16.82	657.14	20.00	28
Argentina	12.32	357.79	20.00	8540
Aruba	12.33	591.40	20.00	57
Australia	15.27	531.25	20.00	18207
Azerbaijan	16.63	532.90	20.00	2173
Bahrain	21.66	489.77	15.44	2611
Bangladesh	29.33	555.91	20.00	10729
Barbados	20.23	644.86	25.88	114
Belize	23.53	484.38	25.75	84
Benin	27.47	666.67	36.36	58
Brazil	17.26	158.59	20.00	51399
British Virgin Islands	19.28	714.29	44.65	28
Brunei Darussalam	37.28	658.85	20.00	757
Bulgaria	18.14	354.33	20.00	3719
Republic of Cabo Verde	15.14	600.00	34.99	56
Cambodia	36.18	400.46	20.00	1527
Cameroon	70.85	278.26	20.00	2811
Canada	14.54	128.46	20.00	43459
Cayman Islands	24.23	684.93	20.00	83
Chile	14.97	416.88	20.00	5793
China	17.51	544.36	20.00	652412

Colombia	12.50	181.07	20.00	4638
Comoros	34.70	714.29	25.73	29
Republic of the Congo	84.71	395.52	20.00	1664
Cook Islands	36.79	400.00	99.98	28
Costa Rica	14.92	33.04	20.00	921
Côte d'Ivoire	43.57	410.75	20.00	2278
Croatia	18.81	210.98	20.00	1380
Cuba	17.16	602.03	20.00	1588
Cyprus	24.06	599.61	20.00	552
Democratic Republic of the Congo	73.44	25.36	20.00	3760
Denmark	14.51	221.42	20.00	2336
Djibouti	15.92	666.67	125.65	29
Dominica	18.24	529.41	41.00	28
Dominican Republic	16.04	550.88	20.00	1275
Ecuador	20.76	155.84	20.00	3224
Egypt	14.80	464.43	20.00	13538
El Salvador	32.76	185.98	20.00	1029
Equatorial Guinea	59.75	492.96	20.00	352
Eritrea	13.79	688.89	36.80	57
Estonia	14.44	481.22	20.00	487
Falkland Islands / Malvinas	12.84	500.00	297.19	18
Faeroe Islands	15.74	428.57	27.20	41
Fiji	15.11	289.47	20.00	84
Finland	14.51	145.54	20.00	5084
France	16.63	67.39	20.00	41465
French Polynesia	19.54	471.43	27.11	85
Gabon	41.24	397.38	20.00	498
The Gambia	21.58	700.00	36.66	57
Georgia	26.58	111.55	20.00	1590
Germany	18.87	365.48	0.18	395
Ghana	26.61	361.20	20.00	2654
Greece	15.19	353.34	20.00	3855
Greenland	16.56	133.33	20.00	57

Grenada	18.39	714.29	30.99	29
Guam	21.15	670.33	20.00	200
Guatemala	41.74	320.64	20.00	2874
Guinea-Bissau	28.90	750.00	50.94	29
Guinea	54.57	208.63	20.00	721
Guyana	23.79	642.28	20.00	145
Haiti	17.40	606.06	20.00	83
Hawaii	15.89	700.19	20.00	578
Honduras	19.04	375.10	20.00	1126
Iceland	16.40	28.56	20.00	1492
India	19.13	637.18	20.00	145171
Indonesia	19.45	623.16	20.00	27238
Iran	21.47	492.68	20.00	36098
Ireland	14.44	363.61	20.00	2382
Israel	36.91	548.03	20.00	11885
Italy	18.45	340.79	20.00	24598
Jamaica	17.31	519.54	20.00	364
Japan	16.82	478.55	20.00	75259
Kazakhstan	15.78	641.10	20.00	8348
Kenya	19.69	86.22	20.00	1112
Kiribati	32.89	666.67	131.04	29
Latvia	14.92	223.93	20.00	411
Lebanon	33.82	594.75	20.00	2888
Liberia	67.26	304.35	20.00	292
Libya	16.72	550.42	20.00	2616
Lithuania	15.20	244.60	20.00	282
Madagascar	13.51	483.25	20.00	143
Malaysia	32.44	548.61	20.00	24725
Maldives	55.29	651.52	20.00	175
Malta	22.20	441.44	20.00	236
Mauritania	13.80	526.60	20.00	139
Mauritius	19.03	611.11	20.00	248
Mexico	16.78	399.85	20.00	26365
Montenegro	19.51	326.26	20.00	328
Montserrat	17.48	1000.00	551.25	28

Morocco	15.64	610.41	20.00	3033
Mozambique	19.79	126.63	20.00	1822
Myanmar	28.39	344.36	20.00	23155
Namibia	14.66	63.69	20.00	112
Nauru	101.77	750.00	34.99	29
New Caledonia	17.37	610.12	20.00	300
New Zealand	14.03	132.43	20.00	2809
Nicaragua	14.54	354.21	20.00	345
Nigeria	41.14	376.99	20.00	5917
North Korea	17.33	157.79	20.00	1242
Norway	15.90	27.55	20.00	11648
Oman	17.38	488.24	20.00	3011
Pakistan	21.50	366.05	20.00	15022
Palestine	37.97	465.12	20.00	175
Panama	18.46	192.14	20.00	1044
Papua New Guinea	16.09	526.75	20.00	376
Peru	12.54	230.65	20.00	3267
Philippines	16.29	580.91	20.00	8170
Poland	15.08	660.12	20.00	12323
Portugal	18.42	219.05	20.00	4173
Puerto Rico	19.00	681.47	20.00	1587
Qatar	21.81	489.79	20.00	5096
Romania	17.87	255.88	20.00	4805
Russian Federation	15.60	359.94	20.00	82127
Saint Kitts and Nevis	17.32	681.82	32.83	28
Saint Lucia	19.39	685.71	38.24	57
Saint Pierre and Miquelon	14.77	800.00	104.95	20
Saint Vincent and the Grenadines	17.92	500.00	42.84	29
Samoa	25.84	470.59	31.89	29
São Tomé and Principe	75.69	600.00	33.55	59
Saudi Arabia	18.22	571.34	20.00	28558
Senegal	17.68	523.13	20.00	479
Seychelles	19.63	615.38	20.00	58

Sierra Leone	76.12	47.62	20.00	87
Solomon Islands	20.86	727.27	47.61	29
Somalia	14.55	634.15	20.00	29
South Africa	18.88	715.68	20.00	18480
South of Korea	16.94	458.08	20.00	48289
Spain	17.84	193.86	20.00	20498
Canary Islands	15.95	552.00	20.00	544
Sri Lanka	15.98	463.00	20.00	1223
Sudan	16.80	264.01	20.00	1361
Suriname	22.15	356.44	20.00	204
Sweden	14.48	45.82	20.00	11879
Syria	23.39	541.17	20.00	1831
Taiwan	14.60	573.28	20.00	19449
Tanzania	25.20	366.75	20.00	993
Thailand	31.87	506.64	20.00	28931
Bahamas	17.10	698.11	20.00	190
Timor-Leste	30.15	698.11	25.99	87
Togo	25.21	460.32	20.00	87
Tonga	19.66	625.00	79.11	28
Trinidad and Tobago	17.96	491.41	20.00	748
Tunisia	17.14	468.23	20.00	1800
Turkey	16.35	430.40	20.00	24988
Turkmenistan	15.28	490.19	20.00	1645
Turks and Caicos Islands	15.12	703.70	26.94	27
Ukraine	17.52	240.17	20.00	13060
United Arab Emirates	69.39	461.84	12.98	30012
United Kingdom	14.48	268.33	20.00	20142
United States	16.51	379.26	20.00	314046
United States Virgin Islands	17.97	685.71	28.60	84
Uruguay	17.24	147.28	20.00	1276
Vanuatu	17.78	571.43	97.29	28
Venezuela	12.24	212.48	20.00	5472
Vietnam	13.79	448.22	20.00	16069
Yemen	13.45	543.91	20.00	257

A2. Interactive web map

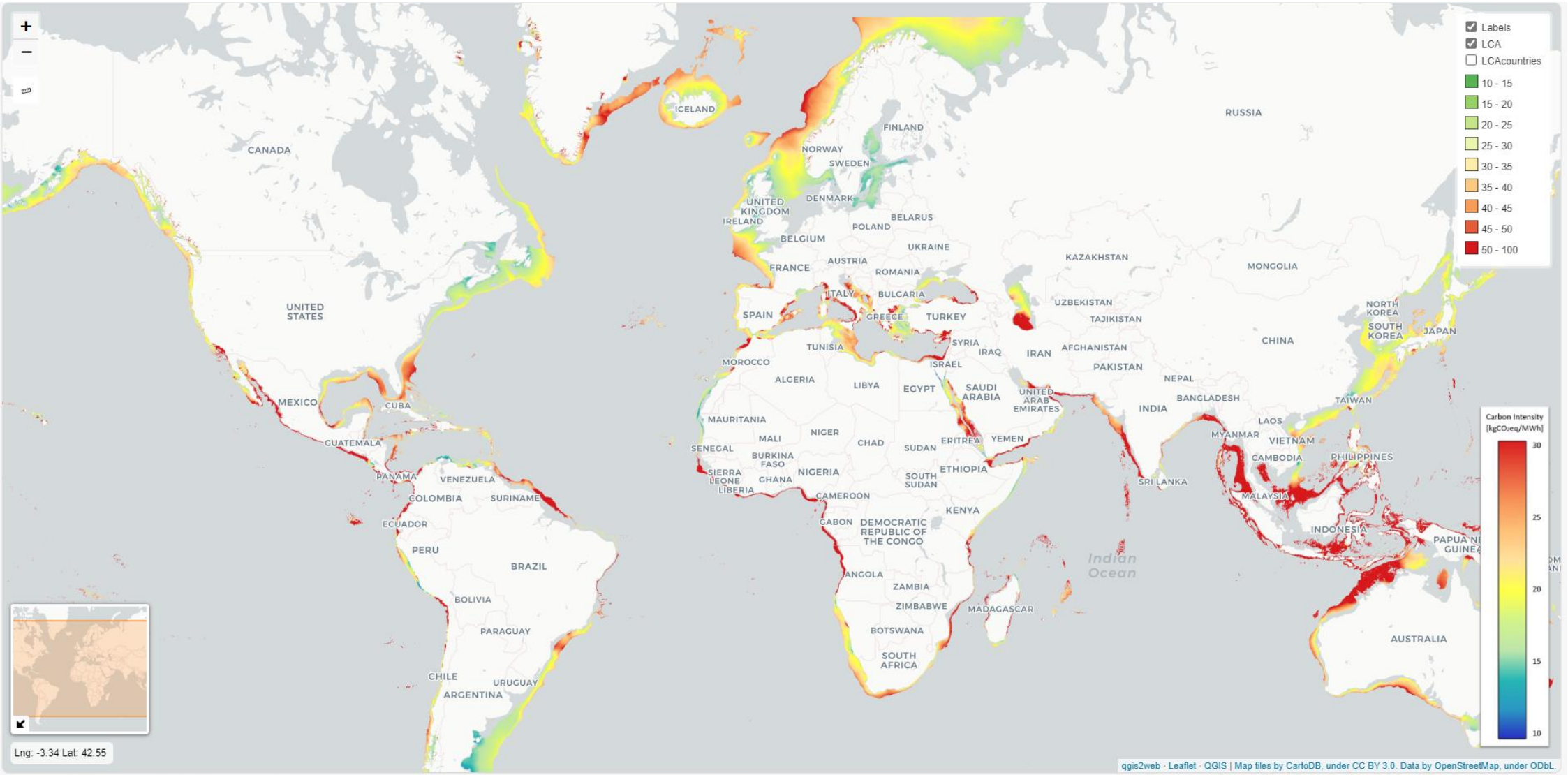
Labels
LCA
LCAcountries
10 - 15
15 - 20
20 - 25
25 - 30
30 - 35
35 - 40
40 - 45
45 - 50
50 - 100
Carbon Intensity [kgCO2eq/MWh]
30
25
20
15
10
Lng: -3.34 Lat: 42.55
qgis2web · Leaflet · QGIS | Map files by CartoDB, under CC BY 3.0. Data by OpenStreetMap, under ODbL.
ICELAND
CANADA
RUSSIA
FINLAND
NORWAY
SWEDEN
DENMARK
UNITED KINGDOM
IRELAND
BELARUS
POLAND
BELGIUM
UKRAINE
AUSTRIA
FRANCE
ROMANIA
ITALY
BULGARIA
KAZAKHSTAN
MONGOLIA
UZBEKISTAN
TAJIKISTAN
SPAIN
GREECE
TURKEY
SYRIA
IRAQ
IRAN
AFGHANISTAN
PAKISTAN
CHINA
NORTH KOREA
SOUTH KOREA
JAPAN
TUNISIA
MOROCCO
ISRAEL
ALGERIA
LIBYA
EGYPT
SAUDI ARABIA
UNITED ARAB EMIRATES
NEPAL
BANGLADESH
INDIA
TAIWAN
LAOS
MYANMAR
VIETNAM
CAMBODIA
PHILIPPINES
SRI LANKA
MALAYSIA
INDONESIA
PAPUA NEW GUINEA
UNITED STATES
MEXICO
CUBA
GUATEMALA
PANAMA
VENEZUELA
COLOMBIA
SURINAME
ECUADOR
PERU
BRAZIL
BOLIVIA
PARAGUAY
CHILE
URUGUAY
ARGENTINA
MAURITANIA
MALI
NIGER
CHAD
SUDAN
ERITREA
YEMEN
SENEGAL
BURKINA FASO
SIERRA LEONE
LIBERIA
GHANA
NIGERIA
ETHIOPIA
SOUTH SUDAN
CAMEROON
KENYA
GABON
DEMOCRATIC REPUBLIC OF THE CONGO
ANGOLA
ZAMBIA
ZIMBABWE
MADAGASCAR
BOTSWANA
SOUTH AFRICA
AUSTRALIA
Indian Ocean

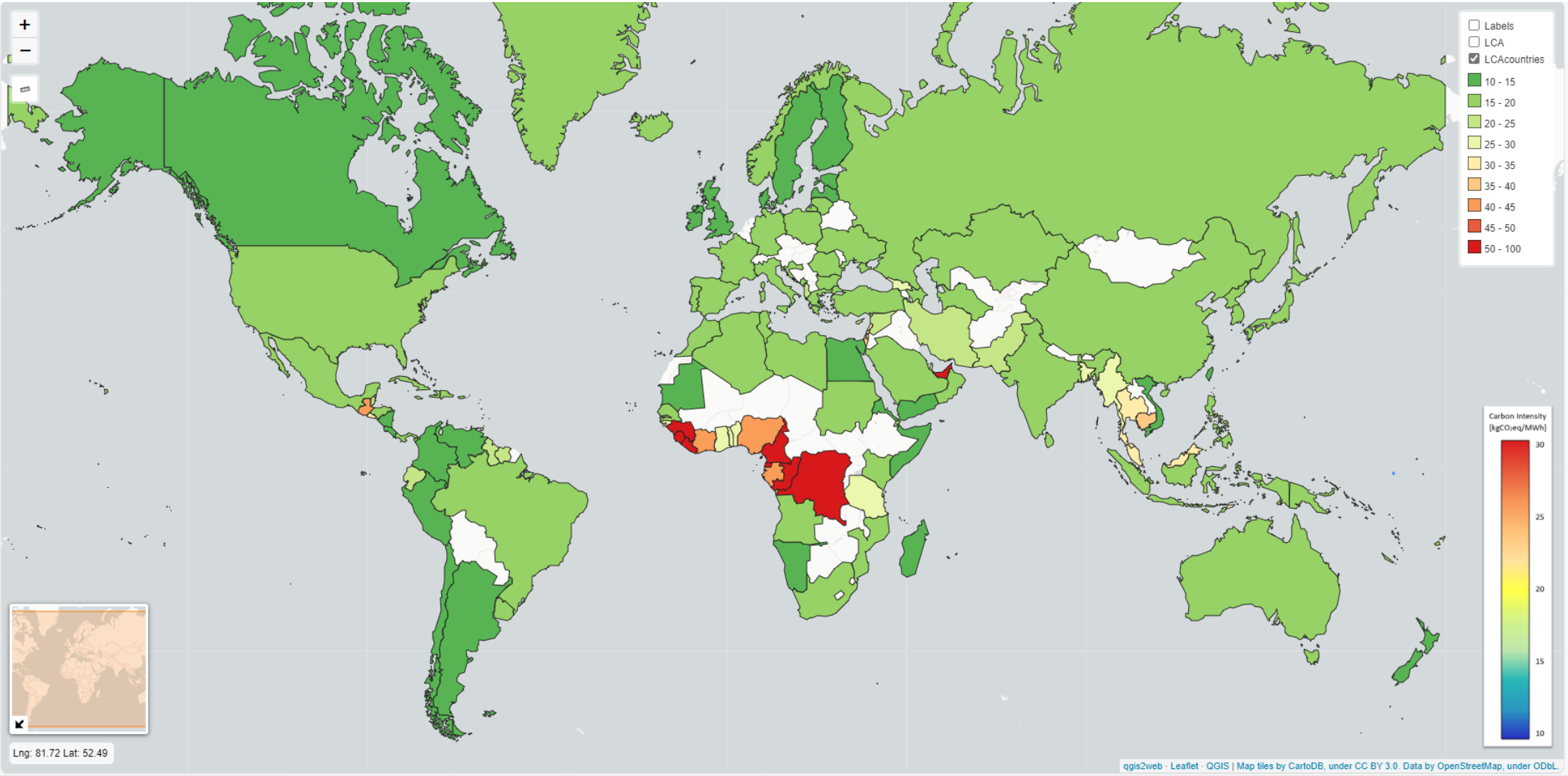
Labels
LCA
LCAcountries
10 - 15
15 - 20
20 - 25
25 - 30
30 - 35
35 - 40
40 - 45
45 - 50
50 - 100
Carbon Intensity
[kgCO2eq/MWh]
30
25
20
15
10
Lng: 81.72 Lat: 52.49
qgis2web · Leaflet · QGIS | Map tiles by CartoDB, under CC BY 3.0. Data by OpenStreetMap, under ODbL.

Popup information window per country.